AN ABSTRACT OF THE THESIS OF

Hong Gao for the degree of Master of Science in Forest Products presented on March 12, 1990

Title: X-ray Computerized Tomography of Particleboard to Predict Through-thickness Density Profile

Signature redacted for privacy.

Abstract approved: _____

James B. Wilson

Particleboard is a widely used composite panel product consisting of consolidated wood particles and adhesive. On a macro level the panel appears to be homogeneous, however, its density varies both throughout the plane of the panel as well as through its thickness. Of concern for this thesis is the through-thickness density profile which strongly influences the panel's mechanical properties such as modulus of rupture, modulus of elasticity and internal bond strength. Panel manufacturers realize this importance and, as a result, have begun to use some methods to measure the density profile in their laboratories for quality control. However, present methods provide data for only a small portion of the production and often hours if not days after the panel was produced. This study proposes and evaluates a method using a X-ray computerized tomography technique to predict the through-thickness density profile.

Three types of commercially produced particleboards were scanned using a system consisting of an X-ray densitometer and a computer acquisition system to collect the attenuation data. The density profile of each sample was then predicted by using a computer algorithm (C language) in which two mathematical models were applied. A two-degree polynomial regression function was used to evaluate the accuracy of the models.

Comparisons were made of the predicted to actual density profiles for the same sample. A good agreement, a correlation value of $r^2 = 0.822$, between the predicted and actual density profiles was found indicating that this technique does provide good estimation of density profiles.

This study provides the necessary knowledge to design a valuable nondestructive testing tool for use in monitoring the quality of particleboard and other similar composite products on the production line and on a real time basis.

X-ray Computerized Tomography of Particleboard to Predict Through-thickness Density Profile

by

Hong Gao

A THESIS

submitted to

Oregon State University

in partial fulfillment of
the requirements for the
degree of

Master of Science

Completed March 12,1990

Commencement June 1990

APPROVED:

Signature redacted for privacy.

Professor of Forest Products in charge of major

Signature redacted for privacy.

Head of Department of Forest Products

Signature redacted for privacy.

Dean of Graduate School

Date thesis is presented: March 12, 1990
Typed for Hong Gao

ACKNOWLEDGEMENTS

I would like to thank Dr. Jim Wilson, my major professor, for his guidance in my graduate study and research.

I would also like to thank Milo Clauson and Bob Heald for their generous help.

Table of Contents

List of Figures

List of Figures (Continued)

List of Figures (Continued)

List of Tables

X-RAY COMPUTERIZED TOMOGRAPHY OF PARTICLEBOARD TO PREDICT THROUGH-THICKNESS DENSITY PROFILE

INTRODUCTION

Particleboard is a panel product composed of wood particles and adhesive that have been consolidated and cured under sufficient pressure and heat to permanently densify the board. Due to processing conditions the panel varies in density throughout its plane as well as through its thickness. Although variations throughout the panel are not advantageous, a controlled density gradient through the thickness can be advantageous. The through-thickness density profile contributes significantly to both the physical and mechanical properties of the panel. A typical through-thickness density profile of particleboard has densities for the face layers of the panel greater than the density of its core.

Gamma-ray scanners exist for monitoring density variations throughout the plane of the panel as it travels along the production line. However, presently no equipment is being used on-line to monitor through-thickness density gradient. Equipment does exist to monitor the through-thickness gradient in the laboratory, however the panel must be cut into small 2- x 2-inch

samples and scanned with a X-ray beam from face-to-face to measure the gradient. Because of the importance of the through-thickness density gradient to quality control, and a lack of existing equipment for in-line monitoring, this thesis will focus on the subject of finding a through-thickness density monitoring technique that could be used in-line. The reviewed literature will address only through-thickness density variations in terms of its effect on panel properties and the equipment used to monitor the profile.

The through-thickness density profile affects the mechanical properties of modulus of rupture (MOR), modulus of elasticity (MOE), and the internal bond strength (IB) of the panel -- all properties important in the manufacturing process. The higher density face layers influence MOE and MOR, while the lower density core influences IB. Increasing or decreasing the density of the layers has the same influence on its respective mechanical property. The through-thickness density gradient is affected by the manufacturing process parameters which can be controlled to some extent.

X-ray computerized tomography is a technique which provides remarkably precise images of density variations of an object without destroying the object. This technique is widely used in medical diagnoses and as a quality control tool in many industries, but is little used in forest

products manufacturing. X-ray computerized tomography of particleboard to predict the density profile could be used to nondestructively monitor every product on-line. This material monitoring technique should give useful information to the panel manufacturer who is interested in improving product quality.

OBJECTIVES

The primary objective of this study is to present a practical, nondestructive method for predicting the through-thickness density profile of particleboard on the production line. An additional objective was to demonstrate the feasibility of applying a X-ray computerized tomography technique in forest products manufacturing.

LITERATURE REVIEW

Effects of Density Profile on Mechanical Properties of Particleboard

The processing of particleboard generally results in a density variation throughout the panel. Part of the variation is designed into the product to influence board properties, but part of the variation results from uncontrolled parameters in the manufacturing process. The density gradient perpendicular to the panel is called the through-thickness density profile (Figure 1). The density profile of particleboard depends directly on several manufacturing parameters and strongly influences mechanical properties such as MOR, MOE, and IB. As a result, density is an important factor frequently used to monitor particleboard quality.

Density Profile of Particleboard

Strickler (1959) demonstrated the relative influence of the hot pressing operation, moisture content, and moisture content distribution on the through-thickness density profile of Douglas-fir flakeboard. Panel density variations depended primarily upon the pressure of the hot

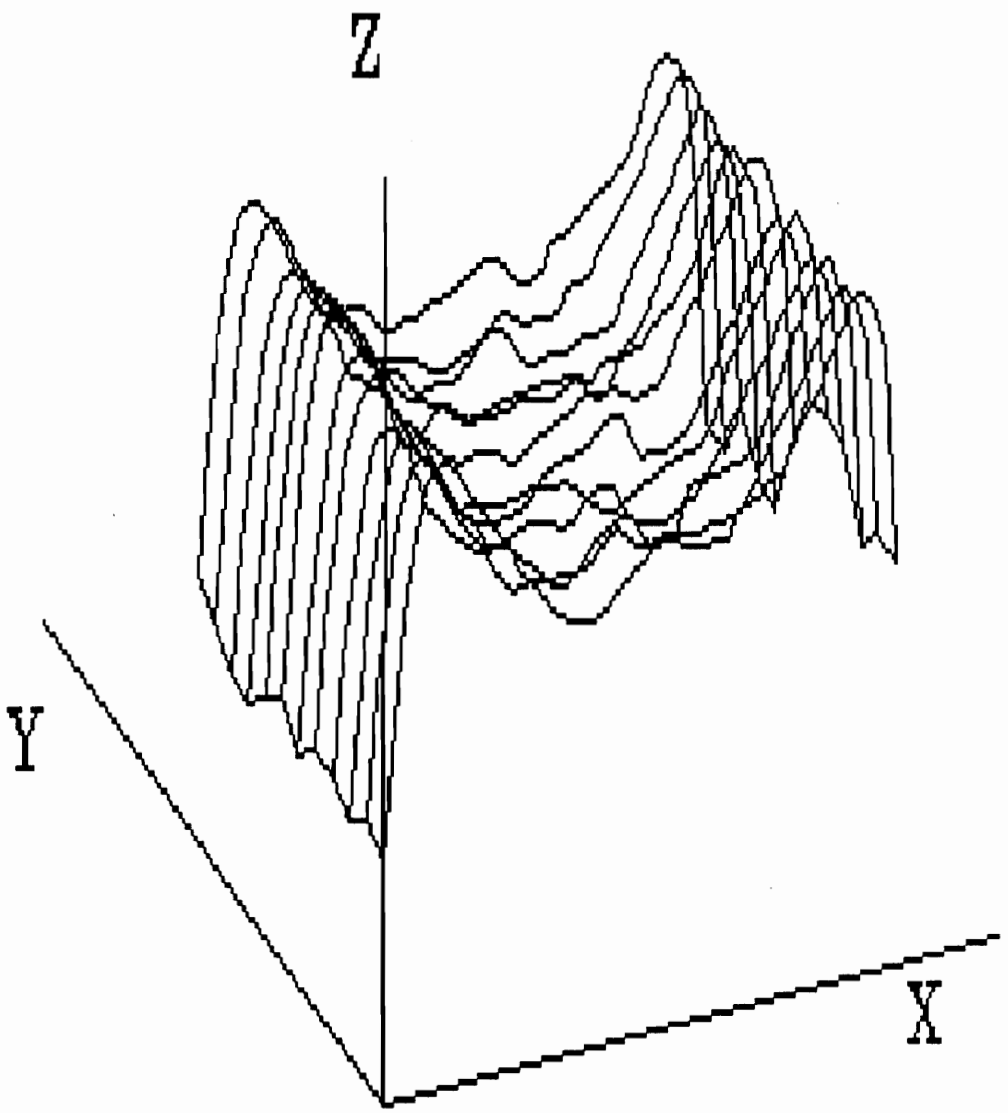

Figure 1. - A three-dimensional density profile of particleboard sample, where X-axis represents thickness, Y-axis represents length, and Z-axis represents density.

press and the moisture content distribution in the panel when the adhesive bonded the wood particles together. Strickler observed that the density gradient decreased as the press closure time increased. High surface density was the result of a high initial pressure during the pressing cycle. The effect of moisture content on density profile was highly significant, but extremely complex. Moisture content affected both heat conduction and water vapor transfer in the panel which influenced the relative densities of the layers. Nonuniform density distribution throughout the panel in turn impacted heat and moisture transfer. Strickler also found that high surface and low core moisture content within board caused the surface density to increase and core density to decrease.

Carroll (1963) also pointed out that the density profile was affected by the close-time of hot press. His conclusions regarding the relationship between layer-density and press close-time agreed with Strickler's results. As the closing time increased, the maximum density gradient began to shift from the face towards the core of the panel.

In order to control the through-thickness density gradient of particleboard in the manufacturing process, Suchsland (1967) studied the behavior of the particleboard mat during the pressing process. He reported that low initial pressures produced a more uniform density profile.

Heebink et al. (1972) showed the influence of moisture content and the press closure time on the density profile of particleboard. Essentially, the higher the moisture content of the mat, the greater the gradient between the face and core layer of the panel. The density rose sharply from the surface to a maximum in the face layer and then declined gradually to a minimum in the core. As the closing time increased, the face density decreased and the core density increased. Decreasing the press temperature produced a more uniform density profile.

Harless et al. (1987) also showed that a steeper gradient in the density profile was produced by increasing the press temperature. However, the density gradient did not appear to be sensitive to the closing rate, which is contrary to the findings of Heebink et al..

Effects of Density Profile on Mechanical Properties

Mechanical properties of particleboard, such as modulus of elasticity (MOE), modulus of rupture (MOR) and internal bond strength (IB), are strongly affected by the through-thickness density profile. Strickler (1959) studied the effect of flakeboard density on strength properties. Unexpectedly, the modulus of rupture was not closely correlated with the density of the surface layer. However, the high density material just below the surface did give

correspondingly high MOR strength. It appeared that the particleboard's MOR was related to the density beneath the surface.

Suchsland (1967) theorized that MOE can be expressed in terms of the face density, the difference between the face and core density, and the ratio of face thickness to total thickness of the panel.

Woodson (1977) evaluated the through-thickness density profile of fiberboard using X-rays to predict MOE and MOR. He found a good statistical relationship between the MOE or MOR and density profile.

Preheating particleboard was studied by Huang and Mori (1978). They found a linear relationship between the density of the board surface and MOE with a correlation coefficient of $r = 0.82$. The IB had a linear relationship to the density of core, with higher core density resulting in higher IB of the boards. Similarly, Strickler (1959) and Carroll (1963) found moderately good correlations between core density and IB if press cycle and moisture content treatments were constant.

May (1983) found ample evidence of the relationship between board properties and the through-thickness density in particleboard. When surface material is removed during sanding to obtain a uniform thickness, the MOE changes. May showed that the shape of the density profile determined the difference in MOE before and after sanding. However,

he suggested that the influence of density profile on MOE and IB was less than the influence of the glue content in different layers of the board.

Other mechanical properties of particleboard besides MOE, MOR and IB were affected by the through-thickness density profile. The relationship between the layer-strength and layer-density was demonstrated by Shen and Carroll (1970). Using a torsion-shear technique, they determined the relative strength of the surface and core layers. A gravimetric method was used to measure the density profile. They found that layers with high density had high strength. A close correlation ($r = 0.89$) was found between torsion-shear strength and density. This indicated that layer density could be used to predict layer-strength of particleboard. A few years earlier, Suchsland (1967) had already found that the shear strength was a function of core density only.

Additionally, Sekino and Morisaki (1987) reported that the lateral nail resistance of low-density particleboard was affected by the density profile. Given the same average density of all boards, the one with the larger through-thickness density variation had the smaller lateral nail resistance. This knowledge is very useful to the manufacturer who produces particleboard to meet a customer's special requirement.

To summarize, close relationships were found between

the through-thickness density profile and mechanical properties of particleboard. IB was found to have a linear relationship to core density while MOE and MOR were found to be related to surface density, surface-to-core density gradient, and other factors.

Density Profile Measurement and Predicting Methods

There are several techniques to measure the through-thickness density profile of particleboard. These are normally divided into two major groups: (1) direct measurement methods and (2) indirect measurement methods.

Direct Measurements

The gravimetric method is the oldest technique for measuring the density profile of particleboard. Stevens (1977) used an apparatus to incrementally cut slices as thin as 0.25 mm parallel to the face of a sample. Each slice was then weighted and the thickness measured with a micrometer. The density of each slice was calculated by simply dividing its weight by its volume. The results of this test were accurate to within ±11%. However, there are several obvious problems with this technique, surface roughness influenced thickness measurements and particle tear-outs caused errors in weight measurements. Both

problems contributed to the large variances observed. Stevens (1978) suggested that the errors could be reduced to acceptable levels by increasing the slice thickness and averaging the test results.

Indirect measurements

The earliest study to indirectly measure density profiles used radiography. Nearn and Bassett (1967) transmitted an X-ray beam parallel to the face of the board and recorded the radiation passing through the board onto photographic film. On a positive X-ray print, areas of high density in the board resulted in dark regions on the films while the light areas represented low densities. Steiner et al. (1978) used a similar method in applying X-ray densitometry to measure the density profile of waferboard. The calibration was done by scanning various thicknesses of a waferboard with a known density. X-ray exposures were recorded on photographic film. The results were used to identify the relationship of density to IB.

Laufenberg (1986) investigated a gamma radiation-based density gradient measurement system similar to the X-ray technique used by Nearn and Bassett. Gamma-ray attenuation was measured using a scintillation detector rather than a piece of photographic film. Sample densities were calculated by using assumed mass attenuation coefficients

for wood-based composites. Laufenberg's results showed:(1) small measurement error due to the random nature of radiation impinging on specimen, (2) low sensitivity to the resin content and wood species, (3) large error in predicted density caused by moisture within the sample, and (4) inability to measure density of the sample's edge layers as the result of the gamma-ray beam width.

Another procedure was developed by Paulitsch and Mehlhorn (1973) to evaluate the density profile by measuring the moment of inertia of thin layers sliced from particleboards. They investigated the calibration curve between the moments of inertia and the layer densities for certain particleboards. Using this technique, the density profile can be measured with high resolution (as thin as 0.2 mm).

The limitations of a traditional direct measurement technique for density are that it destroys the material and is time consuming. The shortcoming of the indirect measurement techniques is that they cannot be used on the production line and as a real-time quality control tool because they require cutting samples to be scanned.

Mathematical Prediction Model

To obtain a nondestructive determination of the density profile, a group of scientists at the Mississippi Forests

Products Utilization Lab (Harless et al., 1987) researched computer simulation models to predict the density profile of particleboard. The characteristics of the hot pressing proces in terms of rate of closure, press temperature, initial mat temperature, and other parameters were used as model inputs. The model simulated the hot press process by analyzing heat conduction and gas transport. This study provided some knowledge of how the manufacturing process affected the density profile. No comparison between the model-predicted and real density profile was presented. How well this model agreed with the actual situation is unknown.

Another mathematical model was generated by Hänsel, Niemz and Brade (1988). Density was considered as a function of chip moisture content, compression time, density of wood species, and other process factors. The influence of different factors on the density profile was determined by changing one variable while holding all the others constant. Good agreement was found between calculated and experimentally determined density profiles with a mean coefficient of determination of 0.70.

X-ray absorption

In 1895, Wilhelm Konrad Roentgen excited the world with the discovery of X-rays which is currently one of principal

radiation sources for computed tomography. X-rays are identical to visible light in all respects except in wavelength. X-rays have a wavelength in the range 0.06Å to 10Å. Both have the fundamental characteristics of electromagnetic waves. When X-rays pass through matter, some of the radiation is absorbed by it. As the result, the intensity of the X-ray beam decreases. The attenuation of X-rays follows the exponential equation (Beer's law):

$$I = I_0 e^{-(\rho \mu_m d)} \quad (1)$$

where I_0 denotes the initial intensity of radiation; I is the attenuated intensity after the X-rays pass through an object with a thickness of d, and density of ρ; e is the base of natural logarithms; and μ_m is a proportionality factor defined as the mass attenuation coefficient (Kaelble, 1967). The mass attenuation coefficient is dependent upon the wavelength of the X-ray beam and the elements constituting the material, but is independent of the chemical or physical state of the elements.

Variable moisture content (MC) throughout the material will change the relative proportions of materials and moisture, which changes the mass attenuation coefficient of the bulk material. Loos (1961) investigated relationships between gamma-ray absorption coefficients and moisture content. The results indicated that the linear absorption coefficient ($\rho \mu_m$) changed proportionally to the percent

moisture content. Laufenberg (1986) pointed out, however, that if the equilibrium moisture content was less than twelve percent (oven-dry basis), the effects of MC on absorption coefficient could be ignored when working with particleboard.

Hoag (1988) identified attenuation coefficients for Douglas-fir at several X-ray energy levels. He used a cellulose acetate calibration wedge having the same chemical composition as natural wood. The results showed that mass attenuation coefficients were quite different at different energy levels. Therefore, the mass attenuation coefficient is energy dependent.

Another thing that should be pointed out is the amount of energy absorbed by air. From the data given by the National Bureau of Standards (Kaelble, 1967), the air-absorption correction factor was a function of the distance the beam travels through the air and of the X-ray energy level. If the voltage is 20.0 Kv and the distance through air is less than 10.0 cm, the correction factor is above 0.96 (Kaelble, 1967). Less than a 5% loss occurs due to air absorption before the X-rays reach the scanning sample. Therefore, absorption of X-rays in the air is quite small and normally can be ignored when working with typical X-ray systems.

Development of Tomography

X-ray computerized tomography (CT) is a radiological imaging technique which provides extraordinary accuracy and internal structural images of an object. The technique is based on the cross-sectional image generated by CT scanners. X-ray computerized tomography was originally developed for medical applications which require low dosage and high speed. This technique refers to multiple scanning of an object and to collecting a large number of radiation intensity measurements. With the aid of a computer, the internal structure of the scanned material is then reconstructed.

Since its introduction by Hounsfield in 1972, computerized tomography has undergone considerable development. Physically, computerized tomography consists of one or more X-ray sources and detectors which are used to scan an object. Early scanners sent a single narrow parallel beam of X-rays through the object, and the attenuated X-ray beam was received by a precisely aligned detector. Advantages of this method are in its simplicity and flexibility. Later scanners combined a fan-shape X-ray beam source with a circular array of detectors, thus removing any equipment motion during data collection. With such a system, the entire imaging process can be completed in seconds and attenuation differences as small as 0.1% can

be measured accurately within an interior region of 2 mm^2 or less (Wellington, 1987).

Parallel to the rapid development in scanning hardware, developments in the mathematics of reconstruction theory have resulted in a reduction in computation time. Reconstruction techniques can be largely classified into two distinct groups: (1) the convolution and back projection, and (2) iterative methods. Each has its own advantages and disadvantages which will be described later (Webb, 1987).

Many of the applications of CT are in the field of diagnostic medicine where this technique's high resolution and low X-ray exposures are advantageous. Grauer et al. (1984) published the results of their study on body fat distribution and demonstrated that computerized tomography "can be done quickly (average 15 minutes), at low cost (less than $100), and with only minimal hazard (radiation exposure less than one rad)." Recently, computerized tomography (CT) has been validated as a reliable diagnostic tool (Enzi, 1986).

Computed tomography systems designed for industrial applications can be used on objects with a wide range of sizes and have higher sensitivity than medical systems to accommodate objects with widely varying characteristics. CT has been widely applied in petrophysics (Vinegar, 1986), aerospace and other industrial engineering fields providing

nondestructive inspection of the internal structure and composition of materials. Instruments have been developed which can image objects such as rocket motors. Systems providing very high resolution (15μm) have also been developed (Sato,1984). The application of CT has changed from primarily detecting, locating and sizing an object to measuring the absolute density, calculating quantitative accept/reject criteria, and providing information for engineering design analyses. CT can provide information on the geometry and internal characteristics of logs, making more accurate sawing decisions possible.

Principles of Computerized Tomography

Computerized tomography is a mathematical reconstruction technique which generates a computer image from data collected as radiation transmits through an object. The basic apparatus of CT is shown in Figure 2. It consists of a radiation source, such as X-ray, located on one side of an object and detector on the opposite side of the object. The collimated radiation passes through the object in a thin column and is measured by the detector. A thin ray of radiation is emitted from the source with an initial intensity I_0; the radiation is partially absorbed by the material being scanned, and the remainder is transmitted to the detector with intensity I. The

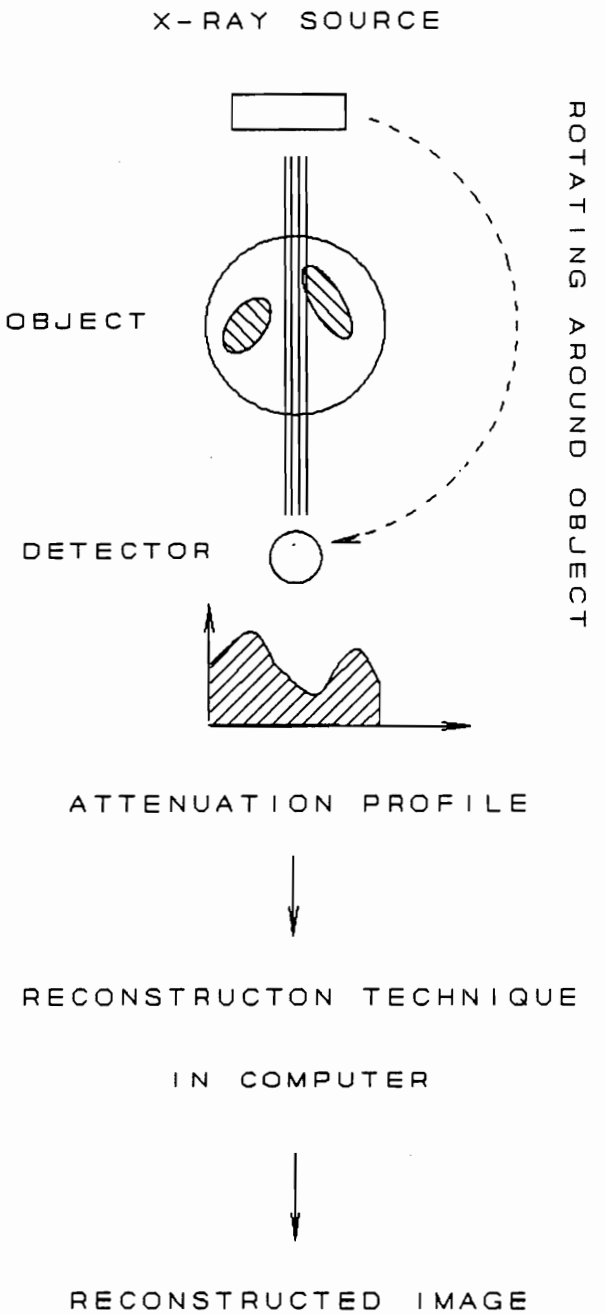

Figure 2. - Principle of Computed Tomography

relationship between initial intensity and attenuated intensity follows Beer's Law (Kaelble, 1967). When the object is a succession of layers of thickness d_i, the total attenuation is the sum of attenuation through each layer:

$$I = I_0 e^{-\sum_{i=1}^{n} \mu_i d_i} \qquad (2)$$

where: I = attenuated intensity, (intensity remaining after passing through object).

I_0 = initial intensity.

μ_i = attenuation coefficient.

d_i = thickness of layer.

n = number of layers.

The attenuation coefficient in a layer is proportional to its density. Data is collected by repeatedly rotating the scanned object slightly, and collecting a new intensity measurement. Rotating the object a total of at least 180 degrees produces a measurement projection with full spatial coverage. With the aid of a computer, a cross-sectional digitized image is generated by computing the value of the attenuation coefficients. This provides a highly accurate view of a slice of the object. Stacking the cross sections produces a three-dimensional image of the object. Theoretically, a reconstruction algorithm is simply a set

of calculations for combining a series of measurements to produce attenuation values. The mathematical procedures needed to fulfill this task are not simple. One equation is obtained for each measurement taken resulting in a huge system of linear equations to be solved. Mathematical problems such as incomplete data stimulate many mathematicians to devote their time to this topic. If it were not for the practical problems related to data generation and collection, the CT equations could be solved explicitly since there is enough data from the projections to reconstruct the internal image.

There are several reconstruction methods: (1) filtered back-projection algorithm, (2) algebraic reconstruction technique, (3) Fourier algorithm, and others (Natterer, 1986). The back projection algorithm is the simplest and oldest procedure. Acting like a filter, the algorithm reconstructs the image by filtering selected points from back-projecting measurements. If different transmissions pass through the same point as the X-ray source and the detector rotates about the object, it becomes a unique, distinguishable point. This technique proves very successful in minimizing noise in the reconstructed image. This principle is the basis for all the other methods developed later.

The algebraic reconstruction technique (ART), also called the iterative method, actually forms a large family

of reconstruction algorithms. All ART methods use iterative solutions to solve the linear system; they differ from each other by using different estimate functions. This method is more appropriate when data sets are incomplete or have errors. The main drawback is its computational cost, which makes it infeasible for large dimension images.

The Fourier transform plays a preponderant role in studies on the use of parallel beam X-ray reconstruction techniques because of its translation invariance. The major advantage of this method is that it requires a relatively small amount of computer storage and shorter computation time than other methods.

The most popular method in CT image generation is the convolution method for divergent X-ray beams. This method combines the Fourier and back-projection techniques. It is a natural extension of the back-projection method in that it uses a Fourier-transform function to transform measurements forming a filter before performing back-projections. This method is fast and yields excellent results (Webb et al., 1987).

Applications of CT in Forest Products

In recent years X-ray computerized tomography has been used to detect the internal structures of logs. Taylor et

al. (1984) investigated locating knots by industrial tomography. The logs, which were freshly cut from trees and kept green, were scanned by a tomographic scanning system to produce black and white photographs. Log perimeter and knot detection were based on grey levels corresponding to the various wood densities. The results of the study showed favorable identification of knots and their locations. The authors indicated that even better identifications could be achieved if the photographs used in this study were replaced by the raw data representing the tomogram. They also suggested that computed tomography was a reliable technique providing automatic image analysis of freshly sawn logs to assist in sawing decision.

A group of Japanese scientists (Onoe et al. 1985), developed portable CT scanners which could be transported for testing live trees, standing columns of an old temple, and utility poles. They used a collimated X-ray beam plus a filtered back projection algorithm. In addition to the annual rings shown by reconstruction, a good correlation was observed between the X-ray profile and the moisture content profile. This data was then used to detect heartwood decay in utility poles. Additionally, different X-ray absorption coefficients were measured with various tree species.

Funt and Bryant (1987) suggested the feasibility of using automatic interpretation of computer tomography

images to detect internal logs defects. They used a Siemens Somatom DR2 scanner and an International Imaging Systems image processor to collect and interpret the data. Three classes of features were used in computer algorithms: (1) lightness or darkness of a region, (2) the shape of a region of a particular brightness, and (3) brightness textures or patterns. The boundary between various density regions was determined by calculating the second and third derivatives of a frequency-intensity histogram. The high density region represented knots, while low density and rough texture areas represented rotten wood. Finally, the interpreted CT image was represented by a false color photograph. The results matched the actual log very well. Even though the speed of the computer program was not fast enough to permit operation in a sawmill, there is no doubt that the future use of CT scan systems in the mill has the potential to increase both the quantity and quality of yield by detecting the internal characteristics of logs. A major problem shown by this study was the impact of moisture content on the image. The effect was so dramatic that it was difficult to uniquely identify knots or other defects.

Applications of computerized tomography in forest products industry are becoming more possible, but is, at present, limited to the research laboratory. There are some ongoing research efforts to develop processing systems

which could operate in the mill (McMillin 1982).

MATERIALS AND PROCEDURES

Methodology

As a careful review of the literature revealed, X-ray computerized tomography (CT) is the technique that is being widely used with substantial success in research and industry to nondestructively determine the internal properties of materials. Therefore, CT is deemed to be the most appropriate for predicting the through-thickness density profile through the thickness of particleboard without cutting the panel.

However, it is quite difficult to obtain a complete data set because of the limitations of scanning the entire particleboard panel from all directions. Using only limited data, as in this study, sufficient prediction of density profiles cannot be achieved. As a result, the CT technique is applied to predict density profiles using a different approach rather than is conventionally done. This method can reconstruct data by using theoretical mathematical models and making some assumptions. The procedure is shown in Figure 3.

The intensity of X-rays after attenuation through the object depends on the source intensity, linear attenuation coefficient and thickness of absorbing materials.

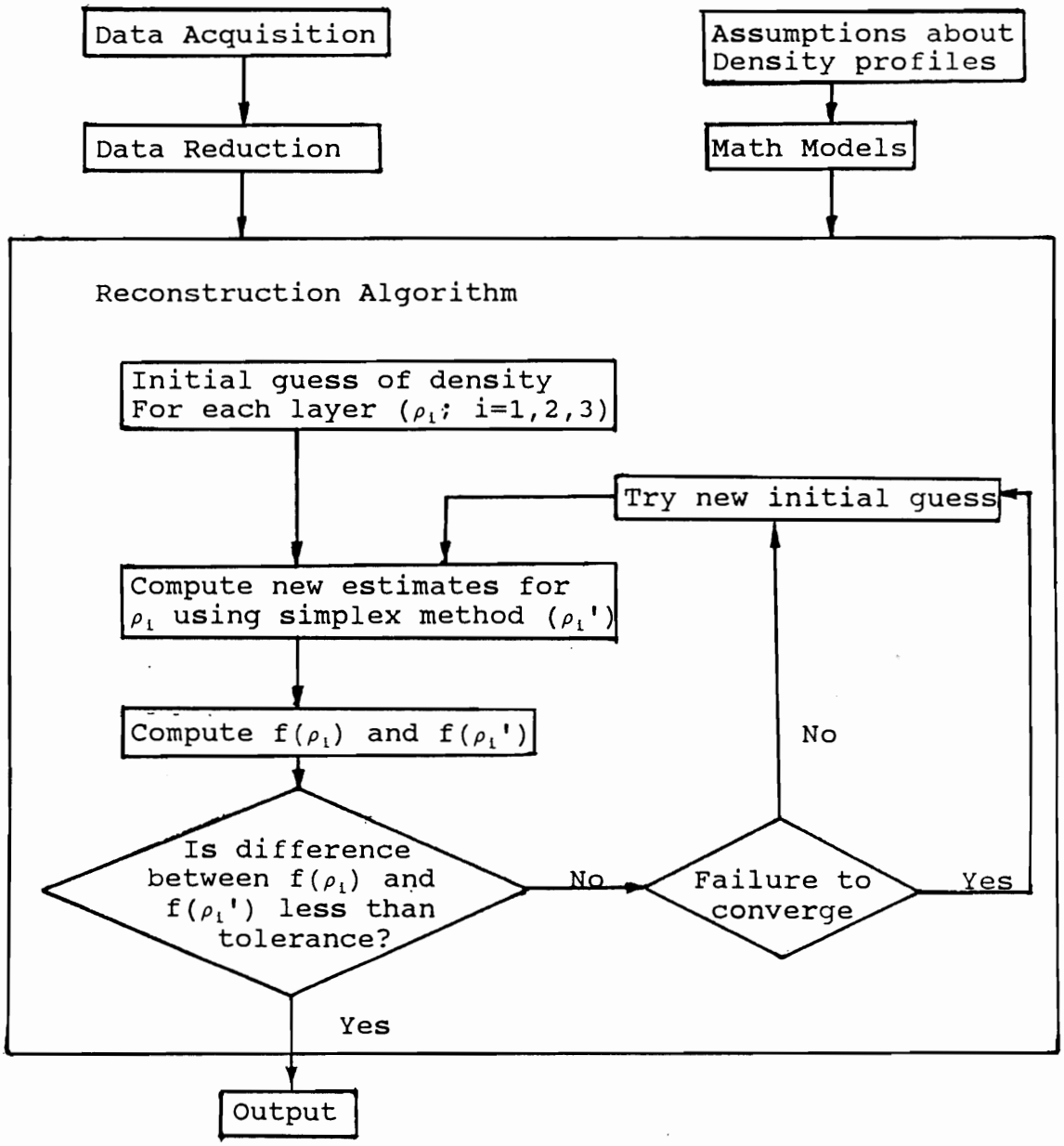

Figure 3. - Flow diagram of the procedure.

Furthermore, linear attenuation coefficients are related to mass attenuation coefficients. The relationship among these leads to the expression:

$$I = I_0 \, e^{-\sum_{i=1}^{n}(\rho_i \mu_m d_i)} \tag{3}$$

where: I = attenuated intensity

I_0 = source intensity

μ_m = mass attenuation coefficient

ρ_i = density of object

d_i = thickness of layers

n = number of layers.

Taking the natural logarithm of both sides gives:

$$\ln(I_0) - \ln(I) = \sum_{i=1}^{n} (\rho_i \mu_m d_i) \tag{4}$$

As a result, it is possible to reconstruct the CT density image by using attenuation profiles of the object to be imaged and knowing a mass attenuation coefficient which can be obtained theoretically or experimentally.

Predicting through-thickness density profiles depends on solving a set of simultaneous equations (4). Two simplified mathematical models and a minimization computer program are used in this study.

X-ray computed tomography density prediction amounts to the following processes. The first step involves generating attenuation profiles using the X-ray scans. The

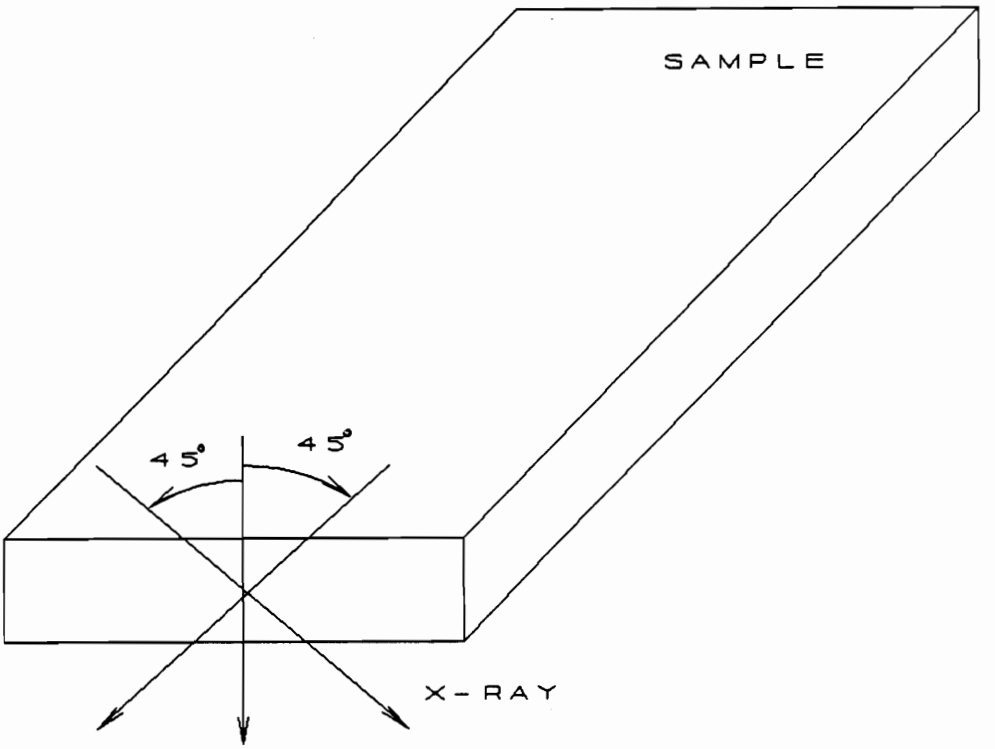

Figure 4. - Illustration of X-ray scanning directions

object to be scanned is laid on a specially designed holder which is positioned on a sliding translation table between the X-ray source and detector. A calibration material of known thickness and attenuation coefficient is placed on the table directly before the sample in each scan in order to determine I_0 in equation (4). Collimated X-rays are transmitted through the sample in three different directions. In one scan, X-rays are transmitted through

the specimen perpendicular to its face. In the other two scans, the sample is rotated and scanned at a 45 degree angle to the surface (as shown in Fig.4). A computer drives a stepper motor, which moves the translation table incrementally at a pre-selected rate. Before the data are collected, the translation table is stopped for a period of time to allow the X-ray sensor to come to equilibrium. This process is repeated again and again until the whole sample has been scanned. In the second step of the process, the data are sent to another computer for further reduction. Then the theoretical model predictions are computed by applying pre-selected mathematical models to fit the data. Finally, comparisons are made between the predicted and actual density profiles.

Materials

The test materials consisted of manufactured particleboard (122 cm x 244 cm sheets) having three different unsanded thicknesses of 14.3 mm, 17.7 mm, and 21.0 mm. These are all commercial panels of industrial grade and bonded with urea-formaldehyde adhesive. The average board density is 0.75 g/cm^3.

Samples 2.54-cm and 3.81-cm wide and 121.9-cm long were cut from these boards from an edge of the panel's cross machinery orientation. Three specimens 10.16 cm in length

were cut from these strips at 40.64 cm intervals. The samples were tested at room temperature and humidity without any pretreatment.

Equipment

The equipment for this study consists of an X-ray source, a detector, a sliding translation table, and computer. A Kevex X-ray tube with a tungsten target provides an X-ray source that produces a polychromatic energy spectrum. The X-ray energy level, which is fixed for this study, is 25.3 kilovolts and 2.0 milliamperes. The detector is a Victoreen 500 cesium iodide, photo-diode scintillation sensor which uses cesium iodide crystals to absorb the X-ray energy. The X-ray energy is converted to light, then to an electrical signal in a solid state detector in which the Victoreen 500 electrometer is used as a picoammeter. A slit-type, 0.1 mm x 1.0 mm aperture mounted in the sensor is the primary collimating element of the system. A translation table is driven by a stepper motor with a speed of 0.0053 mm per step. A Hewlett Packard Vectra computer is connected to the data translation system for data collection; data are stored on floppy disks for later processing.

System Evaluation and Quality Assurance

Since the accuracy of CT prediction is entirely dependent on the types of sampling and reconstruction processes, it is very important that some systematic evaluation be done before actual testing. The sampling process depends on X-ray beam width, sampling rate and X-ray energy level, etc. Since attenuation is dependent on the energy of the X-ray beam, all evaluation work has been completed using a fixed energy level which will also be used for actual testing. There was no comparison among different operational levels for this system nor between this and other X-ray systems.

The evaluation of scanner performance consists of noise determination, sensitometry measurement, and sensitivity profile investigations.

Noise determination

Noise, as used here, refers to a variation in the CT predicted values that are not related to the actual attenuation variation in the material. The noise includes the fundamental variation due to the quantum nature of radiation and system variation due to scanner system irregularities. The former may be different for the same object on different scans because of the random variation in photon flux and is impossible to control. However, the

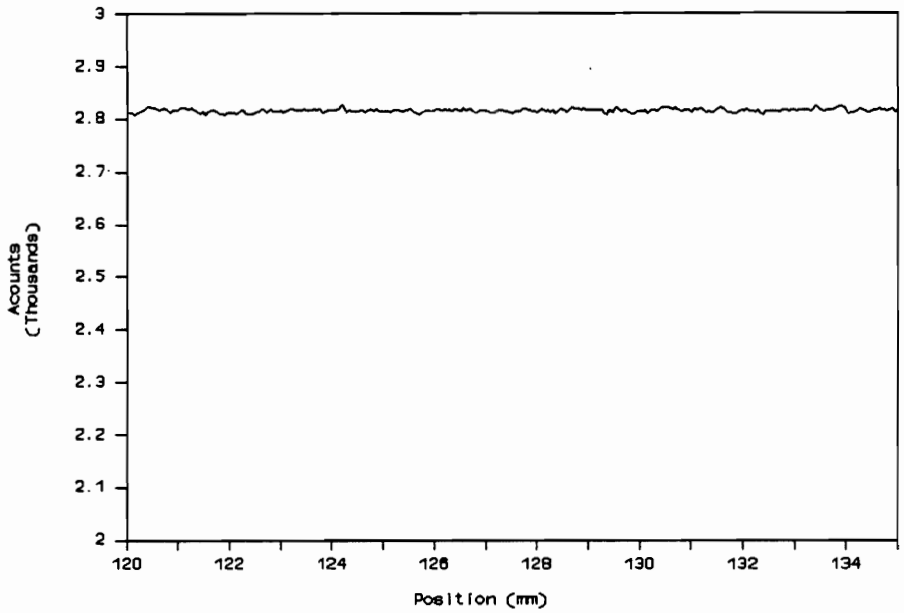

Figure 5. - Noisy profile obtained in homogeneous material scanning. Sampling increment: 0.053 mm/step, sampling rate: four points/second.

latter should be relatively small if the system is operating properly.

The noise characteristics of this system are determined by scanning a uniform cellulose acetate slab. Figure 5 clearly illustrates the random noise throughout one scan.

Figure 6 is the noise histogram showing the frequency of observed intensity. The distribution of noise is approximately normal (with skewness = 0.1001 and kurtosis = -0.0104). Most values are very close to the mean value of 2815.08 counts with only a small standard deviation (3.22

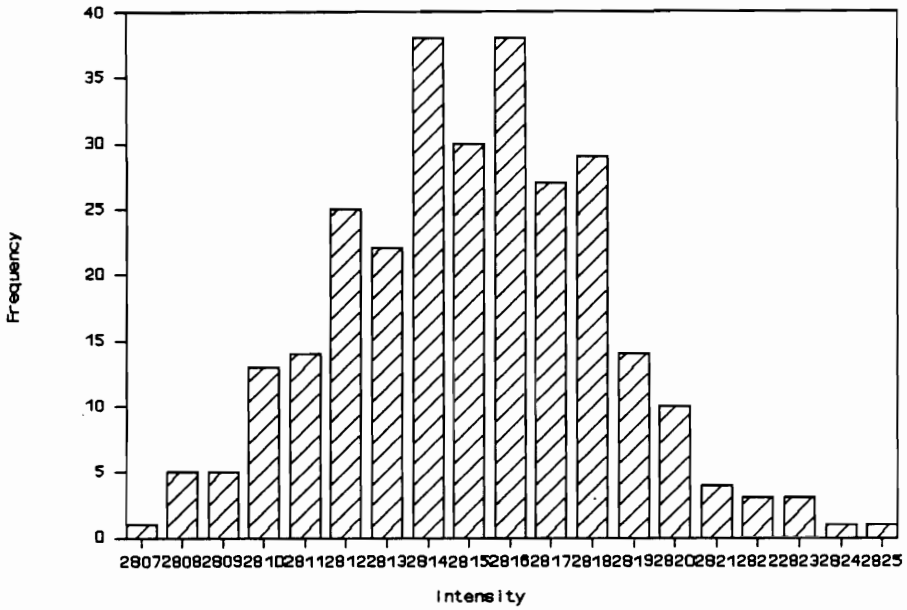

Figure 6. - Histogram of noise during an X-ray scan of the homogeneous material.

counts). There is 95 percent confidence that the true mean value will be in the interval between 2814.70 counts and 2815.46 counts. Since the noise standard deviation is only 3.22 counts, it is regarded as insignificant. Table 1 summarizes statistics of noise for this system. Complete data are included in Appendix A.

Sensitometry

Sensitometry in computed tomography is the determination of the relationship between attenuation

Table 1 - Summarized statistics for noise determination

Sample size	283
Average Intensity	2815.08 (counts*)
Variance	10.40 (counts)
Standard Deviation	3.22 (counts)
Maximum Intensity	2825 (counts)
Minimum Intensity	2807 (counts)
Intensity Range	18 (counts)
Skewness	0.1001
Kurtosis	-0.0104
Confidence Interval for mean (95%)	2814.70 (counts), 2815.46 (counts)

* intensity of the X-ray energy as measured at the computer

Table 2 - Data set for sensitometry

Number of Layers	Intensity	CT Numbers
1	3596.20	0.079688
2	3416.85	0.130846
3	3252.10	0.180264
4	3095.95	0.229470
5	2945.90	0.279151
6	2810.95	0.326043
7	2679.10	0.374085
8	2550.15	0.423414
9	2481.15	0.450843
10	2411.80	0.479192

intensity ratios (I_0/I) and linear attenuation coefficients (μ). Ideally, this relationship should be linear, but is generally non-linear because of a non-linear relationship between the detector readings and the X-ray intensity. Errors brought by such non-linearity might be avoided by correcting actual readings to the expected readings.

A stair-shaped wedge which provided incremental

thicknesses change from 0.51 mm to 5.10 mm was scanned under fixed operational conditions (25.3 KV and 2.0 mA). The effect of the thickness change was used to obtain varying average attenuation. The test results are presented in Table 2, where CT numbers are logarithms of intensity ratios ($\ln(I_0/I)$) and number of layers represents thickness. The relationship of thickness to CT numbers is

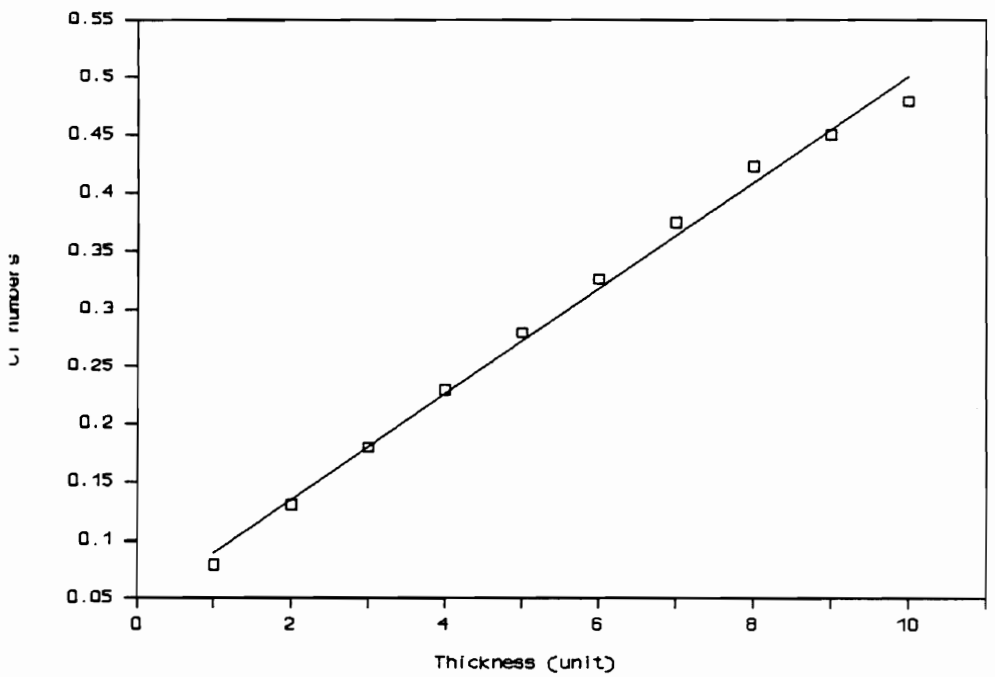

Figure 7. - Sensitometry plot, with a regression line.

plotted in Figure 7. A very high correlation is found between the CT numbers and thickness of object ($R^2 = 0.994$); the standard error of estimate is 0.011 counts. The linear

regression line shows the great consistency of sensitivity for this system.

Sensitivity Profile

A sensitivity profile provides information about effective width which then determines the spatial resolution of a scanner. A narrower X-ray beam will produce finer resolution. For example, if a material which is opaque to X-ray is moved across the beam, the distance on which the intensity drops from the initial intensity to zero is proportional to the width of the beam. However, there is no such thing as a perfect X-ray system in practice. A sensitivity profile of this system was obtained by a simplified measurement. A metal strip, with a width of 9.66 mm, was scanned and a plot of CT values across the strip was produced (Figure 8). The profile is typically an upside-down bell-shaped curve in which intensity falls smoothly from the initial intensity to zero in the center of the slice width. The effective width is defined to be the width between the fifty percent sensitivity points on the sensitivity profile, or 0.26 mm for this system. The resolution, which is the ability of the system to discriminate between closely spaced details in the object, is twice the effective width and not less than 0.52 mm under these operational conditions.

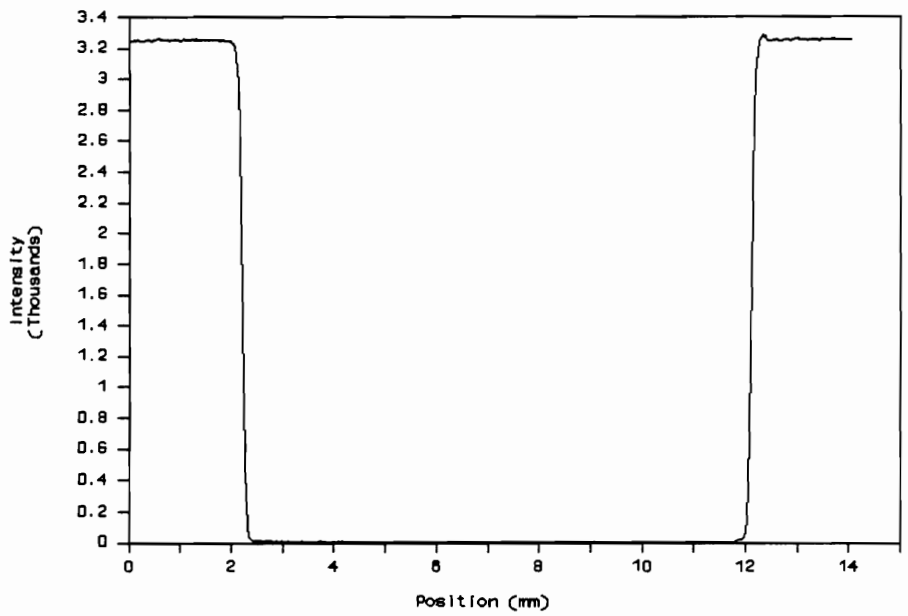

Figure 8. - The sensitivity profile of a metal strip. Width: 9.66 mm; the maximum intensity: 3252.9; effective width: 0.26 mm; energy level: 25.3 kV, 2.0 mA; sampling interval: one second.

Scale Calibration

Scale calibration, which refers to calculation of attenuation coefficients, is very important because it is used to interpret the CT numbers. The attenuation coefficient was determined empirically in this study. A two-step wedge of cellulose acetate, which has similar chemical composition to wood, was used as a calibration material. In general, the attenuation coefficient is a function of X-ray energy. Thus, the operational level used

here (25.3 kV, 2.0 mA) is the same as that which is utilized for later scanning. Table 3 demonstrates the data and calculation results.

The formula used for calculation is:

$$\mu_m = \frac{\ln(I_1)-\ln(I_2)}{\rho d} = 0.755 \ (cm^2/g)$$

where: μ_m = mass attenuation coefficient

I = X-ray intensity

d = thickness of sample

ρ = density of sample.

Table 3 - Attenuation coefficient calculation

Acetate* Layers**	Intensity***	Standard Deviation
1	2811.5	2.37
2	2025.9	4.35

* Density of acetate = 1.35 g/cm^3
** Layer thickness = 3.24 mm
*** Intensities are averages of 25 observations

Data Acquisition and Reduction

ASYST^R software is used as the data acquisition program; it includes several subroutines to handle the sampling and control processes. While one routine drives the specimen carriage, another one collects the X-ray

intensity for that location. The process is repeated until the entire sample has been scanned. After scanning is completed, the intensity data are saved in an ASYST, 16 bit, unsigned binary integer data file which is then transferred to floppy diskettes.

As a sample is being scanned, the translation table is moved in 0.0053 mm steps. A measurement of X-ray intensity is collected after every tenth step or every 0.053 mm. Intensity data are acquired at intervals of 250 ms, or four points per second. The raw data are then extracted by averaging five points together. The purpose of applying this sample-average technique is to eliminate signal noise. The reduced data are stored on hard disk for further model prediction.

Reconstruction Algorithm

The reconstruction algorithm which was used in this study is an approximation method. There are two different classes of methods for the solution of simultaneous linear equations: (1) the direct calculation, and (2) the iterative method. Direct methods solve the simultaneous equations directly. These methods require complete formulations to solve the equations. In other words, the number of equations must be equal to or greater than the number of unknowns. The iterative method can be used to

solve problems in which some formulations may be absent. Therefore, the iterative method is used here to solve a set of simultaneous linear equations which were obtained from the X-ray scans.

Equation (4) can be written in generalized form as following:

$$\sum_{i=1}^{n}\sum_{j=1}^{n} a_{ij}X_{ij} = J_k, \qquad k = 1, 2, \ldots, n \tag{5}$$

where:

X_{ij}: unknown density

a_{ij}: known constant related to attenuation coefficient and thickness

J_k: known constant proportional to the X-ray intensity.

Or, on rearranging:

$$\sum_{i=1}^{n}\sum_{j=1}^{n} a_{ij}X_{ij} - J_k = 0, \tag{6}$$

There are several ways to solve these equations. The method used here is to change the problem into one of finding the best-fit solution which minimizes the square of the difference between $\Sigma\, a_{ij}X_{ij}$ and J_k. This is called nonlinear least-squares approximation. This means that one aims to find values of X_{ij} which give the minimun of

$$f(X_{11}, \ldots, X_{nn}) = \sum_{i=1}^{n}\sum_{j=1}^{n}\sum_{k=1}^{n} (a_{ij}X_{ij} - J_k)^2 \tag{7}$$

Since there is more information about some unknown variables, the weight function is used to allow some control over the approximating function by emphasizing the square error over such sections. That is:

$$\sum_{i=1}^{n}\sum_{j=1}^{n} (a_{ij}X_{ij} - J_k)^2 w(k) = 0, \tag{8}$$

where w(k) is the weighting function.

The simplex method (Jacoby, 1972) is used here for finding a minimum of $f(X_{ij})$ whenever equation (8) is satisfied. This method requires that the function be continuous but does not require derivatives of functions. This is a direct search method based on the comparison of the objective function values of a general simplex.

First of all, an initial estimate of X_{ij} is given:

$$\mathbf{P}_0 = (p_1, p_2, \ldots, p_n), \tag{9}$$

Given a characteristic length scale (l_i), an initial simplex is obtained in the following way:

$$\mathbf{P}^i = \mathbf{P}_0 + l_i\mathbf{e}_i, \tag{10}$$

where $\mathbf{e}_i$ is a unit vector. Then a simplex has the following structure producing a vertices span:

$$\mathbf{P}^0 = (p_1, p_2, \ldots, p_n), \tag{11}$$

$$\mathbf{P}^1 = (p_1 + l_1, p_2, \ldots, p_n), \tag{12}$$

.....

$$\mathbf{P}^n = (p_1, p_2, \ldots, p_n + l_n). \tag{13}$$

The simplex method starts with this vertices span.

Secondly, the function of these vertices are computed. Let Y^h be the Pi corresponding to the highest value of the function, Y^m to the second highest value, and Y^l to the lowest value.

Thirdly, let Y^c be a center point of all P_i except for i = h:

$$Y^c = \frac{1}{n} \sum_{\substack{i=0 \\ i \neq h}}^{n} P^i. \qquad (14)$$

Then move the next estimate point either (Figure 9):

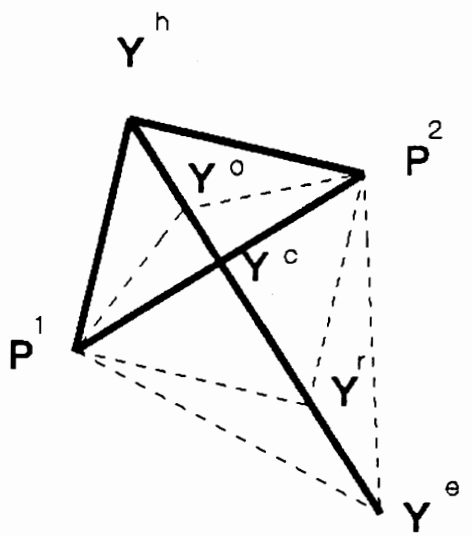

Figure 9. - The reflection, expansion, and contraction operations in the simplex method (Jacoby, 1972)

(a) reflection away from the high point:

$$Y^r = -\alpha Y^h + (1+\alpha) Y^c \qquad (\alpha>0) \qquad (15)$$

(b) reflection and expansion from the high point:

$$\mathbf{Y}^e = \gamma\mathbf{Y}^r + (1-\gamma)\mathbf{Y}^c \qquad (\gamma>1) \qquad (16)$$

(c) contraction along all directions toward the low point:

$$\mathbf{Y}^o = \beta\mathbf{Y}^h + (1-\beta)\mathbf{Y}^c \qquad (0<\beta<1) \qquad (17)$$

The values of coefficients a, b, and c are: a=1, b=0.5, c=2.

Fourthly, replace $\mathbf{Y}^h$ by the highest value of these three tries.

Finally, the standard deviation of the function is calculated and compared with termination criteria to make the decision of when to stop. The equation is defined by:

$$\sqrt{\sum_{I=0}^{m} \frac{(f(Y^h)-f(Y^o))^2}{m}} \leq t \qquad (t>0) \qquad (18)$$

where: t is a preselected tolerance.

In the iterative method, it is necessary to establish the conditions for convergence. A sequence of successive approximations to the solutions is produced from a given set of initial values. Hence, it might not be possible to predict the number of arithmetic operations that would be involved. The process depends on the accuracy required and on how good the initial approximation is. Furthermore, in producing a computer program which implements a numerical method, attention must be paid to its efficiency which depends on time and storage constraints.

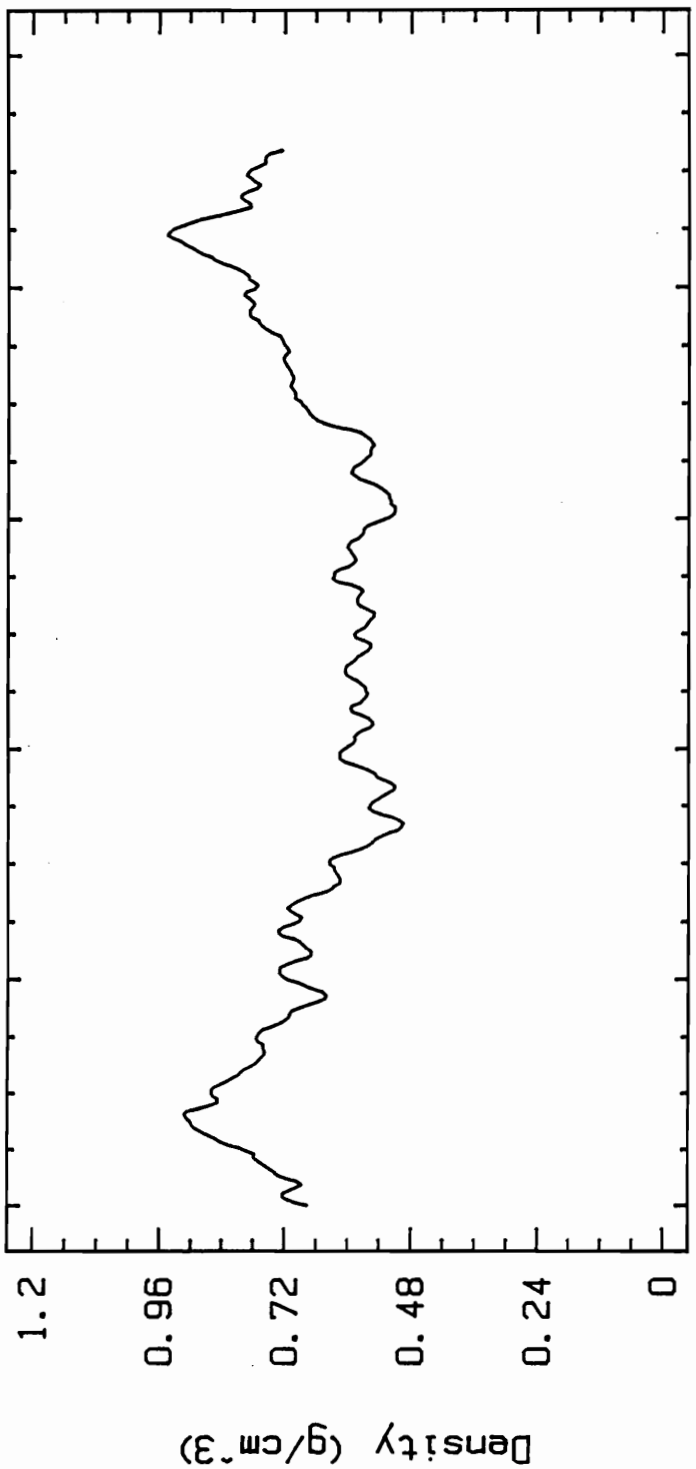

Figure 10. - An example of density profile (sample 20). Sampling interval: one second, sampling increment: 0.027 mm/step.

Selection of Math Models

Figure 10 depicts a typical through-thickness density profile of particleboard using X-ray densitometry, which is obtained by directing X-ray beam parallel to surface of the sample. This graph shows very clearly the density change through the thickness. From a relative low value near the surface the density rises rapidly to a maximum value within two millimeters of the surface, then declines to a minimum in the central core of the board. There is less variability in density within the core portion.

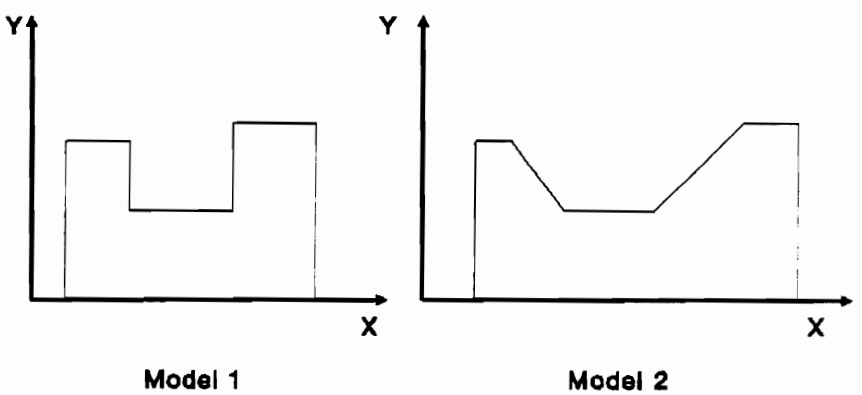

Figure 11. - Two mathematical models.

Two simplified mathematical models are proposed here (Figure 11). Model-1 is stair-step shaped with the abrupt changes in density occurring between the core and face layers. Model-2 has zones of linearly changing density between the core and face layers. For both models, the thicknesses of the layers are pre-selected according to knowledge of actual density profiles of the panels. This is based on a review of 144 known density profiles from twelve boards. The board-average density was used to divide the boards into layers. In other words, a layer with a density higher than the average density is called face material while lower than average density is called core material. In model-2, each intermediate zone between core and face layer is chosen to account for twenty percent of board thickness. The average overall ratios of face to core thickness were used in model prediction.

For this study, the weighting function (w(k)) in equation (8) was chosen to be:

$w(1) = w(3) = 1$, and $w(2) = 2$ for the two diagonal scans, and $k = 2$ for the perpendicular scan.

The following assumptions will be used in the prediction models:

(1) The sample is assumed to be divided into nine rectangular sections of three rows by three columns (Figure 12). Within each section, the density is uniform for both models except that there are

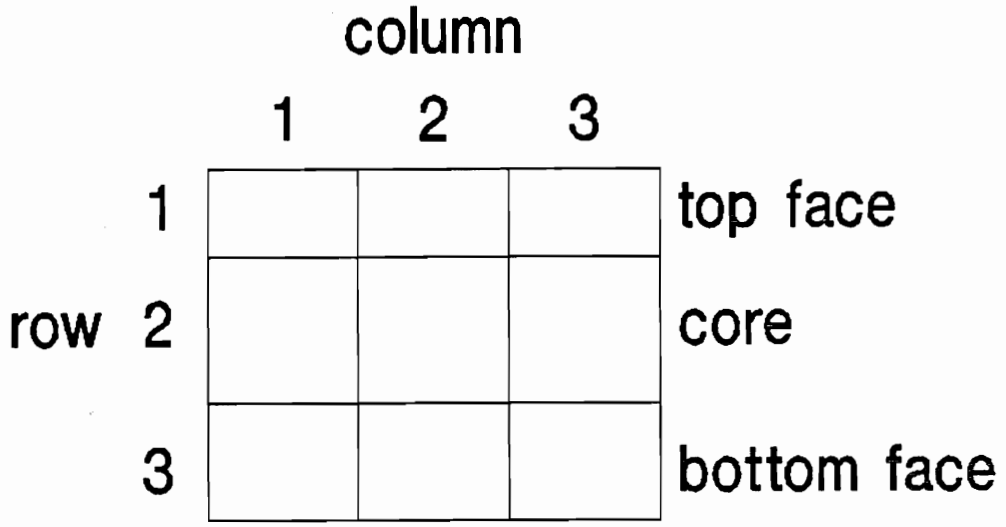

Figure 12. - Simplification of particleboard sample.

intermediate zones between sections for model-2. The three rows representing the top, core, and bottom layers of the sample have different thicknesses. The three columns are of equal width.

(2) The thicknesses of the three layers are assumed to be known and held fixed for a particular product.

(3) Beer's law (1) is assumed to hold for polychromatic

X-ray sources.

(4) This model consists of constraints which prevent negative and too big numbers in prediction. The constraints are: $0 < X_{ij} \leq$ specified number (chosen to be 2.0 in this study).

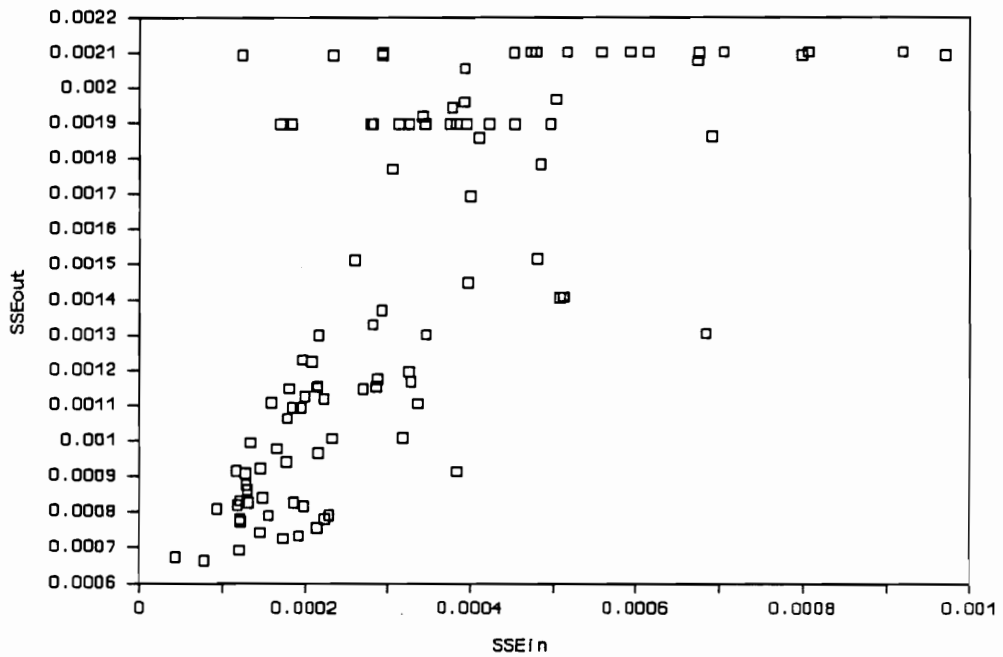

Figure 13. - The result of program testing. SSEin and SSEout represent sum squares of error in input and output data respectively.

Program Testing

A simple test was done to confirm that the program was working correctly. A set of random data was generated. It

was assumed that there were normally distributed (standard error = 0.018) "noise" in the three different density layers. Therefore, the attenuation profiles were affected by this "noise". Using these noisy data to predict the density profile would produce the difference between the "true" and predicted densities. The result of this test is shown in Figure 13.

RESULTS AND DISCUSSION

Theoretical Results and Analyses

Model predictions of density profiles were performed by using the computer program described previously. A two-degree polynomial function was used in regression analyses. Predicted density profiles generated by the computer program were compared to actual density profiles for the same samples. A summary of comparisons is shown in Table 4. A typical plot of actual density profile, first model prediction, and second model prediction is given in Figure 14; the rest of the results and comparisons are contained in Appendix B.

The accuracy of the prediction is quite satisfying. In particular, all second model predictions are better than first model predictions, which suggest that the second mathematical model provides better estimation than the first. Average standard error of estimation for the first and second model predictions are 0.0569 (g/cm^3) and 0.0424 (g/cm^3) respectively. However, the predicted densities are lower than actual densities for the most part. Based on these comparisons, it is unclear whether the error is due entirely to the X-ray attenuation data collection or to the model prediction process.

Table 4 - Summary of density profile predictions

SPECIMEN NUMBER	THICKNESS (mm)	MODEL 1 R^2	MODEL 1 STD*	MODEL 2 R^2	MODEL 2 STD*
1	14.18	0.769	0.0429	0.854	0.0340
2	14.16	0.768	0.0457	0.819	0.0403
3	14.18	0.690	0.0505	0.776	0.0429
4	14.23	0.715	0.0464	0.787	0.0401
5	14.28	0.698	0.0455	0.822	0.0350
6	14.27	0.720	0.0426	0.785	0.0374
7	14.27	0.757	0.0450	0.800	0.0408
8	14.31	0.762	0.0454	0.887	0.0313
9	14.43	0.677	0.0459	0.823	0.0340
10	14.50	0.732	0.0447	0.843	0.0342
11	14.50	0.749	0.0418	0.844	0.0329
12	14.60	0.695	0.0439	0.765	0.0386
13	16.53	0.651	0.0700	0.857	0.0464
14	16.64	0.727	0.0579	0.781	0.0518
15	16.80	0.666	0.0624	0.777	0.0510
16	16.78	0.607	0.0586	0.735	0.0481
17	18.18	0.686	0.0667	0.804	0.0527
18	18.26	0.749	0.0553	0.834	0.0449
19	18.30	0.718	0.0641	0.788	0.0556
20	18.36	0.677	0.0639	0.819	0.0478
21	18.12	0.763	0.0575	0.835	0.0479
22	18.16	0.704	0.0598	0.804	0.0487
23	18.09	0.537	0.0630	0.596	0.0588
24	18.03	0.594	0.0610	0.752	0.0477
25	20.81	0.652	0.0597	0.861	0.0377
26	20.76	0.780	0.0545	0.899	0.0371
27	20.85	0.704	0.0626	0.914	0.0337
28	20.91	0.715	0.0628	0.902	0.0368
29	20.86	0.681	0.0682	0.879	0.0419
30	20.81	0.619	0.0673	0.831	0.0449
31	20.79	0.664	0.0606	0.840	0.0419
32	20.83	0.478	0.0823	0.805	0.0503
33	21.04	0.696	0.0631	0.893	0.0373
34	21.13	0.724	0.0544	0.879	0.0360
35	21.25	0.684	0.0616	0.850	0.0424
36	21.38	0.588	0.0720	0.854	0.0428
Average		0.689	0.0569	0.822	0.0424

STD*: Standard error of Y estimation.

Large deviations from both of the models occurred in samples #12, #23, and #24. This is because all of these

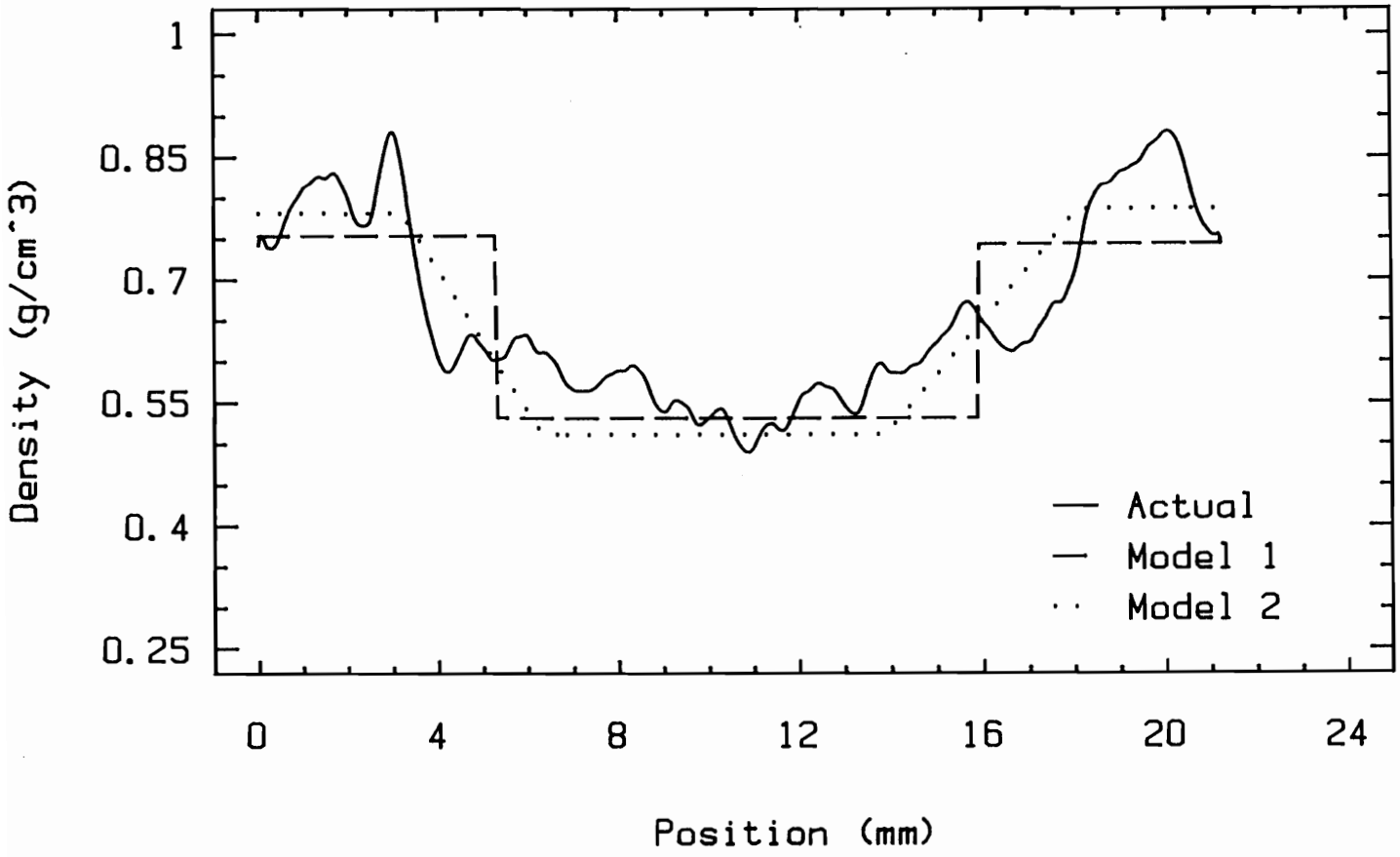

Figure 14. - Comparison of predicted density profile and actual density profile (sample 36).

samples were cut from edges of panels with relatively big thickness deviations. Since the average thickness of the samples was used in the prediction model, an error in thickness through a specimen would result in an error in density prediction.

Big estimate errors occurred in samples #32 and #36 for the first model but not for the second model. Since the same attenuation data were used in both model-1 and model-2 predictions, most of the error for these two samples might be due to the model prediction.

Termination Criterion

Termination criteria determine when the minimization procedure in the model stops. Choice of termination criteria depends on the accuracy of the solutions required. The smaller the value of the criterion, the longer the computation time. A big tolerance will produce premature minimization causing calculation to stop before reaching the real minimum point. On the other hand, the criterion value should never be smaller than the square root of the computer precision. In this study, a tolerance equal to the X-ray scanner's precision was chosen.

Initial Values

From a mathematical standpoint, the constants required in these models are unknown and arbitrary. However, random

choice of initial for these models might cause failure of minimization due to the nature of algorithm. It is possible that one might not find the true solution. Therefore, it is necessary to restart the minimization routine at a point where a minimum is expected. Restarts are easily accomplished by importing new starting values and then running the prediction program again. Further improvement could be made by adding a short subroutine in the program to automatically choose initial values for the constants.

Model Limitations

The implications of assumptions for the model should be considered. Model limitations depend on the knowledge about overall density distributions. How the sample is divided into layers results from this knowledge.

Another problem is the resolution of the predicted density profiles. The two mathematical models used in this study simplify particleboard into three layers of homogenous material resulting in a resolution which is quite low. However, this limitation can be overcome by using more layers than three layers. Applying the same methodology and scanning the specimen in more than three directions, it is possible to get higher resolution density profiles.

CONCLUSION

The application of X-ray tomography was studied for predicting the through-thickness density profile of particleboard. The approach was to develop a nondestructive testing device that could predict the through-thickness density profile by scanning at various angles through the surface of the panel. To accomplish this task two mathematical models were devised by considering the panel to be comprised of three distinct layers of material, tow face and a core. Model 1 consisted of a step function which considered that the face and core each had a fixed density. While Model 2 considered that there was a fixed density for each layer but that there was a gradual transition of the density from face to core and core to face. Three different thicknesses of commercially manufactured particleboards were scanned with X-rays at angles of 45^0, 90^0 and 135^0 to the surface of the panel. The density profile were then predicted using the two models. For comparison, the panels were then scanned normal to the surface and from face to face to establish their actual density profile. This method provided an accurate measurement of the actual profile but would not be useful for in-line scanning in production environment as would be the tomography approach. The agreement of predicted to

actual was best for Model 2. The means of the coefficients of determination (R^2) of thirty-six samples were 0.689 for Model 1 and 0.822 for Model 2. Whereas, the mean of the standard error of estimation was 0.0569 g/cm^3 for Model 1 and 0.0424 g/cm^3 for Model 2.

Use of X-ray tomography to predict the through-thickness density profiles of particleboard has been found to be feasible. Although this study is limited, it appears that it provides the necessary knowledge to design a valuable nondestructive testing tool for use in monitoring the quality of particleboard on the production line. Also, this method can be easily extended for use with other similar composite products.

BIBLIOGRAPHY

Carroll, Murray. 1963. Efficiency of Urea- and phenol-formaldehyde in particleboard. Forest Products Journal 3: 113-120.

Enzi, G., Mauro Gasparo, Pietro Raimondo Biondetti, Davide Fiore, Marcello Semisa, and Francesco Zurlo. 1986. Subcutaneous and visceral fat distribution according to sex, age, and overweight, evaluated by computed tomography. Am J Clin Nutr 44: 739-46.

Funt, B. V., and Edwin C. Bryant. 1987. Detection of internal log defects by automatic interpretation of computer tomography images. Forest Products Journal. Vol.37, No.1: 56-62.

Grauer, Walter O, Albert A Moss, Christopher E. Cann, and Henry I Goldberg. 1984. Quantification of body fat distribution in the abdomen using computed tomography. The American Journal of Clinical Nutrition 39: 631-637.

Habermehl, A. 1982. A new non-destructive method for determining internal wood condition and decay in living trees. Arboricultural Journal, Part 1, Vol 6: 1-8. Part 2, Vol 6: 121-130.

Hänsel, A., P. Niemz and F. Brade. 1988. Investigations to generate a model for density profiles in the cross-section of particleboards. Holz als Roh-and Werkstoff 46: 125-132.

Harless, Thomas E. G., Francis G. Wagner, Paul H. Short, R. Dan Seale, Philip H. Mitchell, and Douglas S. Ladd. 1987. A model to predict the density profile of particleboard. Wood and science, V.19(1): 81-92.

Heebink, Bruce G., and F.V. Hefty. 1972. Reducing particleboard pressing time:exploratory study. U.S.D.A., Forest Service Research Paper.

Hoag, Michael Lynn. 1988. Master's thesis of Oregon State University.

Hovland, H.. 1985. Development in Field X-Radiography, 1931-62. Materials Evaluation (43): 1386-1390.

Huang,Yaw-Fuh, and Minoru Mori. 1978. Pressing of

particleboard with radio-frequency (IV). Effects of distance piece in combined heating method on board properties. Journal of the Japan wood research society. Vol.24, No.2: 97-103.

Humphrey, P. E., and A. J. Bolton. 1989. The Hot Pressing of Dry-formed Wood-based Composites. Holzforschung 43: 199-206.

Jacoby, S.L.S, J.S.Kowalik, and J.T.Pizzo. 1972. ITERATIVE METHODS FOR NONLINEAR OPTIMIZATION PROBLEMS. Englewood Cliffs, N.J.

Kaelble, Emmett F.. 1967. HANDBOOK OF X-RAY. McGraw-Hill, Inc.

Laufenberg, T. L.. 1986. Using gamma radiation to measure density gradients in reconstituted wood products. Forest Products Journal, Vol.36(2): 59-62.

Loos, W. E.. 1961. Gamma ray absorption and wood moisture content and density. Forest Products Journal 3: 145-149.

Marshall, Christopher. 1982. THE PHYSICAL BASIS OF COMPUTED TOMOGRAPHY. Warren H. Green, Inc, St. Louis, Missouri, U.S.A.

May, H.-A. 1983. Relations between properties, raw materials and the distribution of density in particleboards. Part 3: Evaluation of density profiles and industrial application for abrasion control. Holz als Roh- and Werkstoff 41: 189-192.

McMillin, Charles W.. 1982. Application of automatic image analysis to wood science. Wood science. Vol.14, No.3: 97-105.

Nearn, W. T., and Kendall Bassett. 1968. X-Ray Determination and Use of Surface-to-Surface Density Profile in Fiberboard. Forest Products Journal. Vol.18, No.1: 73-74.

Onoe, M., Wen Ysao, H. Yamada, and M. Yoshimatsu. 1983. Computed tomography for use on live trees. Materials Evaluation, 41: 748-749.

Onoe, Morio, Jing Wen Tsao, and et al. 1985. Portable CT scanning for use on live trees and standing columns. The world conference on nondestructive testing. Nov.3-8,85.

Parker, M. L., and L. A. Jozsa. 1973. X-ray scanning machine for tree-ring width and density analyses. Wood and

fiber. V.5(3): 192-197.

Paulitsch, M. and L. Mehlhorn. 1973. A new method for evaluating the density profile in particle boards. Holz als Roh- und Werkstoff 31: 393-397.

Press, Willliam H., Brian P.Flannery, Saul A.Teukolsky, and William T. Vetterling. 1988. NUMERICAL RECIPES IN C. The Press of Syndicate of the University of Cambridge.

Sato, Takuso, Nobuaki Takanshi, and Yoshiki. 1984. Two-dimensional x-ray imaging system for very small objects using scanning slit detection. Applied optics. Vol.23, No.17: 2857-2859.

Sekino, Noboru, and Shin Morisaki. 1987. The effects of board density and board-edge distance of nails on lateral nail-resistance of low-density particleboards. Journal of the Japan wood research society. Vol.33, No.9: 694-701.

Shen, K. C., and M. N. Carroll. 1969. A new method for evaluation of internal strength of particleboard. Forest Products Journal. Vol.19, No.8: 17-22.

Shen, K. C., and M. N. Carroll. 1970. Measurement of Layer-Strength Distribution in Particleboard. Forest Products Journal. Vol.20, No.6: 53-55.

Stevens, R. R.. 1978. Slicing Apparatus Aids in Determination of Layer-Density of Particleboard. Forest Products Journal. Vol.28, No.9:51-52.

Steiner, P. R., L. A. Jozsa, M. L. Parker, and S. Chow. 1978. Application of Z-ray densitometry to determine density profile in waferboard: relationship of density to thickness expansion and internal bond strength under various cycles. Wood science. Vol.11, No.1: 48-55.

Strickler, M. D.. 1959. Properties of Douglas-fir flakeboard. Forest Products Journal. No.7: 203-215.

Suchsland, Otto. 1967. Behavior of a particleboard mat during the press cycle. Forest Products Journal. Vol.17, No.2: 51-57.

Taylor, F. W., Francis G. Wagner, Charles W. McMillin, Ira Lon Morgan, and Forrest F. Hopkins. 1984. Locating knots by industrial tomography--A feasibility study. Forest Products Journal. Vol.34, No.5: 42-46.

Vinegar, H. J.. 1986. X-Ray CT and NMR Imaging of Rocks. Journal of Petroleum Technology, March: 257-259.

Webb, S.. 1987. A review of physical aspects of X-ray transmission computed tomography. IEE Proceedings, Vol.134, Pt.A, No.2: 126-135.

Wellington, S. L., and H. J. Vinegar. 1987. X-Ray Computerized Tomography. Journal of Petroleum Technology, August 885-898.

Woodson, G. E.. 1977. Density Profile and Fiber Alignment in Fiberboard From Three Southern Hardwoods. Forest Products Journal. Vol.27, No.8.: 29-34.

Woodson, G. E.. 1976. Effects of Bark, Density Profile, and Resin Content on Medium-Density Fiberboards From Southern Hardwoods. Forest Products Journal. Vol.26, No.2: 39-42.

Yamada, Kenichi, and Yoshiaki Kido. 1987. Depth profiling by particle-induced x-ray emission analysis using a parameter-fitting technique. J. Appl. Phys. 62(9): 3936-3940.

APPENDICES

APPENDIX A. Noise Distribution in X-ray Scanning

Table 5 - Complete Data of Noise in X-ray Scanning

Position (mm)	Counts (number)	Position (mm)	Counts (number)	Position (mm)	Counts (number)
120.045	2811	122.059	2811	124.391	2813
120.098	2811	122.112	2810	124.444	2813
120.151	2808	122.165	2812	124.497	2813
120.204	2811	122.218	2816	124.550	2816
120.257	2814	122.271	2816	124.603	2816
120.310	2816	122.324	2810	124.656	2812
120.363	2818	122.377	2809	124.709	2816
120.416	2823	122.430	2810	124.762	2818
120.469	2822	122.483	2812	124.815	2814
120.522	2822	122.536	2814	124.868	2819
120.575	2818	122.589	2813	124.921	2814
120.628	2817	122.642	2818	124.974	2813
120.681	2818	122.695	2817	125.027	2813
120.734	2820	122.748	2812	125.080	2813
120.787	2817	122.801	2818	125.133	2812
120.840	2812	122.854	2813	125.186	2815
120.893	2816	122.907	2813	125.239	2817
120.946	2816	122.960	2814	125.292	2816
120.999	2817	123.013	2815	125.345	2814
121.052	2821	123.066	2811	125.398	2814
121.105	2821	123.119	2815	125.451	2815
121.158	2818	123.172	2818	125.504	2818
121.211	2819	123.225	2819	125.557	2816
121.264	2821	123.278	2816	125.610	2812
121.317	2816	123.331	2817	125.663	2810
121.370	2813	123.384	2817	125.716	2808
121.423	2809	123.437	2818	125.769	2814
121.476	2813	123.490	2816	125.822	2815
121.529	2808	123.543	2816	125.875	2815
121.582	2814	123.596	2816	125.928	2814
121.635	2815	123.649	2819	125.981	2817
121.688	2815	123.702	2817	126.034	2819
121.741	2814	123.755	2818	126.087	2819
121.794	2810	123.808	2811	126.140	2816
121.847	2809	123.861	2813	126.193	2818
121.900	2808	123.914	2816	126.246	2816
121.953	2811	123.967	2815	126.299	2818
122.006	2812	124.020	2817	126.352	2814
122.059	2811	124.073	2817	126.405	2818
122.112	2810	124.126	2819	126.458	2818
122.165	2812	124.179	2825	126.511	2814
122.218	2816	124.232	2823	126.564	2820
122.271	2816	124.285	2812	126.617	2817
122.324	2810	124.338	2815	126.670	2818

APPENDIX A. (Continued)

Position (mm)	Counts (number)	Position (mm)	Counts (number)	Position (mm)	Counts (number)
126.723	2818	129.161	2816	131.599	2819
126.776	2812	129.214	2816	131.652	2817
126.829	2812	129.267	2815	131.705	2812
126.882	2817	129.320	2809	131.758	2812
126.935	2815	129.373	2808	131.811	2810
126.988	2815	129.426	2815	131.864	2810
127.041	2813	129.479	2812	131.917	2814
127.094	2812	129.532	2820	131.970	2815
127.147	2812	129.585	2819	132.023	2814
127.200	2814	129.638	2814	132.076	2819
127.253	2816	129.691	2817	132.129	2814
127.306	2815	129.744	2816	132.182	2813
127.359	2813	129.797	2812	132.235	2812
127.412	2813	129.850	2810	132.288	2816
127.465	2812	129.903	2810	132.341	2810
127.518	2810	129.956	2814	132.394	2807
127.571	2814	130.009	2814	132.447	2814
127.624	2813	130.062	2814	132.500	2813
127.677	2814	130.115	2816	132.553	2814
127.730	2819	130.168	2810	132.606	2814
127.783	2819	130.221	2817	132.659	2814
127.836	2816	130.274	2815	132.712	2811
127.889	2814	130.327	2814	132.765	2817
127.942	2814	130.380	2816	132.818	2816
127.995	2812	130.433	2820	132.871	2814
128.048	2813	130.486	2820	132.924	2817
128.101	2818	130.539	2820	132.977	2815
128.154	2814	130.592	2818	133.030	2813
128.207	2815	130.645	2815	133.083	2816
128.260	2812	130.698	2820	133.136	2815
128.313	2815	130.751	2815	133.189	2815
128.366	2809	130.804	2814	133.242	2815
128.419	2814	130.857	2816	133.295	2814
128.472	2818	130.910	2817	133.348	2817
128.525	2817	130.963	2817	133.401	2823
128.578	2812	131.016	2812	133.454	2820
128.631	2815	131.069	2818	133.507	2815
128.684	2822	131.122	2815	133.560	2814
128.737	2819	131.228	2816	133.613	2816
128.790	2819	131.175	2818	133.666	2817
128.843	2816	131.546	2820	133.719	2816
128.896	2818	131.281	2811	133.772	2818
128.949	2816	131.334	2813	133.825	2821
129.002	2817	131.387	2811	133.878	2824
129.055	2816	131.440	2812	133.931	2820
129.108	2815	131.493	2818	133.984	2818

APPENDIX A. (Continued)

Position (mm)	Counts (number)
134.037	2810
134.090	2811
134.143	2811
134.196	2813
134.249	2818
134.302	2816
134.355	2814
134.408	2811
134.461	2811
134.514	2816
134.567	2817
134.620	2818
134.673	2817
134.726	2817
134.779	2814
134.832	2815
134.885	2818
134.938	2812
134.991	2816

APPENDIX A. (Continued)

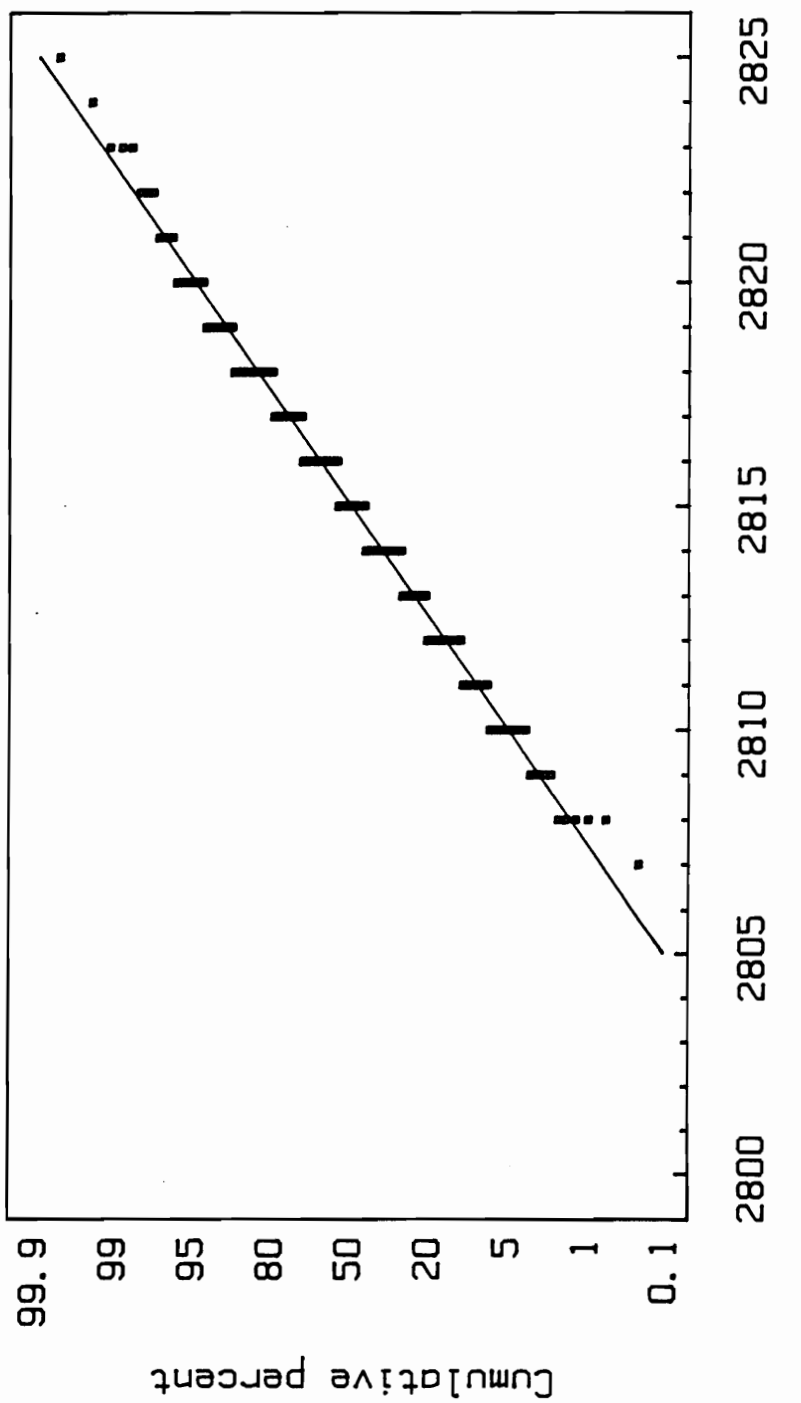

Figure 15. - Normal probability plot.

APPENDIX B. Comparisons of Predicted and Actual Density Profiles

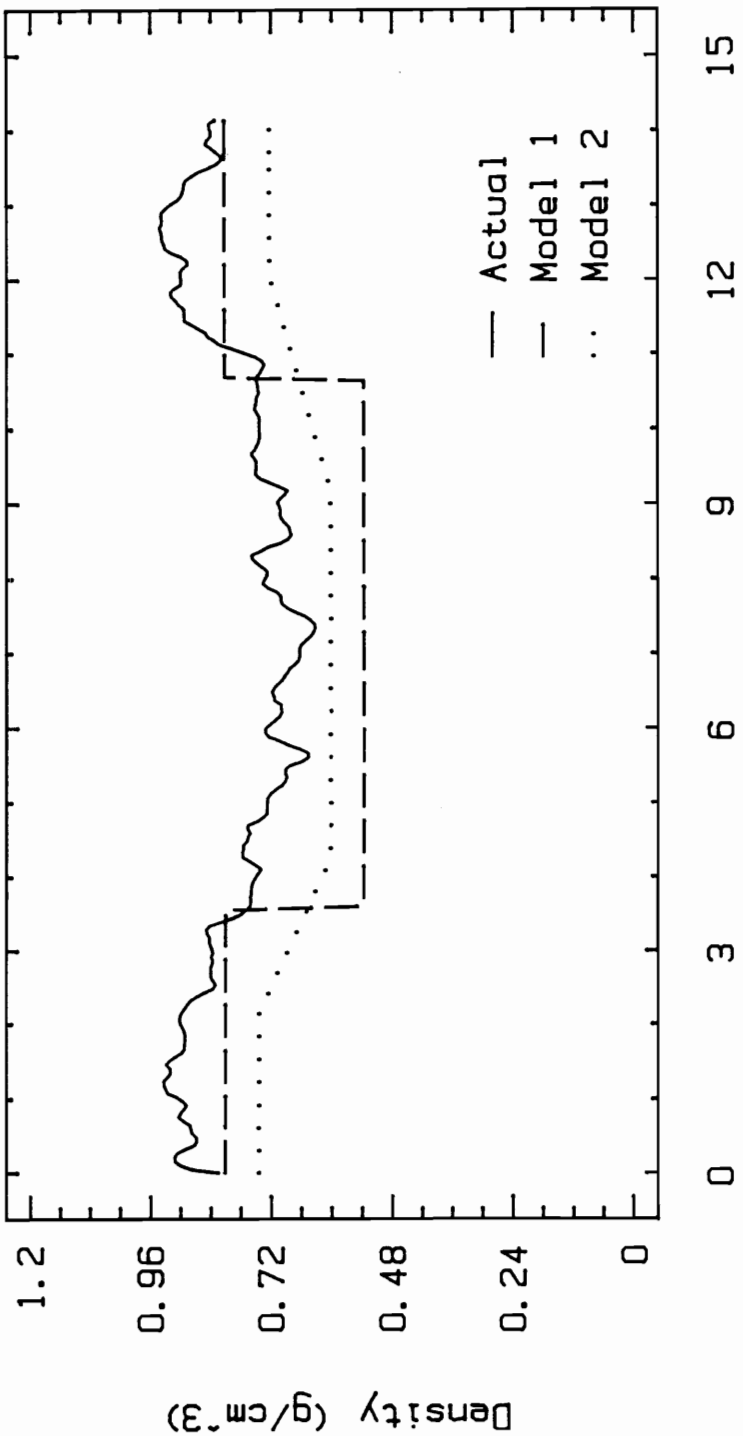

Figure 16. - Comparison of predicted and actual density profile (#1).

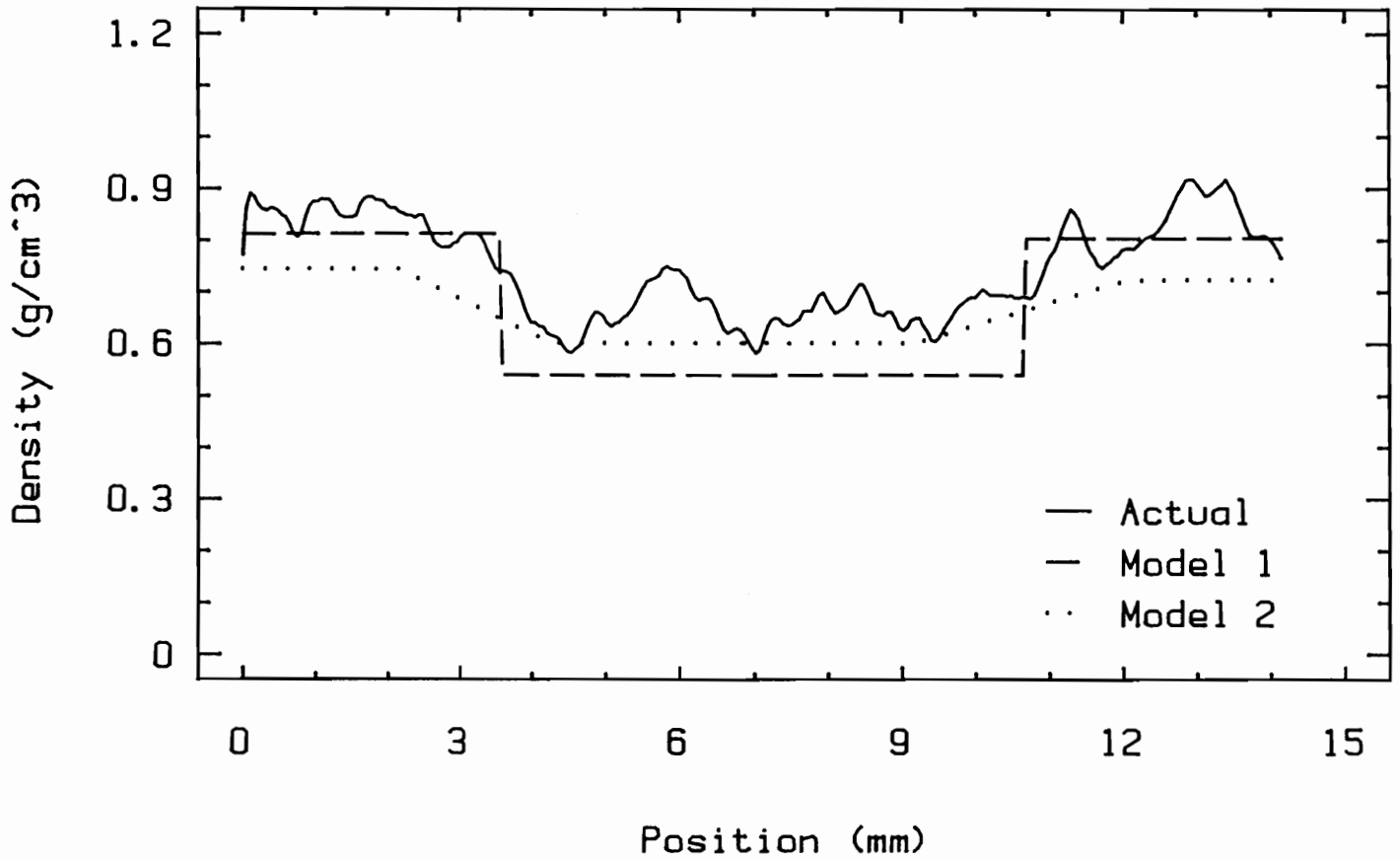

Figure 17. - Comparison of predicted and actual density profile (#2).

APPENDIX B. (Continued)

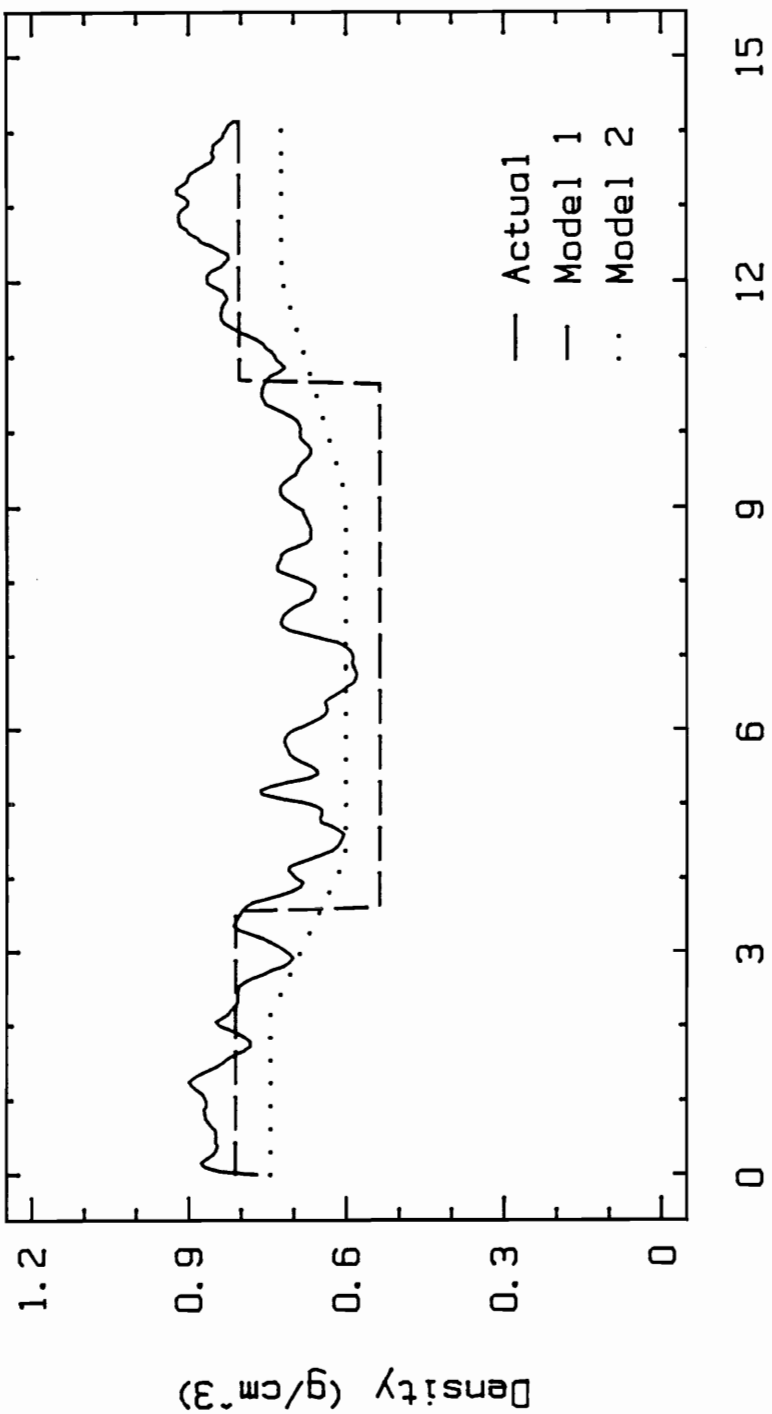

Figure 18. - Comparison of predicted and actual density profile (#3).

APPENDIX B. (Continued)

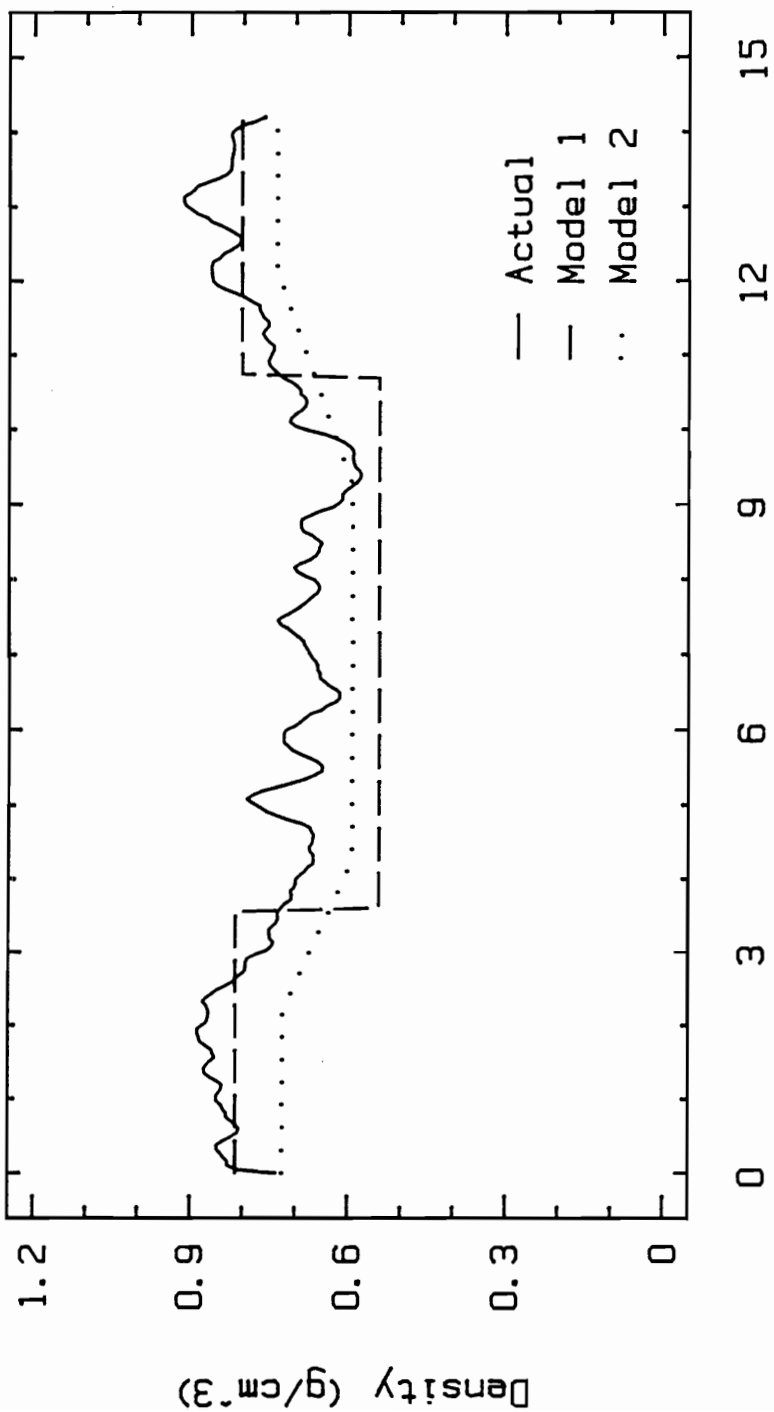

Figure 19. - Comparison of predicted and actual density profile (#4).

APPENDIX B. (Continued)

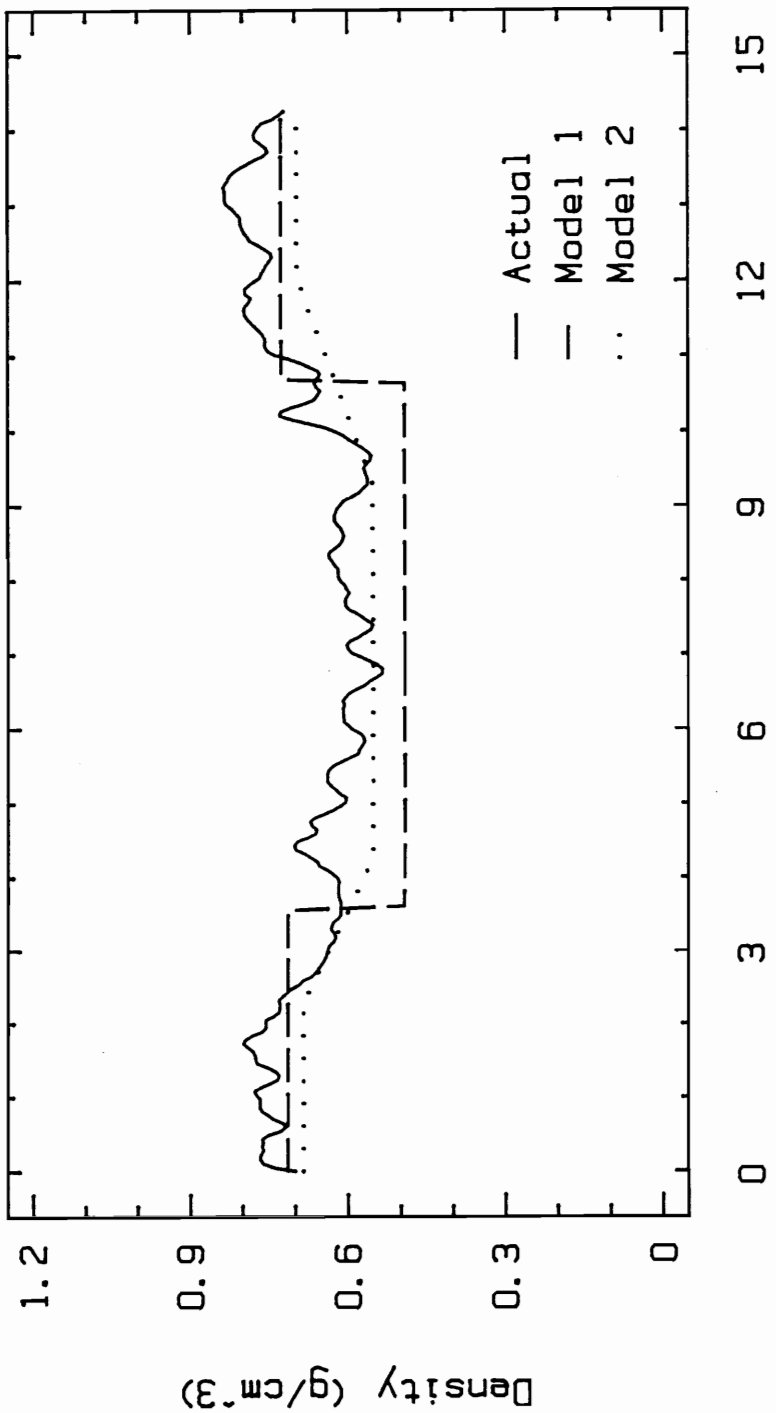

Figure 20. - Comparison of predicted and actual density profile (#5).

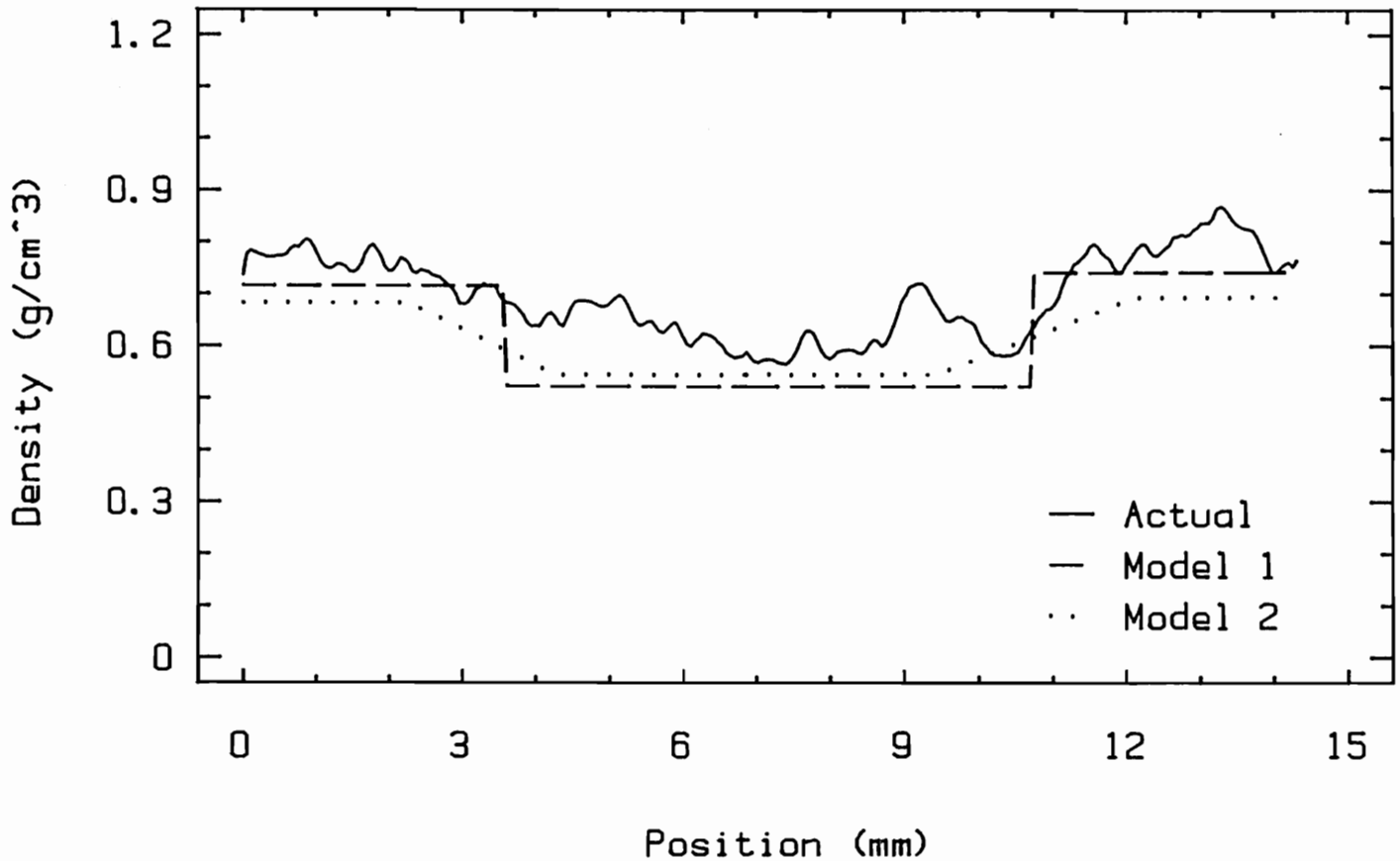

Figure 21. - Comparison of predicted and actual density profile (#6).

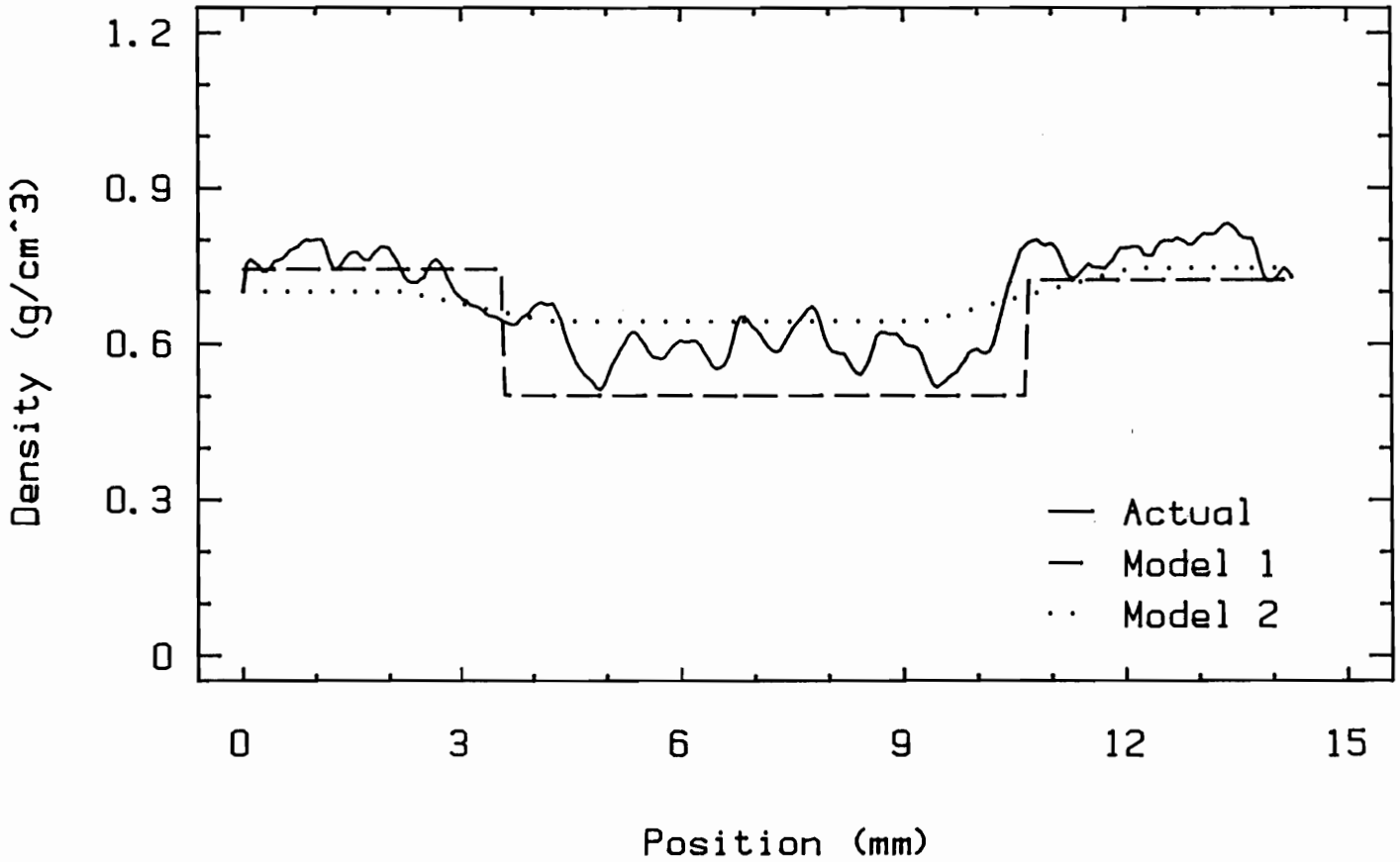

Figure 22. - Comparison of predicted and actual density profile (#7).

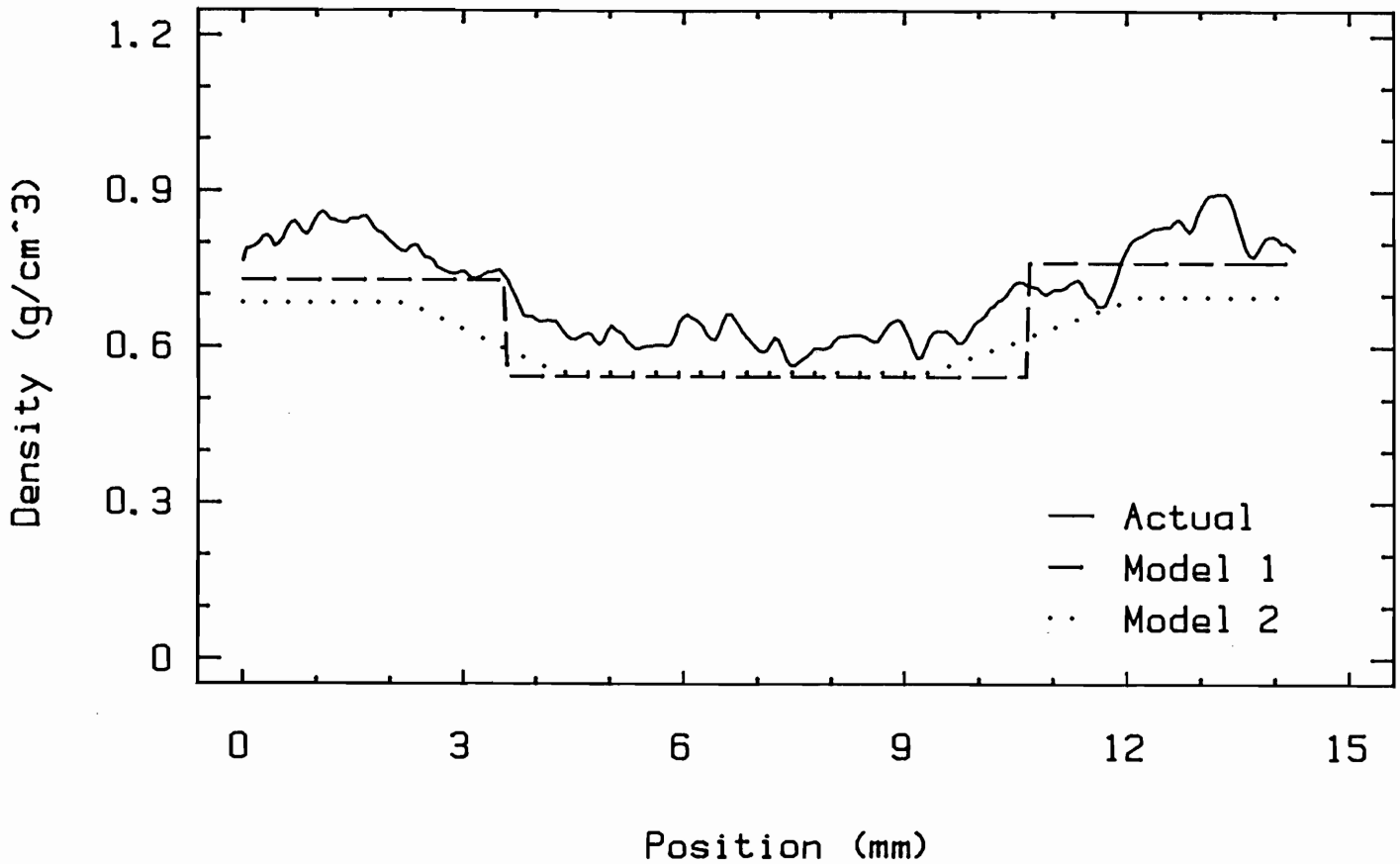

Figure 23. - Comparison of predicted and actual density profile (#8).

APPENDIX B. (Continued)

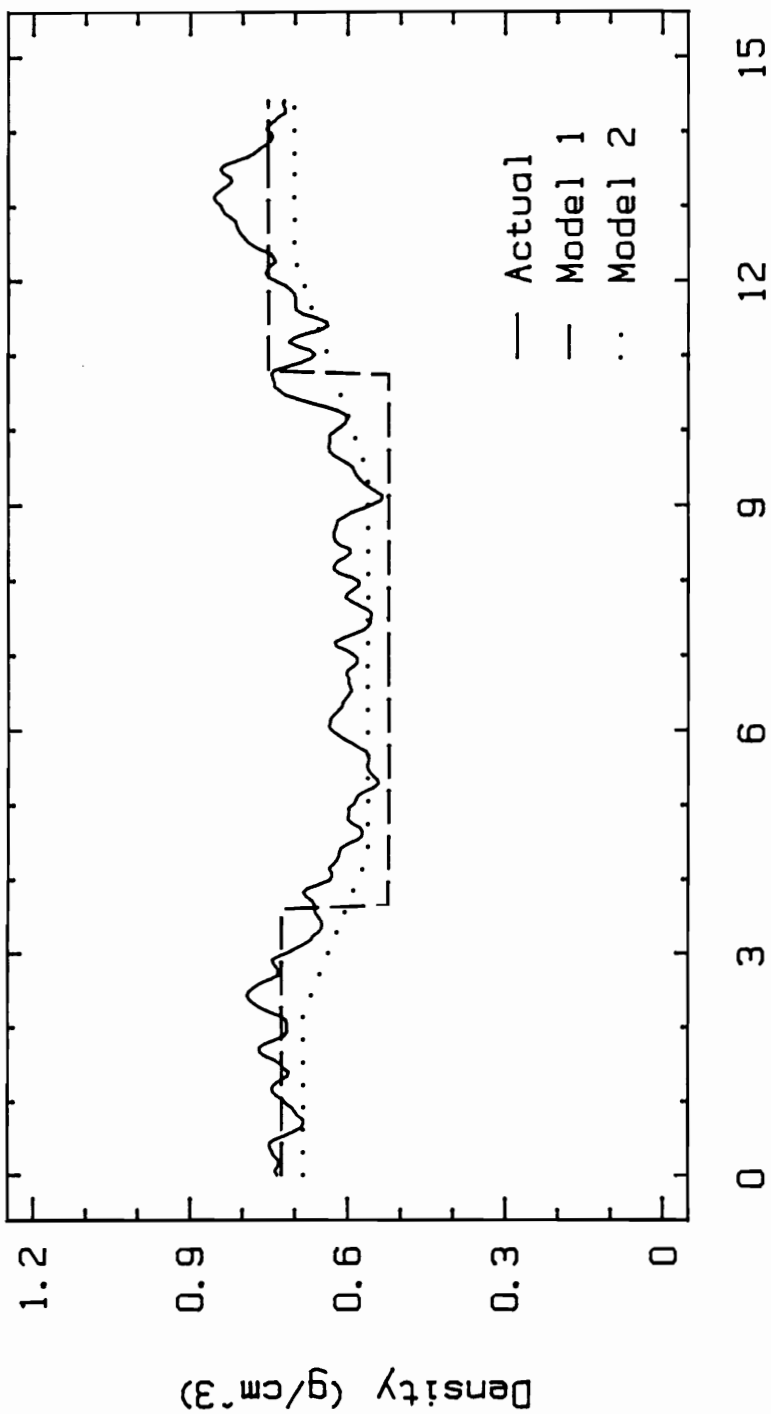

Figure 24. - Comparison of predicted and actual density profile (#9).

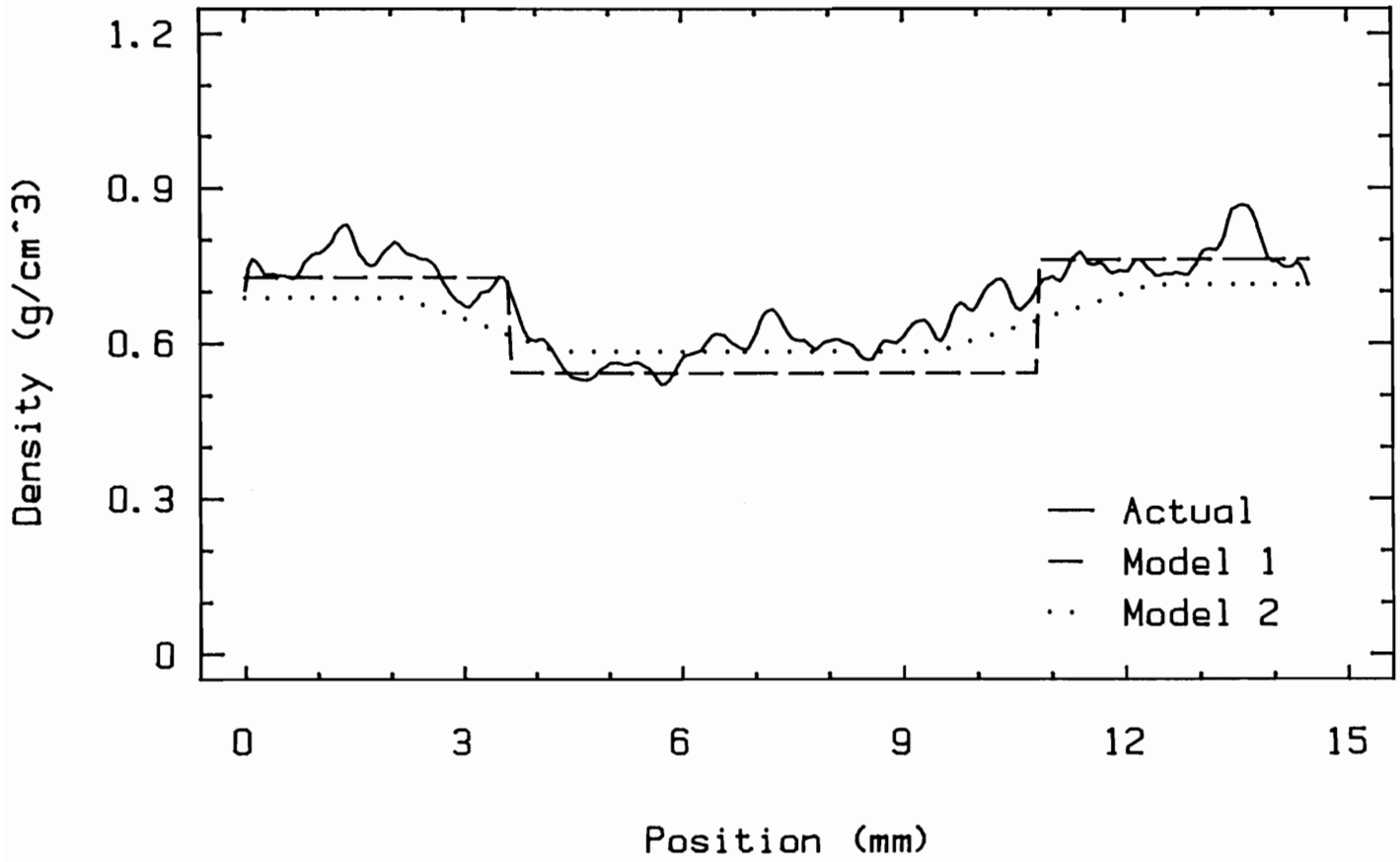

Figure 25. - Comparison of predicted and actual density profile (#10).

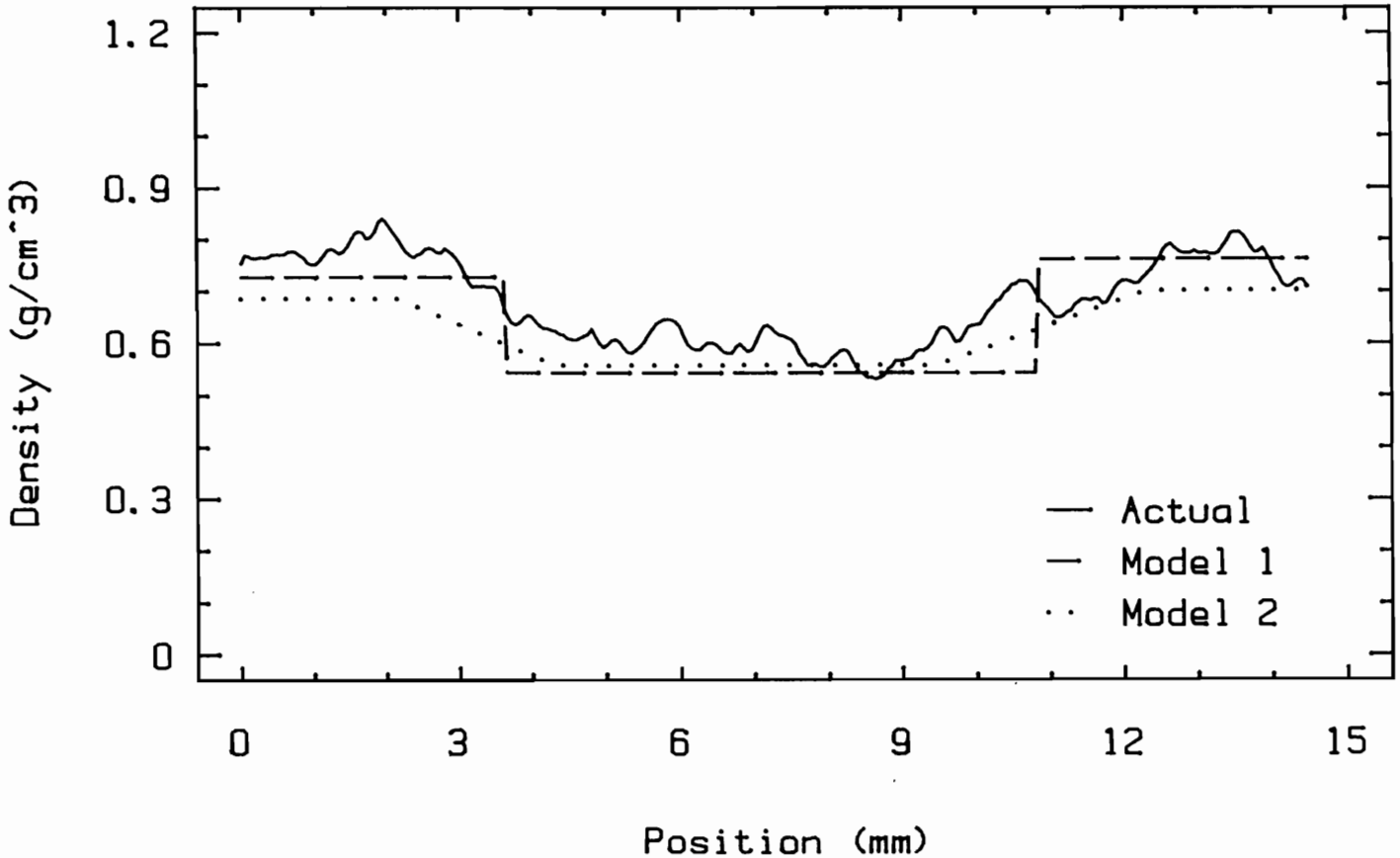

Figure 26. - Comparison of predicted and actual density profile (#11).

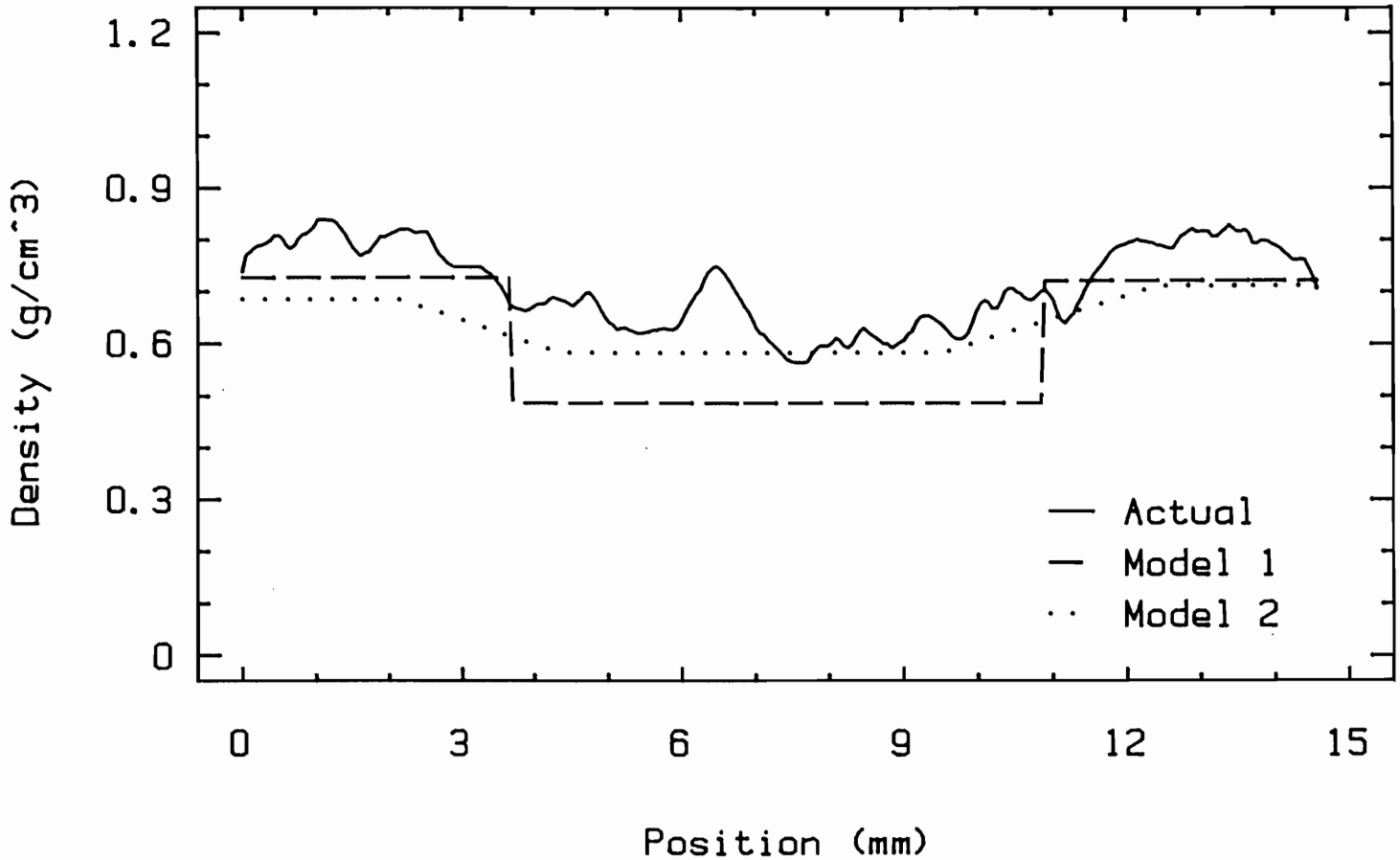

Figure 27. - Comparison of predicted and actual density profile (#12).

APPENDIX B. (Continued)

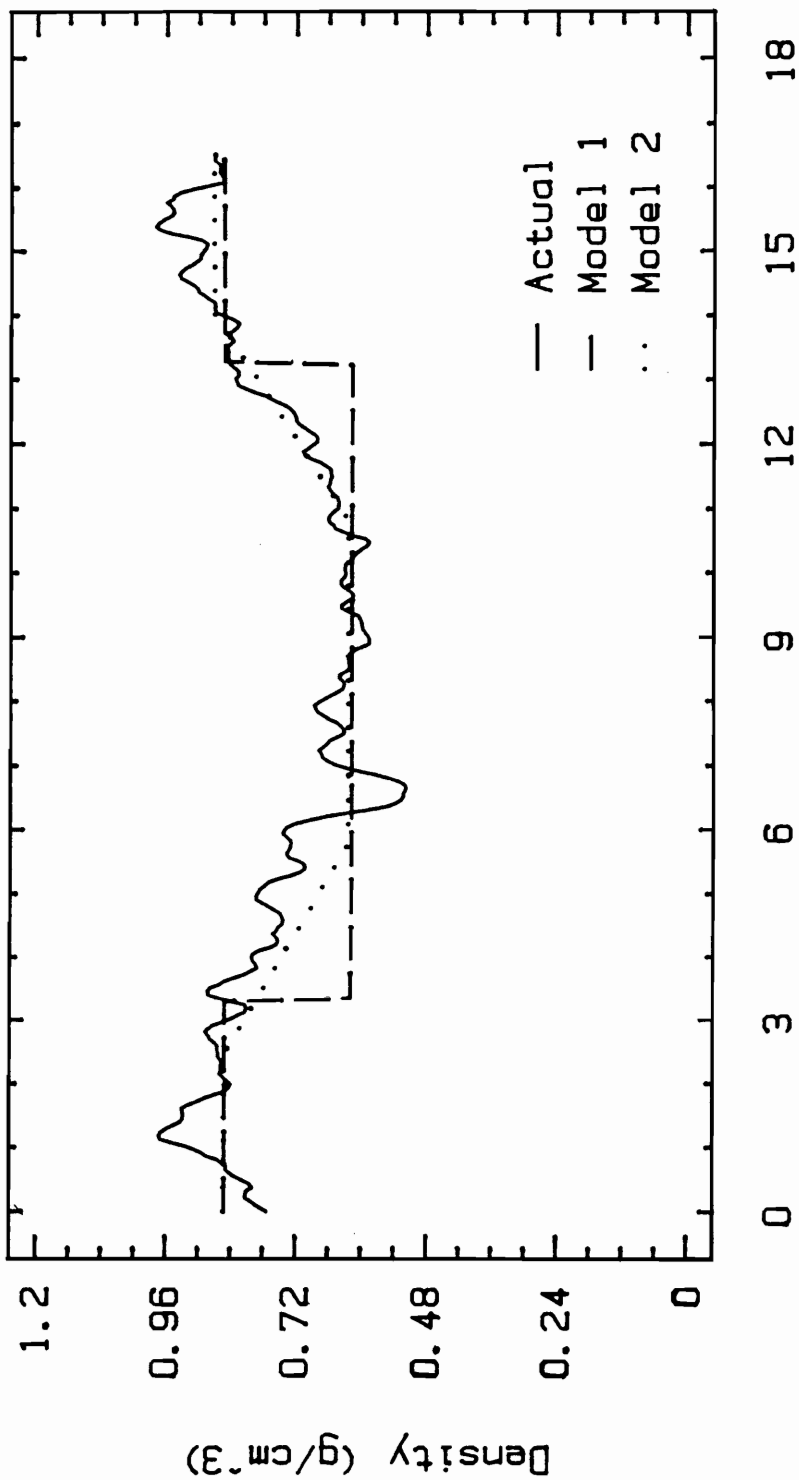

Figure 28. - Comparison of predicted and actual density profile (#13).

APPENDIX B. (Continued)

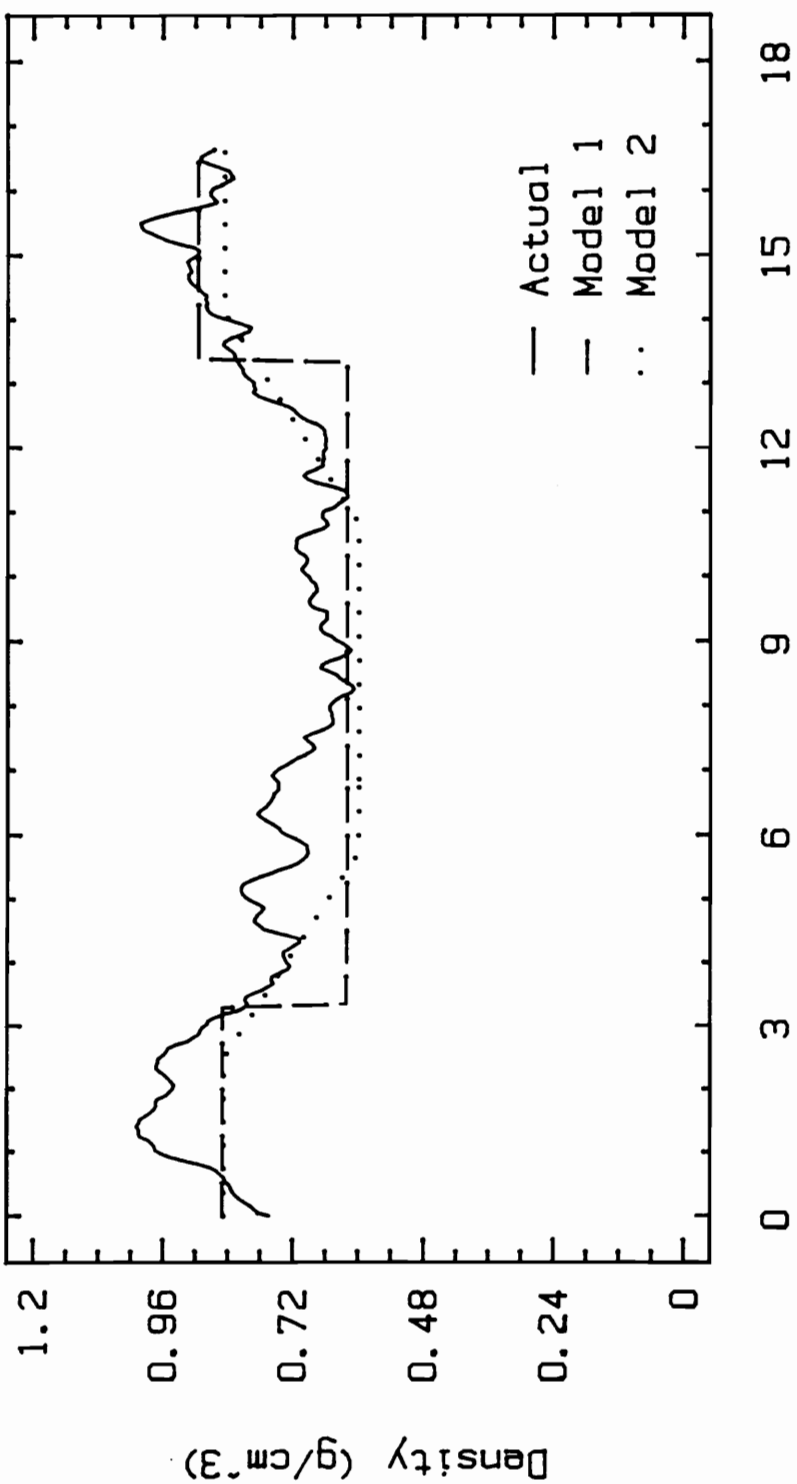

Figure 29. - Comparison of predicted and actual density profile (#14).

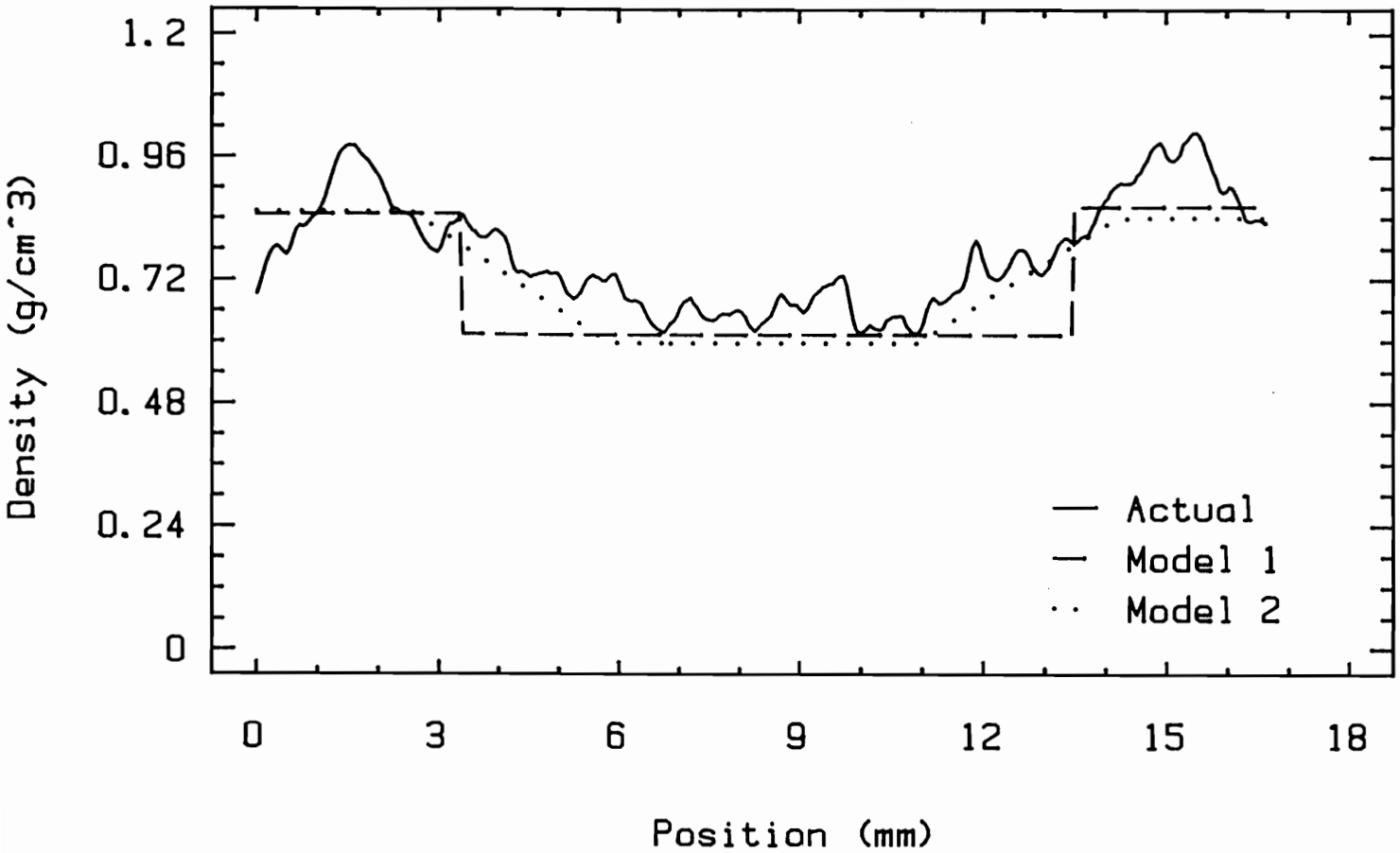

Figure 30. - Comparison of predicted and actual density profile (#15).

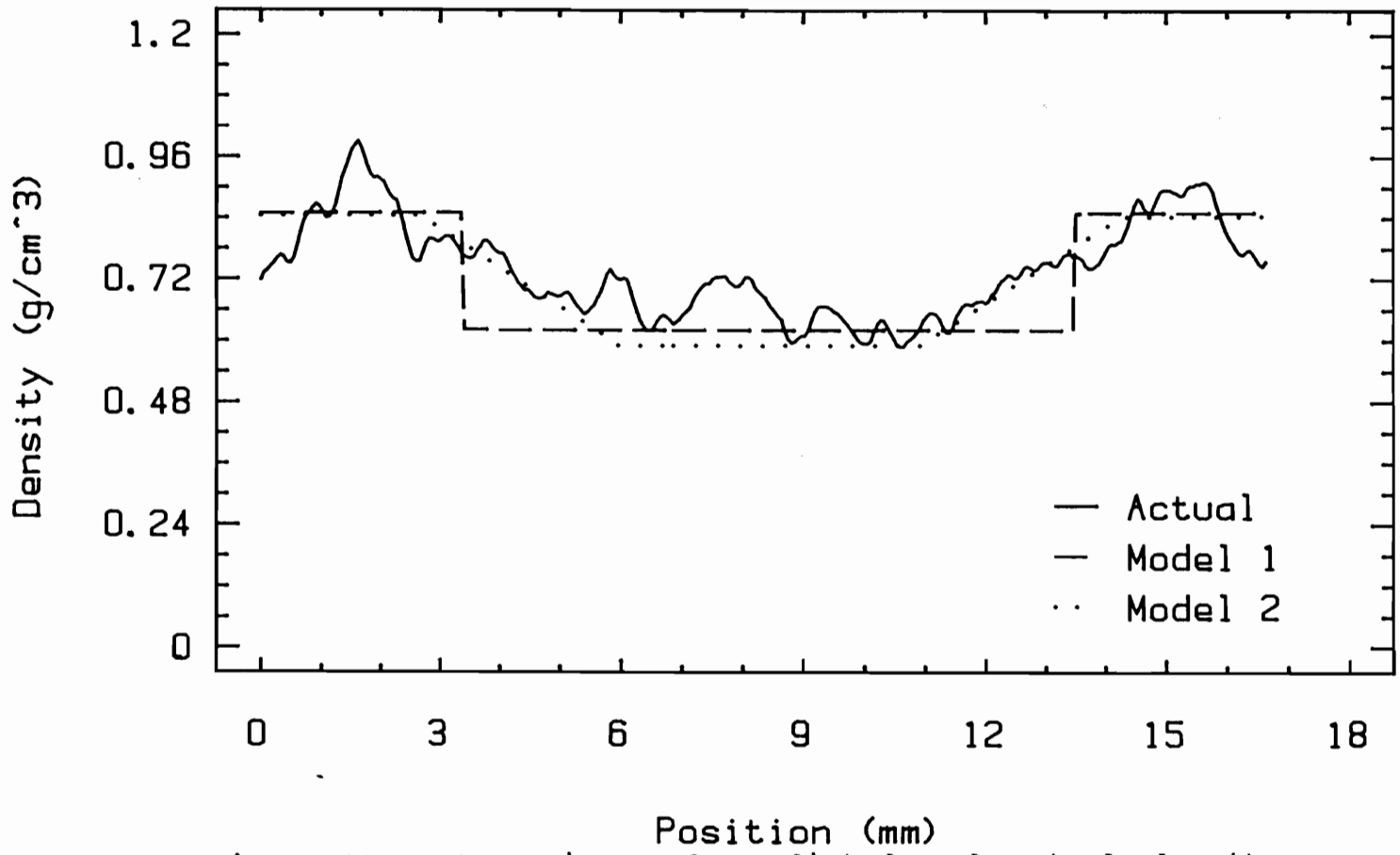

Figure 31. - Comparison of predicted and actual density profile (#16).

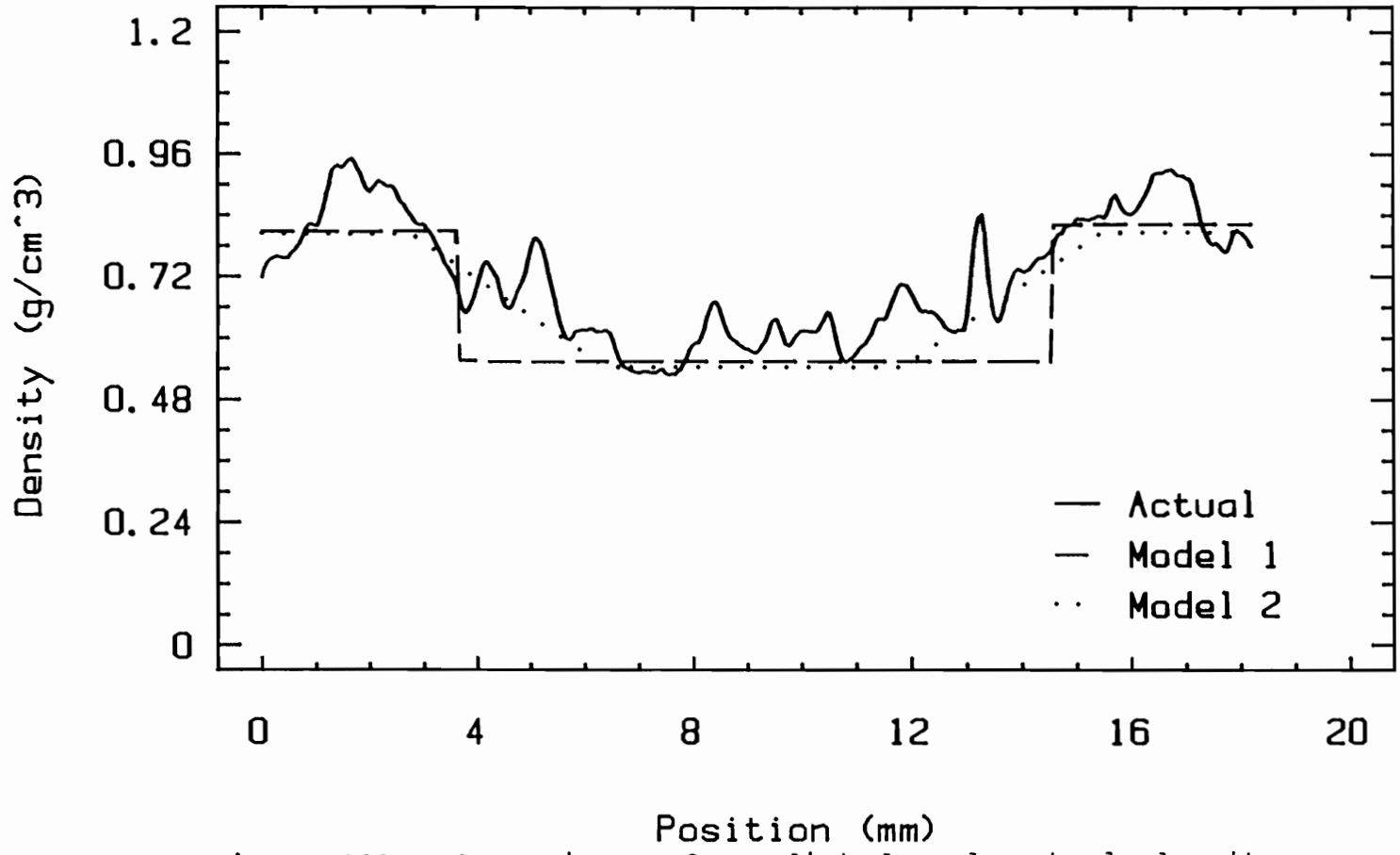

Figure 32. - Comparison of predicted and actual density profile (#17).

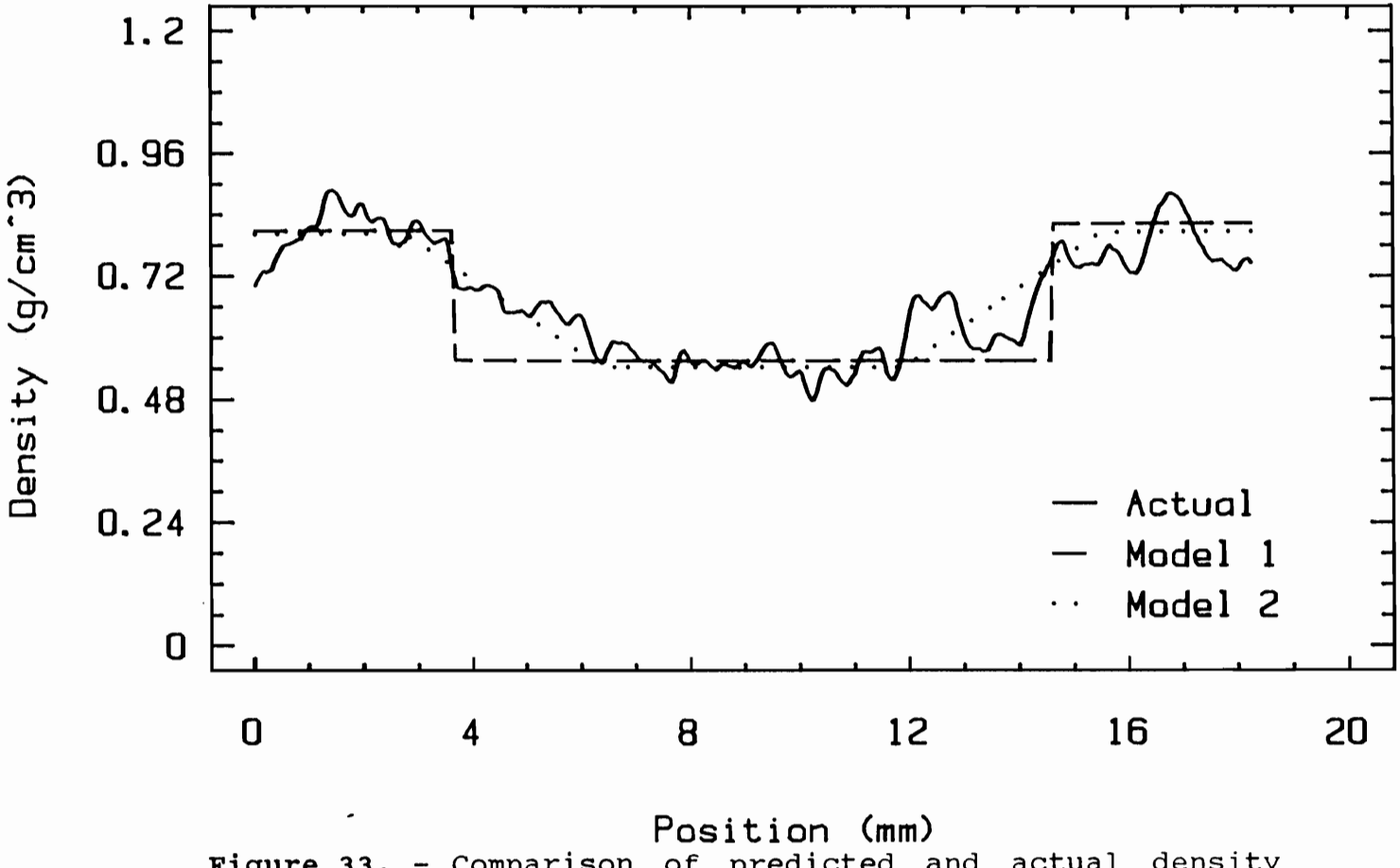

Figure 33. - Comparison of predicted and actual density profile (#18).

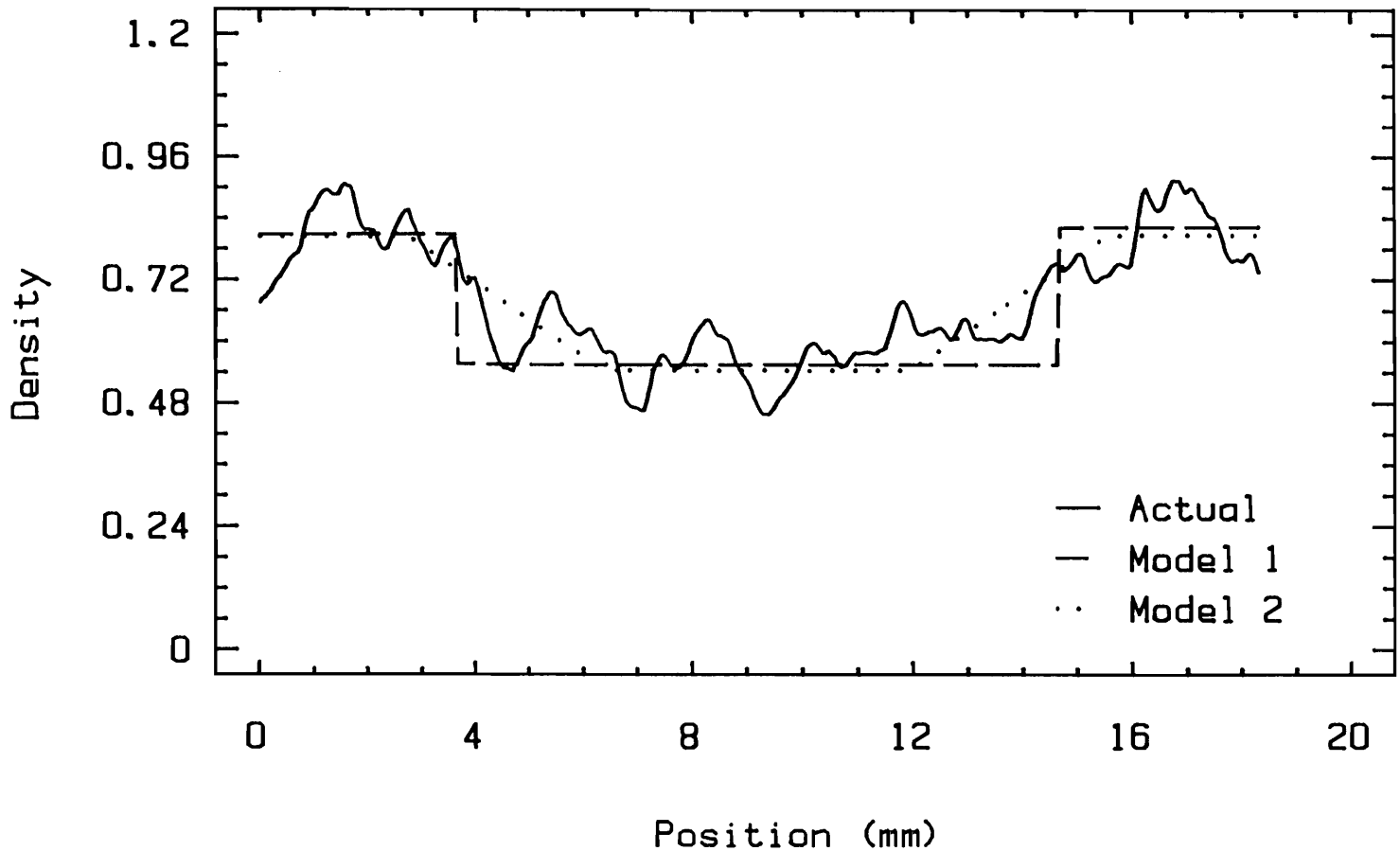

Figure 34. - Comparison of predicted and actual density profile (#19).

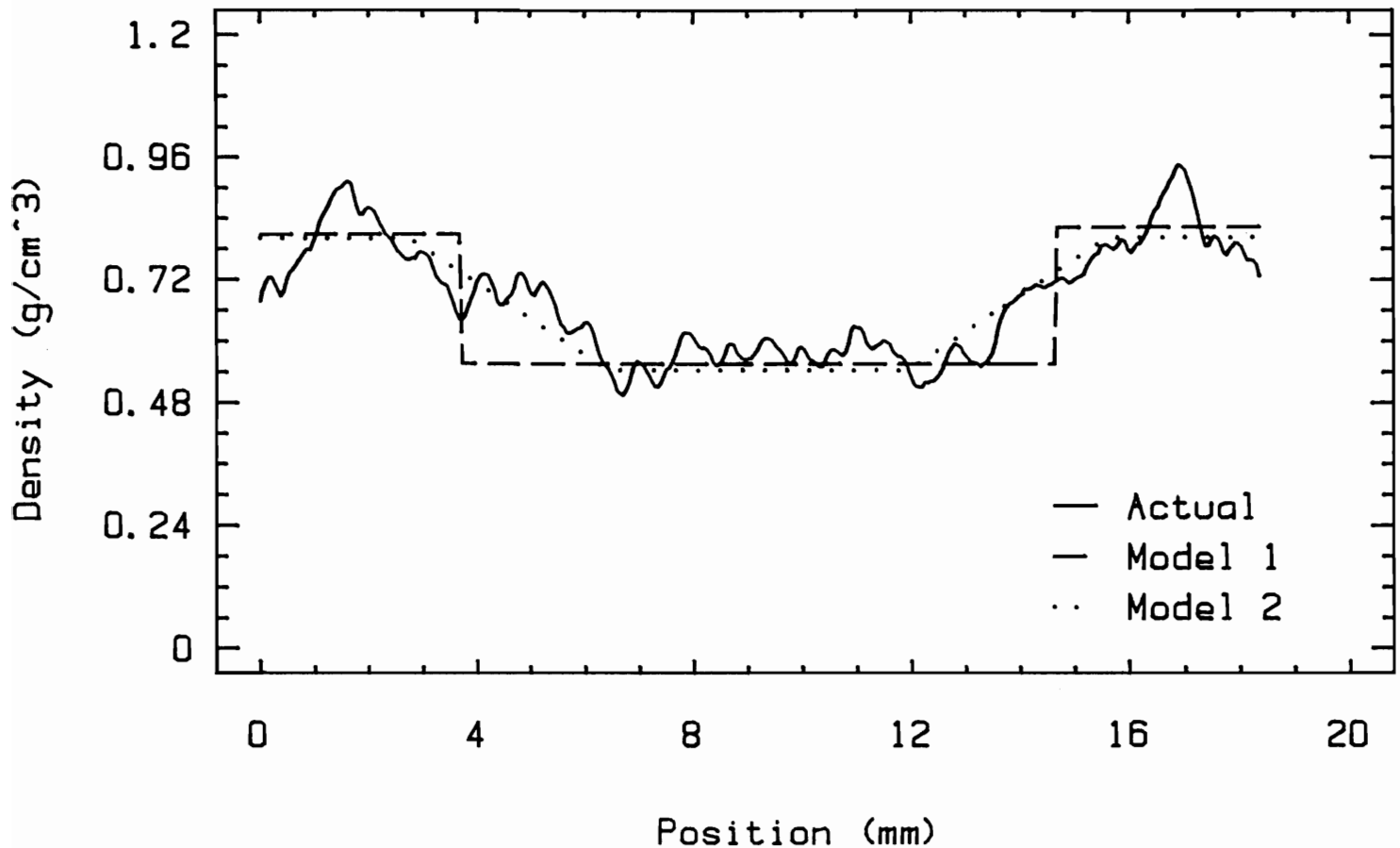

Figure 35. - Comparison of predicted and actual density profile (#20).

APPENDIX B. (Continued)

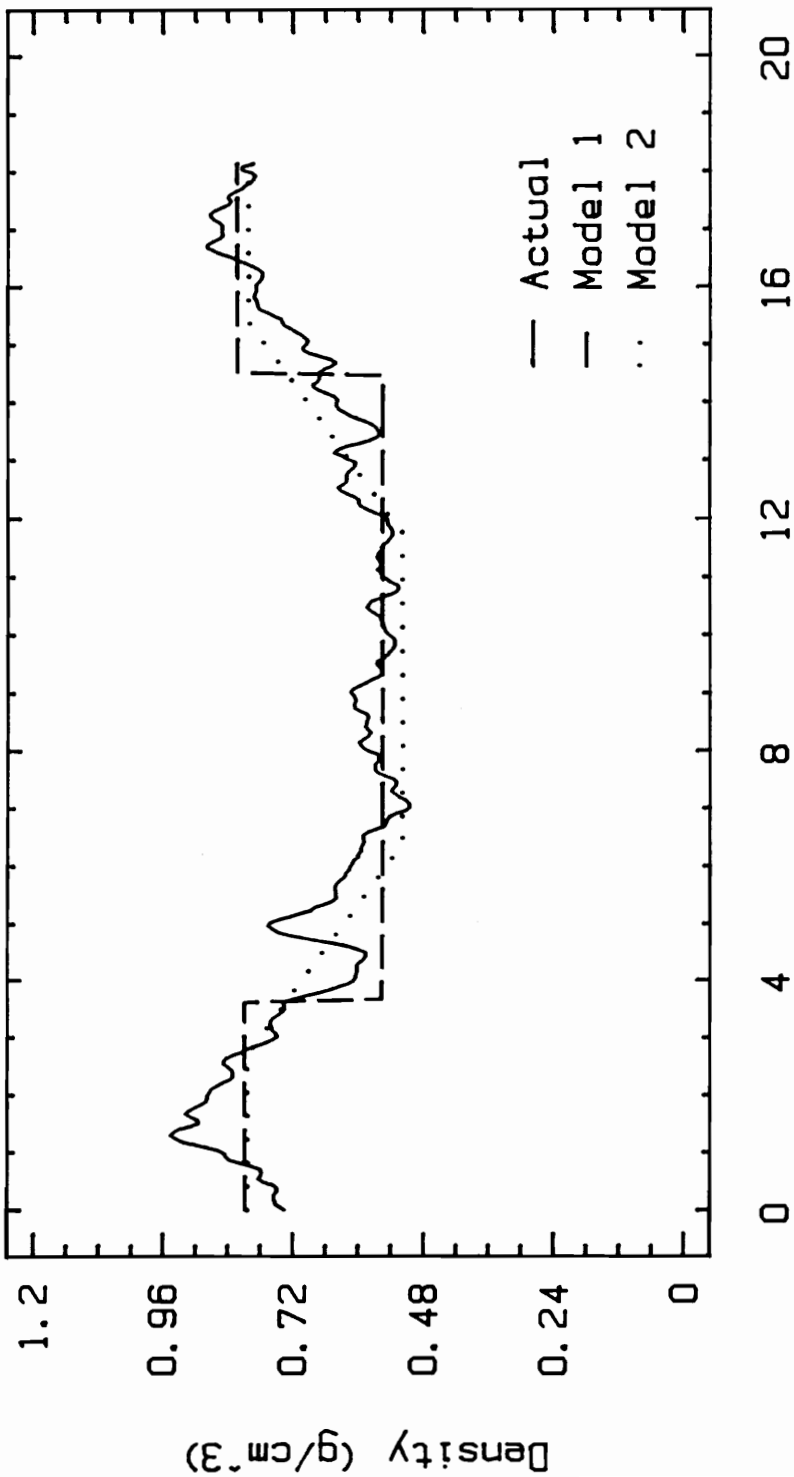

Figure 36. - Comparison of predicted and actual density profile (#21).

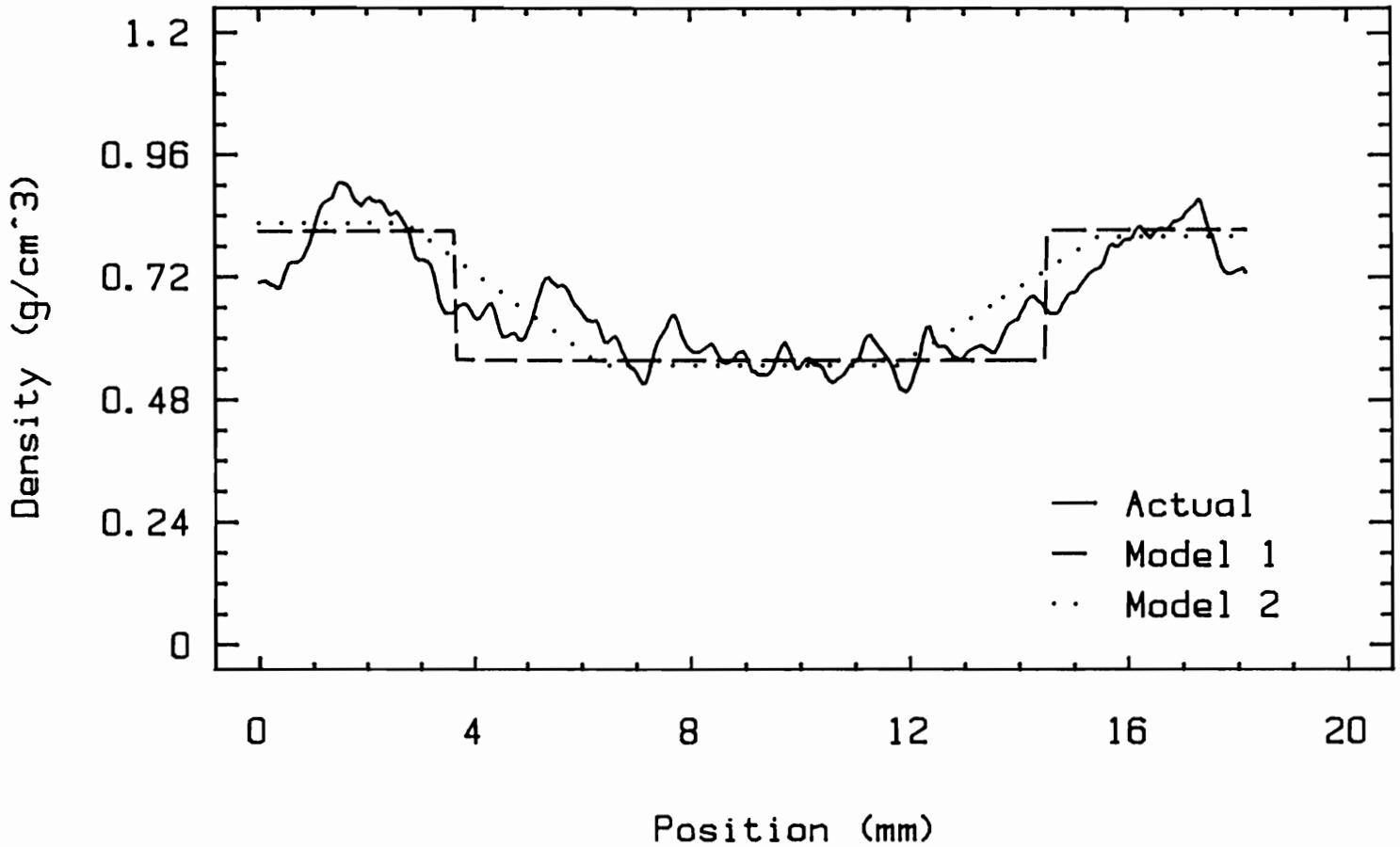

Figure 37. - Comparison of predicted and actual density profile (#22).

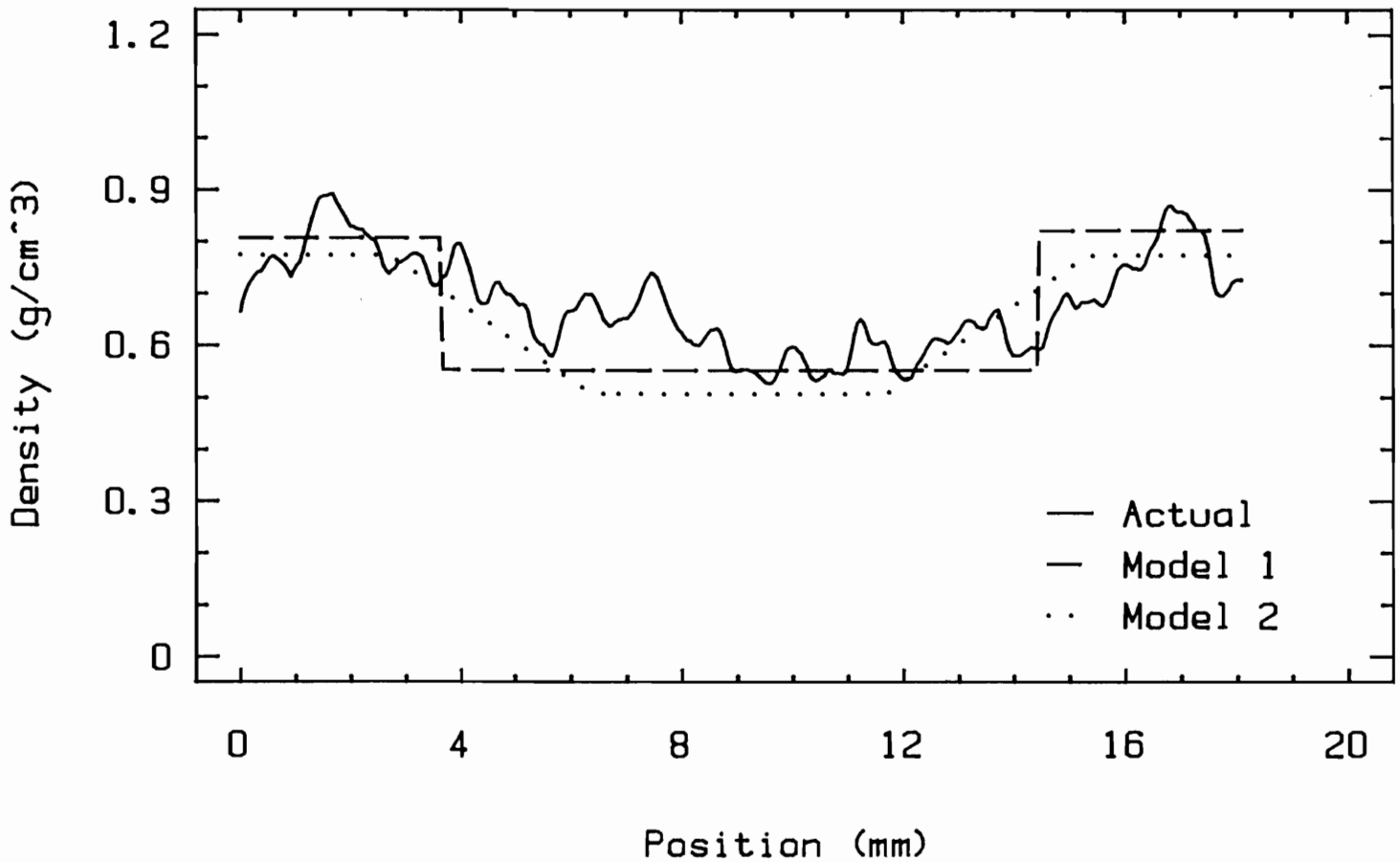

Figure 38. - Comparison of predicted and actual density profile (#23).

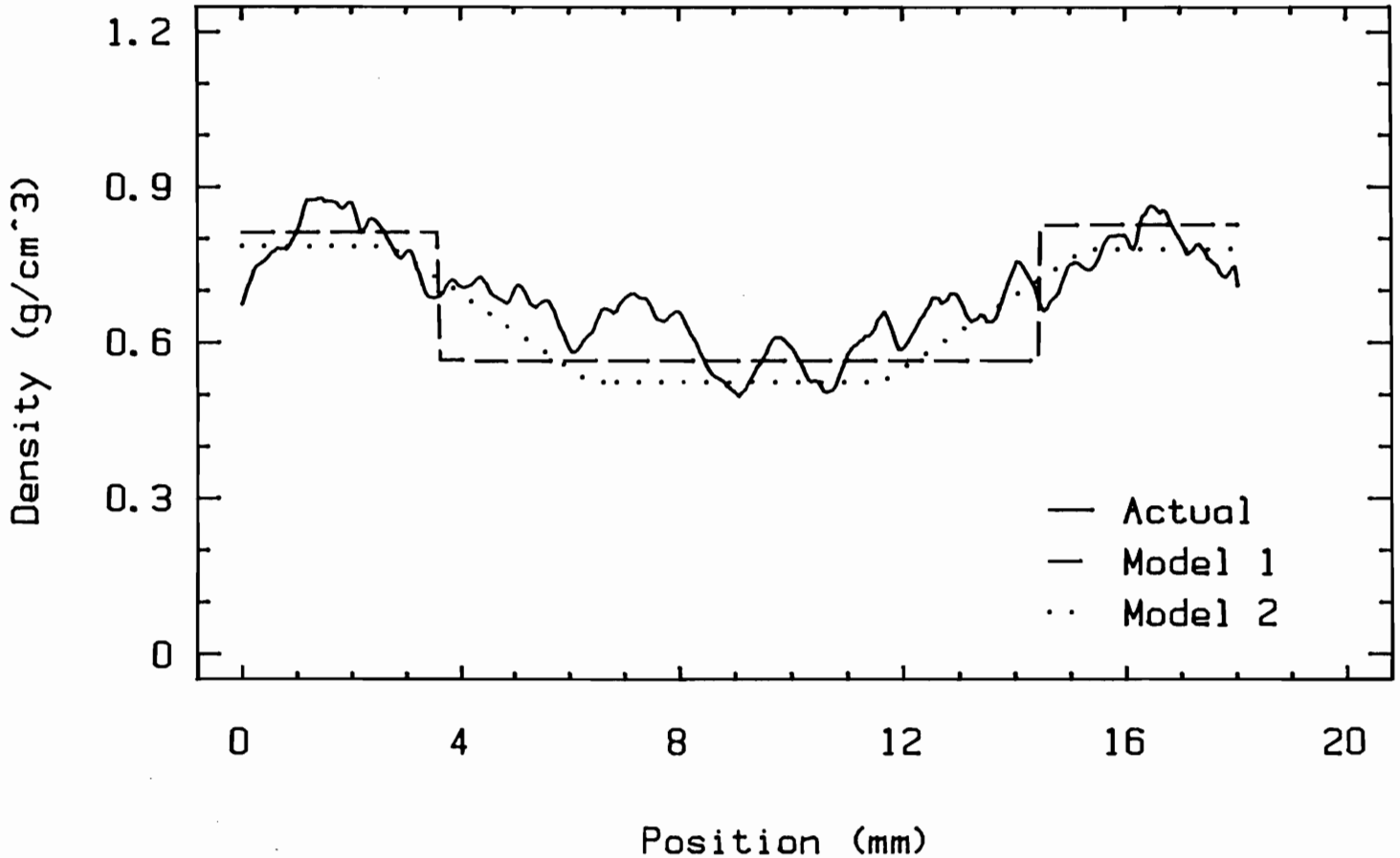

Figure 39. - Comparison of predicted and actual density profile (#24).

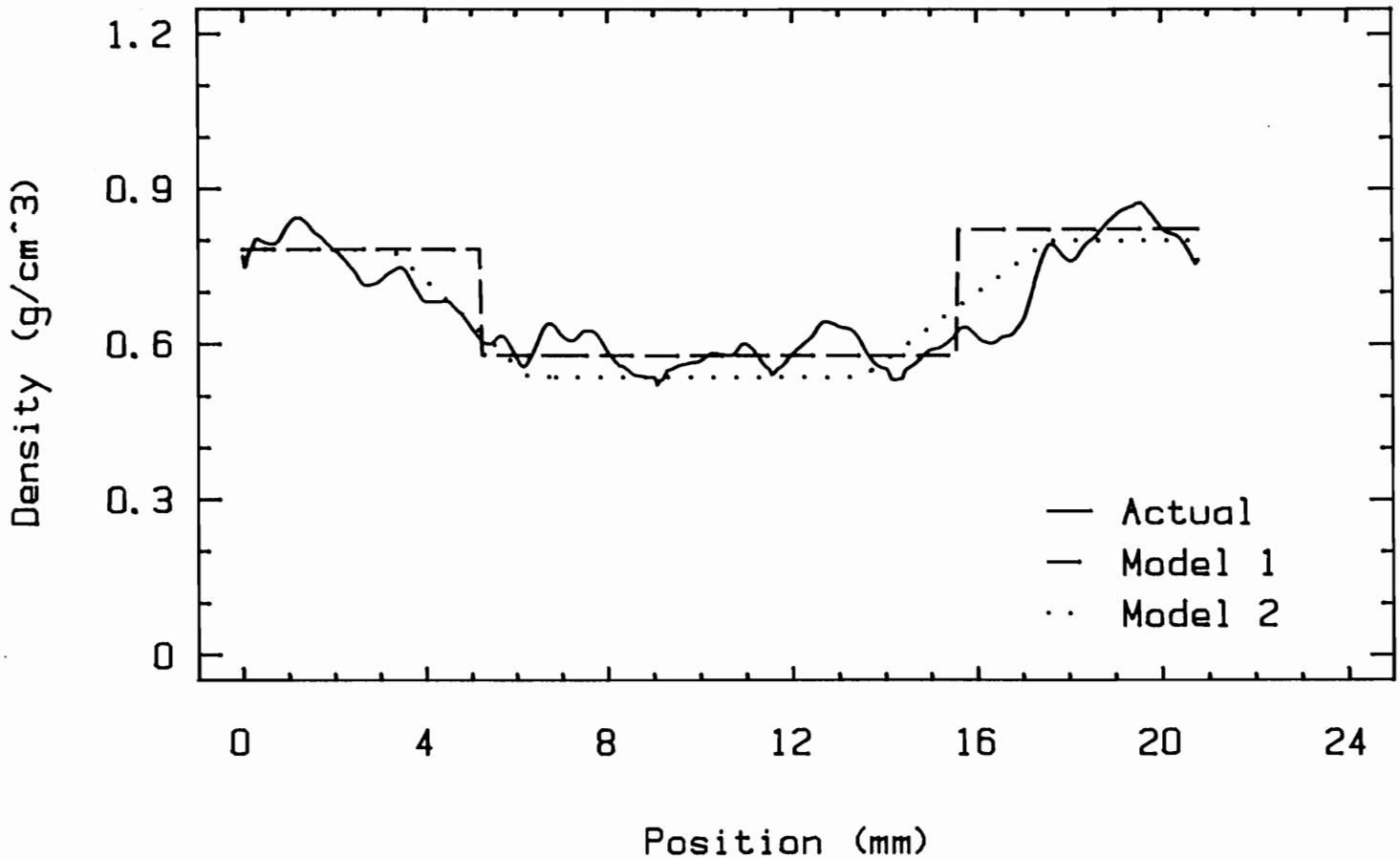

Figure 40. - Comparison of predicted and actual density profile (#25).

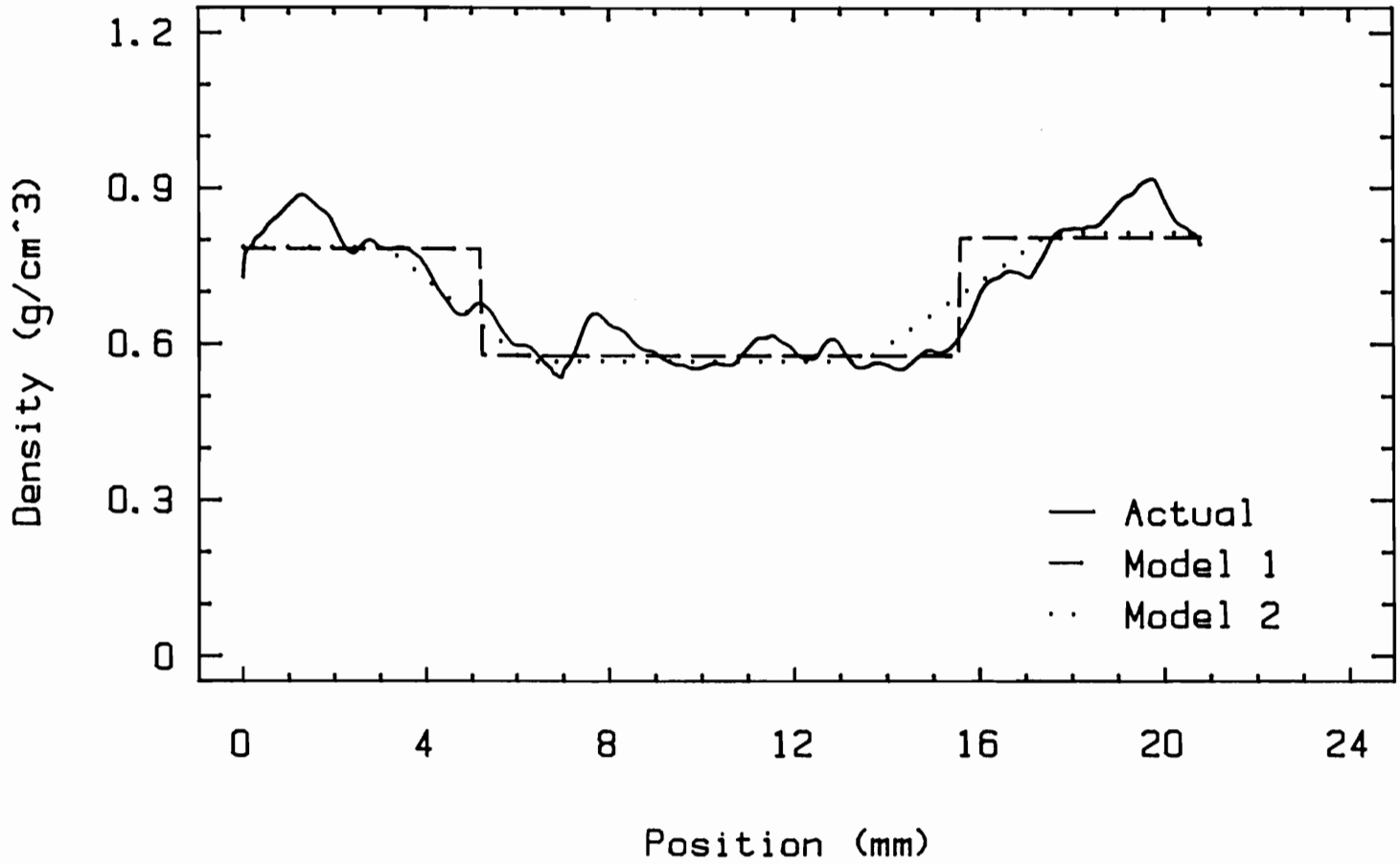

Figure 41. - Comparison of predicted and actual density profile (#26).

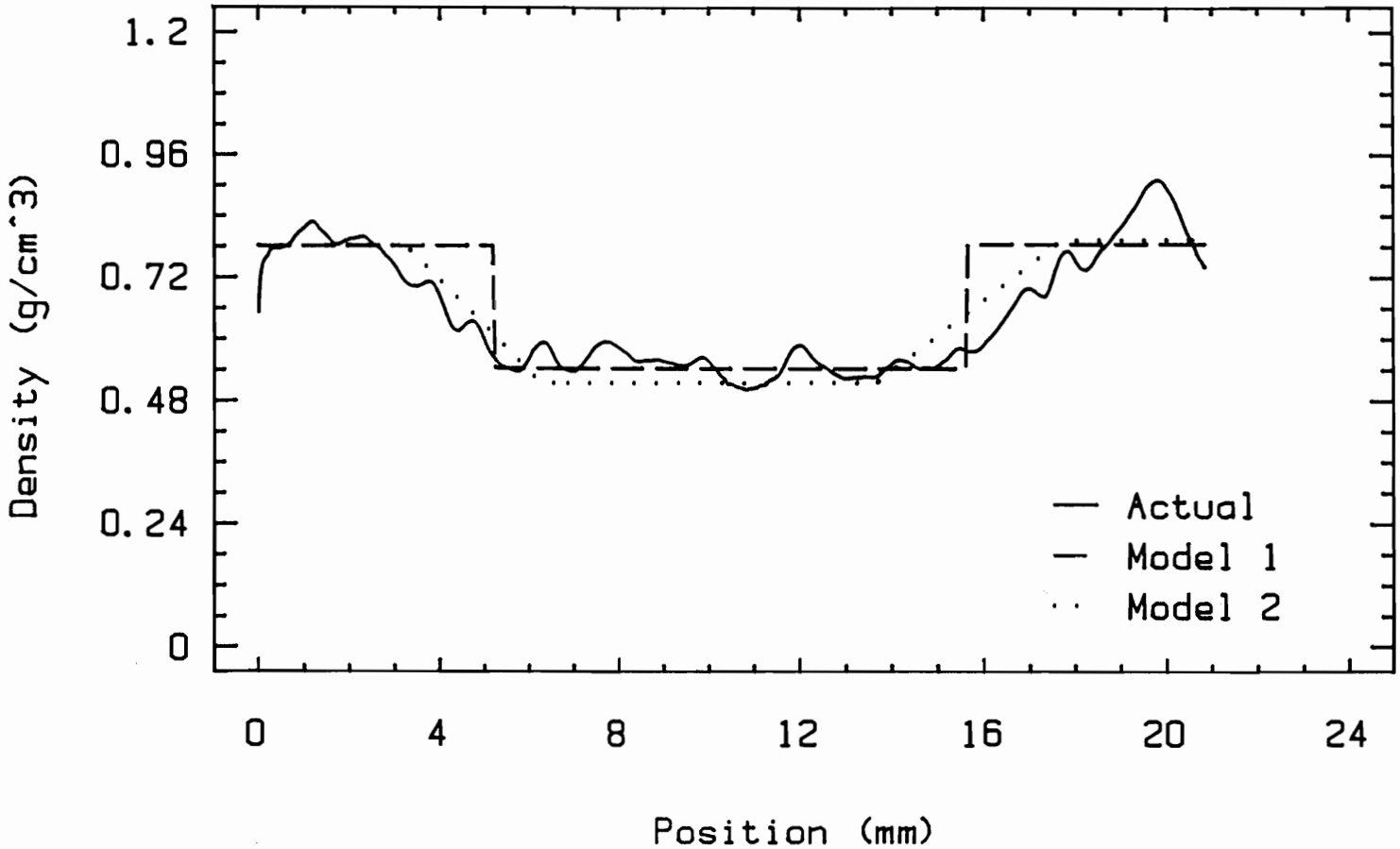

Figure 42. - Comparison of predicted and actual density profile (#27).

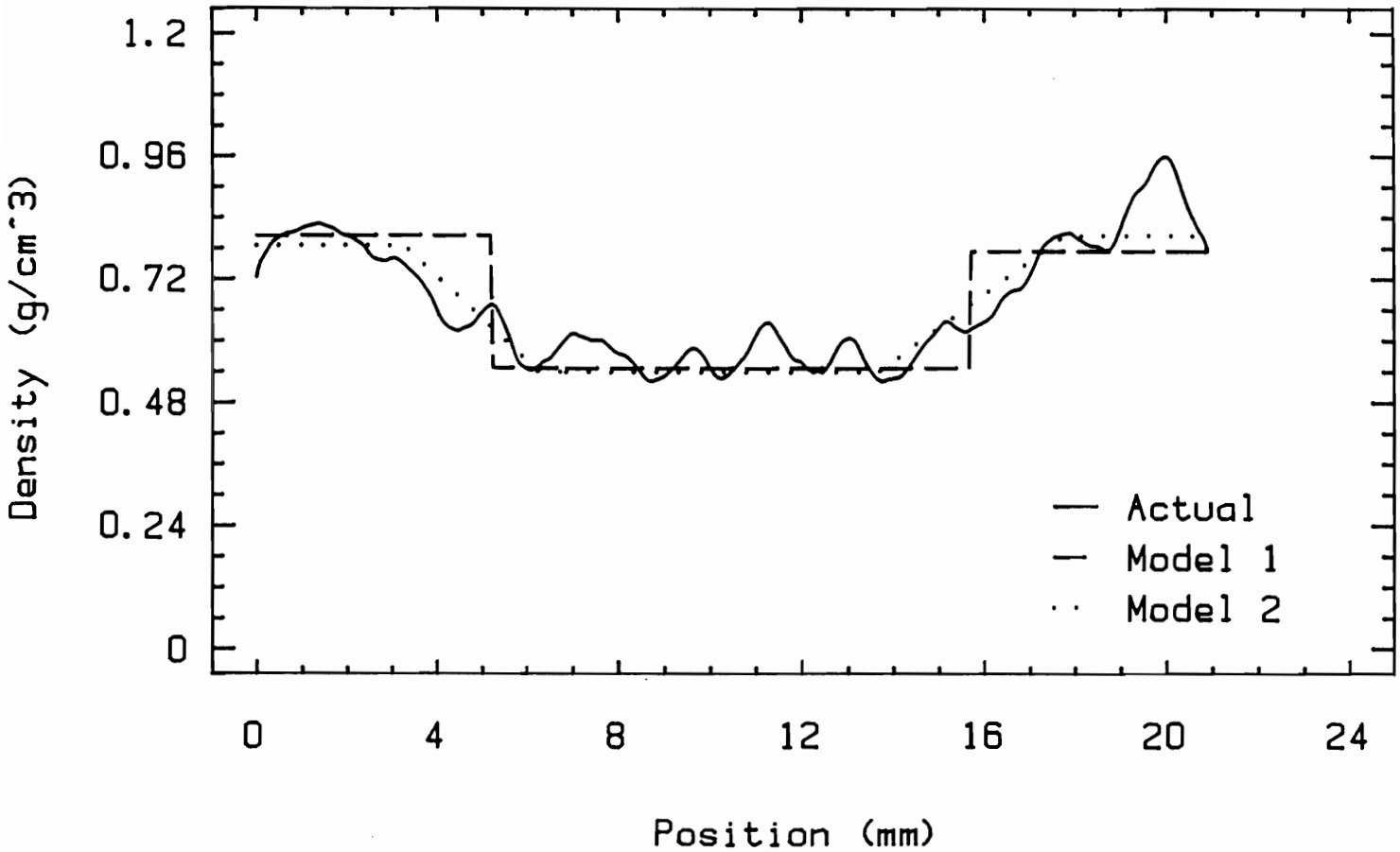

Figure 43. - Comparison of predicted and actual density profile (#28).

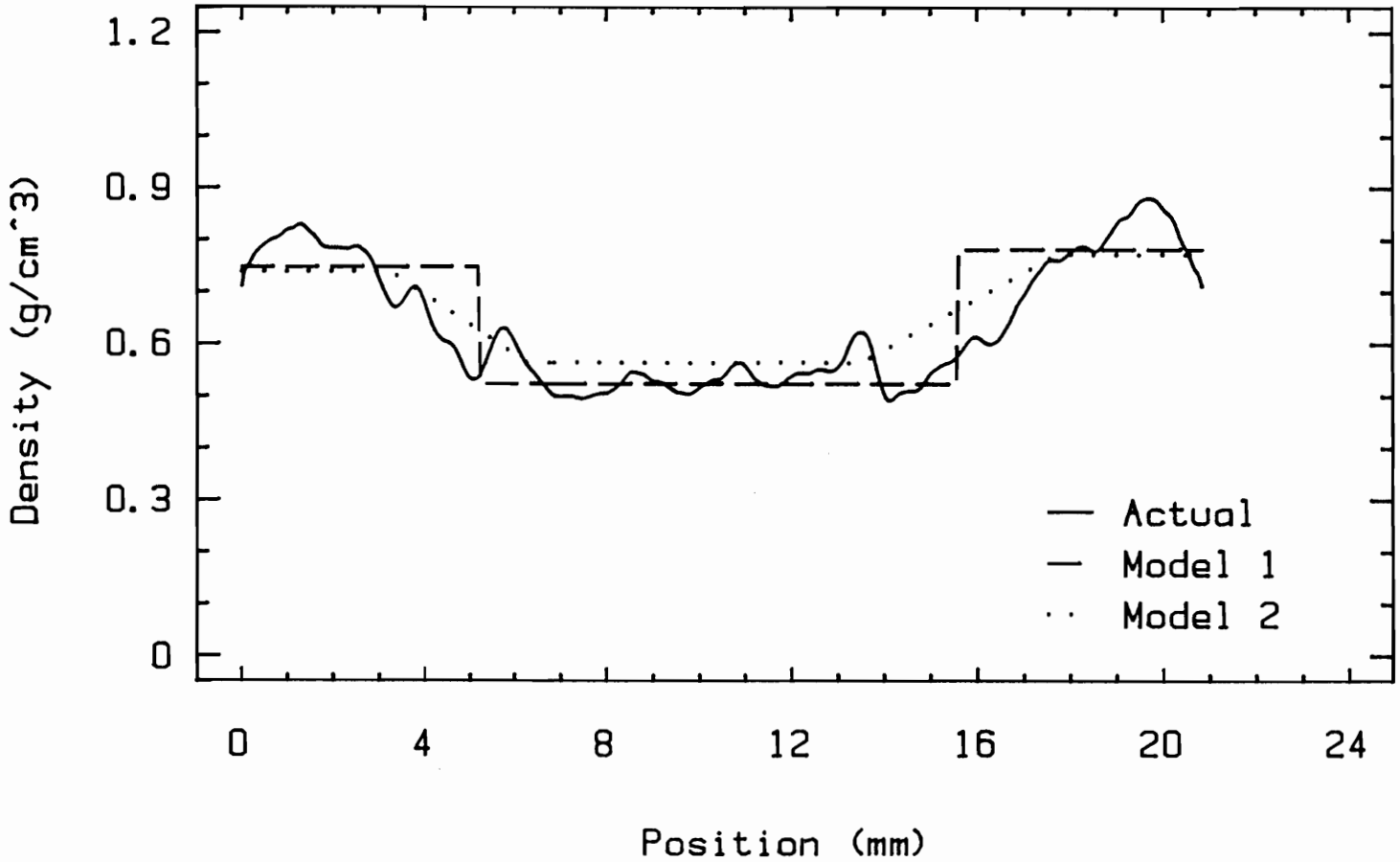

Figure 44. - Comparison of predicted and actual density profile (#29).

APPENDIX B. (Continued)

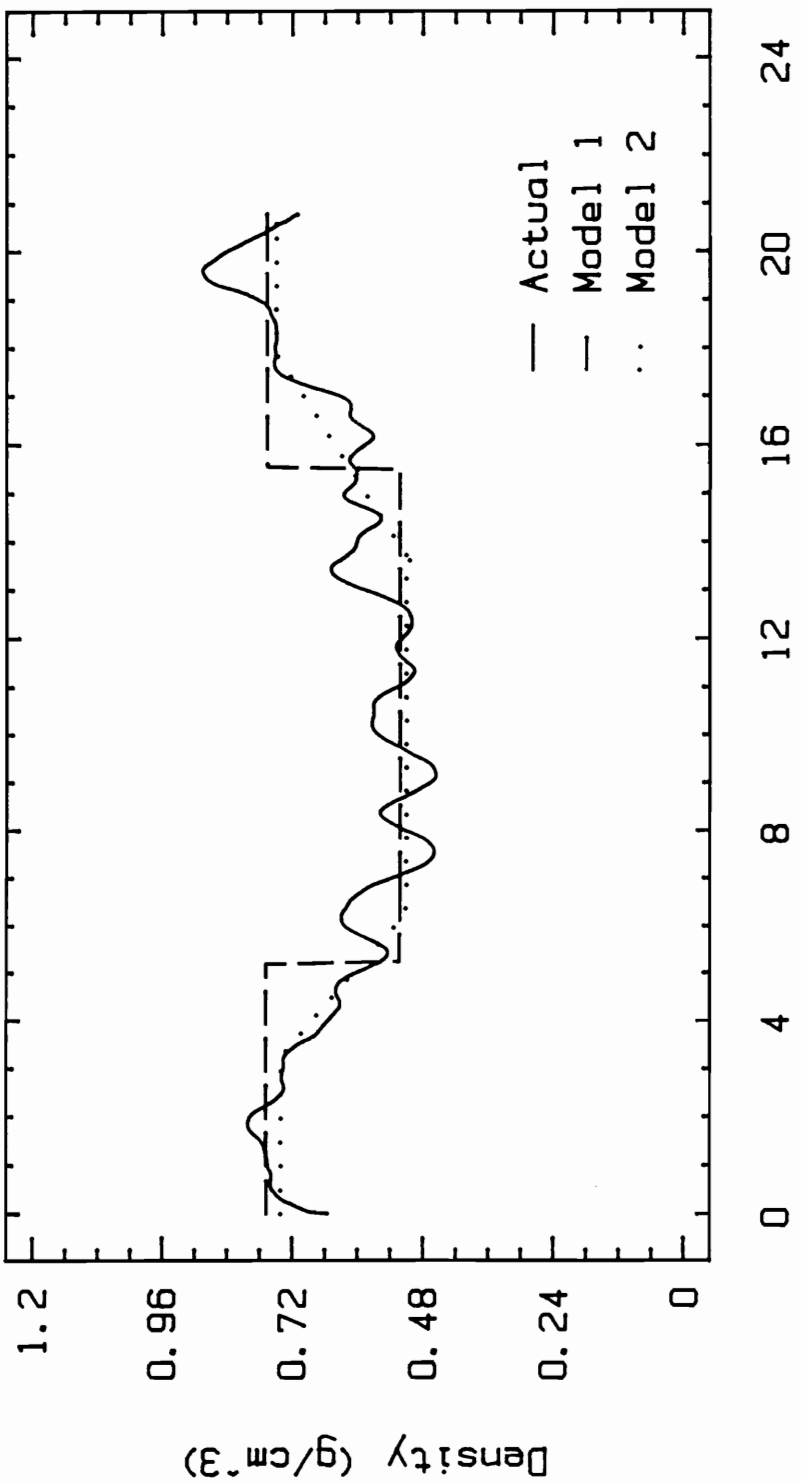

Figure 45. - Comparison of predicted and actual density profile (#30).

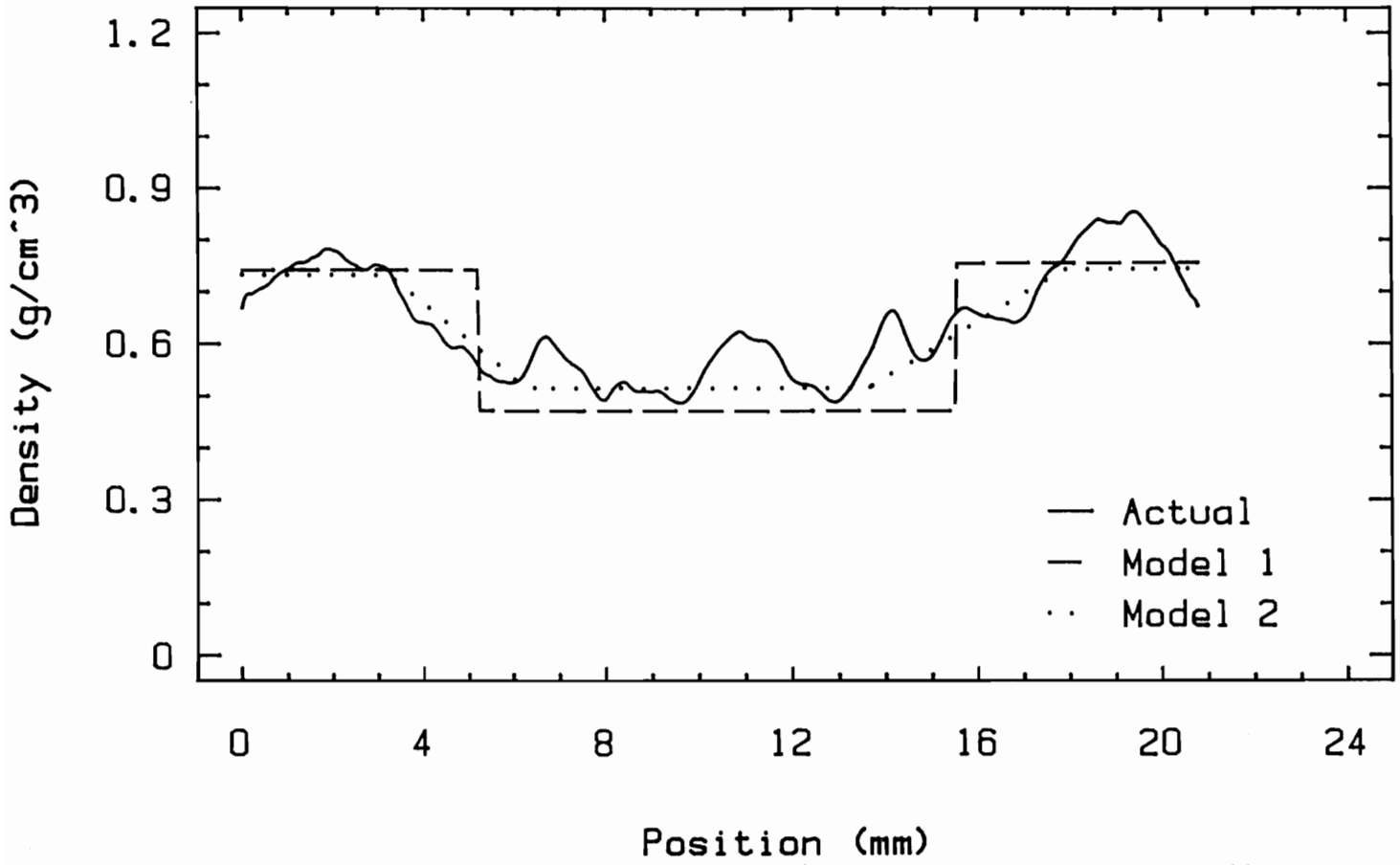

Figure 46. - Comparison of predicted and actual density profile (#31).

APPENDIX B. (Continued)

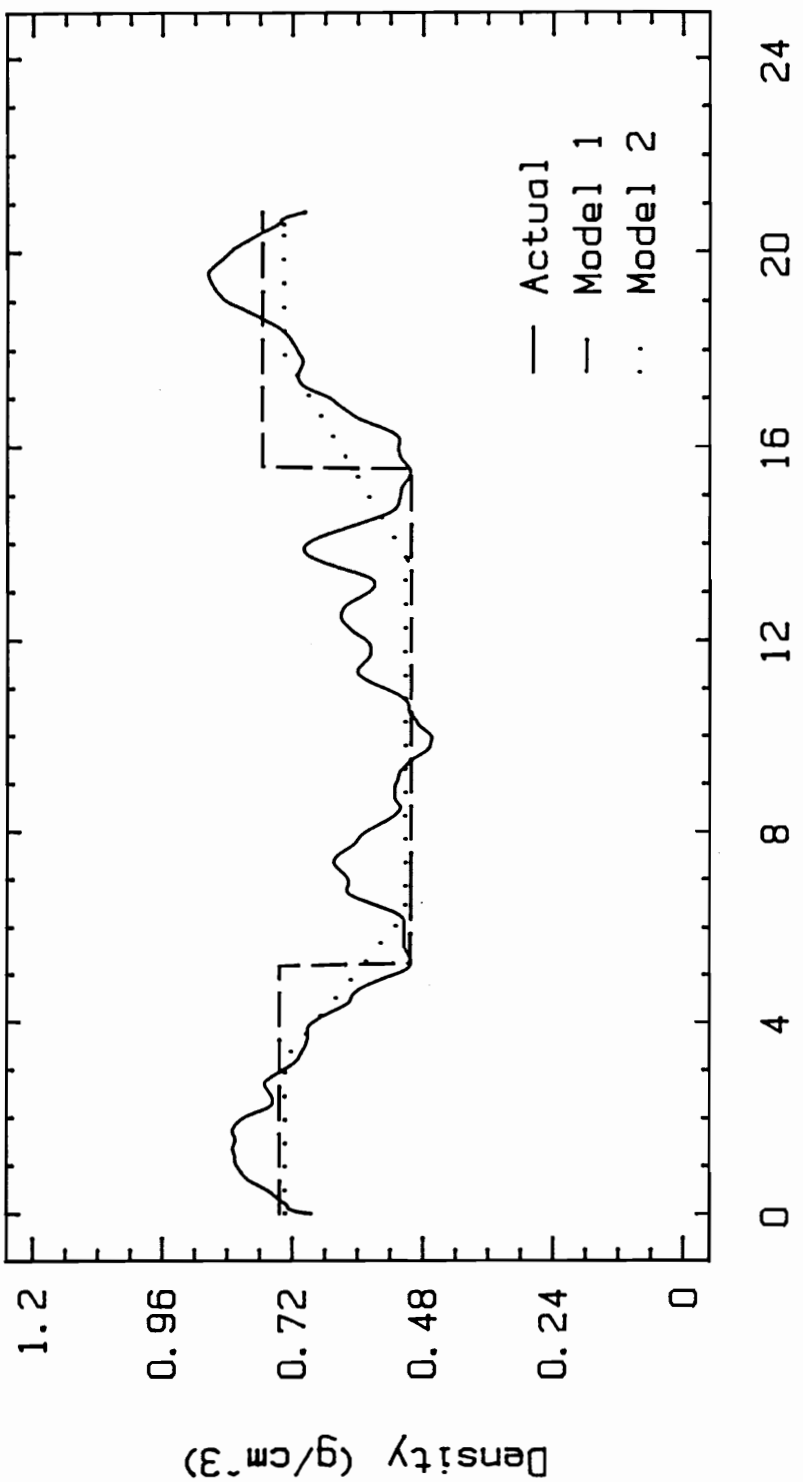

Figure 47. - Comparison of predicted and actual density profile (#32).

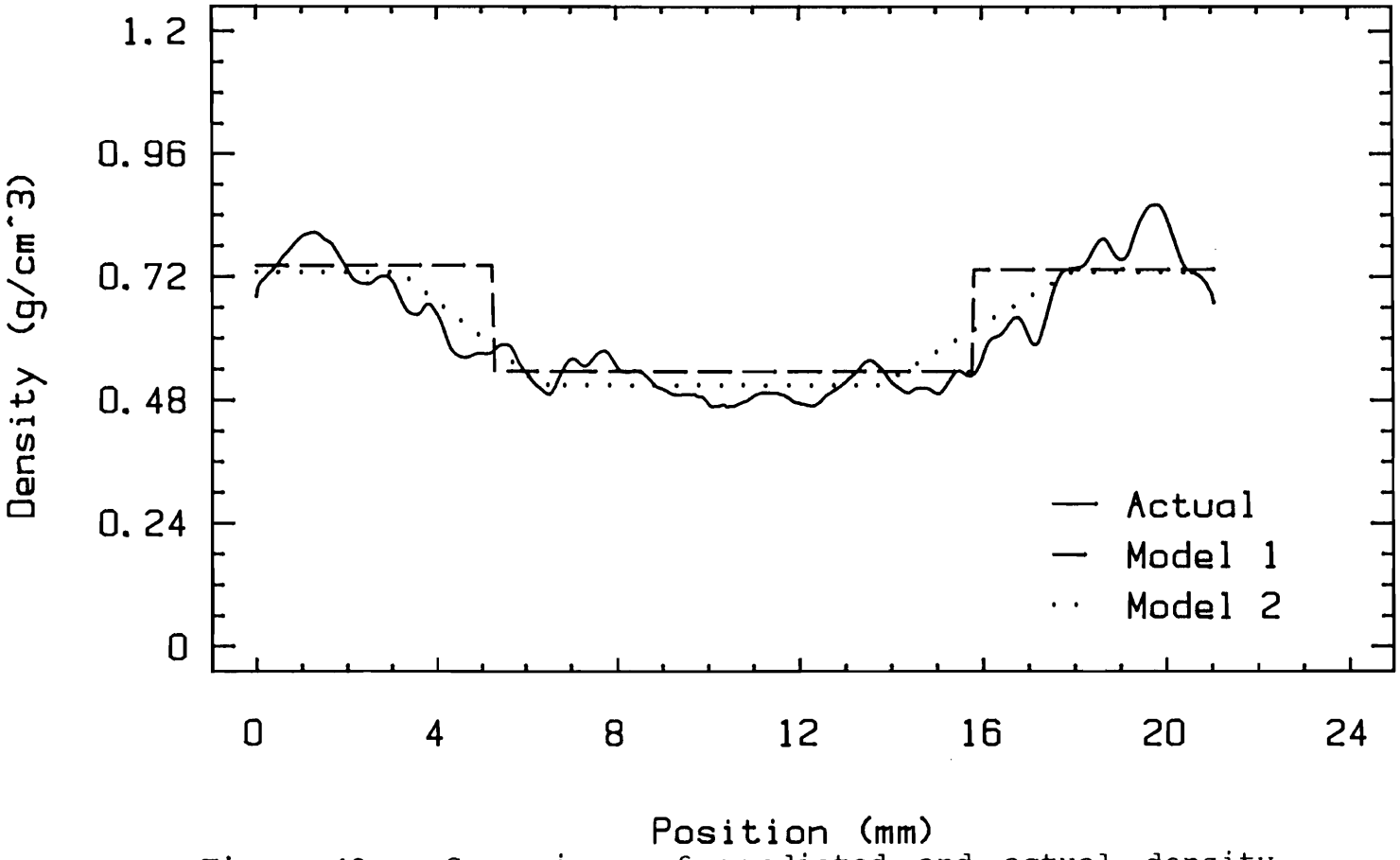

Figure 48. - Comparison of predicted and actual density profile (#33).

APPENDIX B. (Continued)

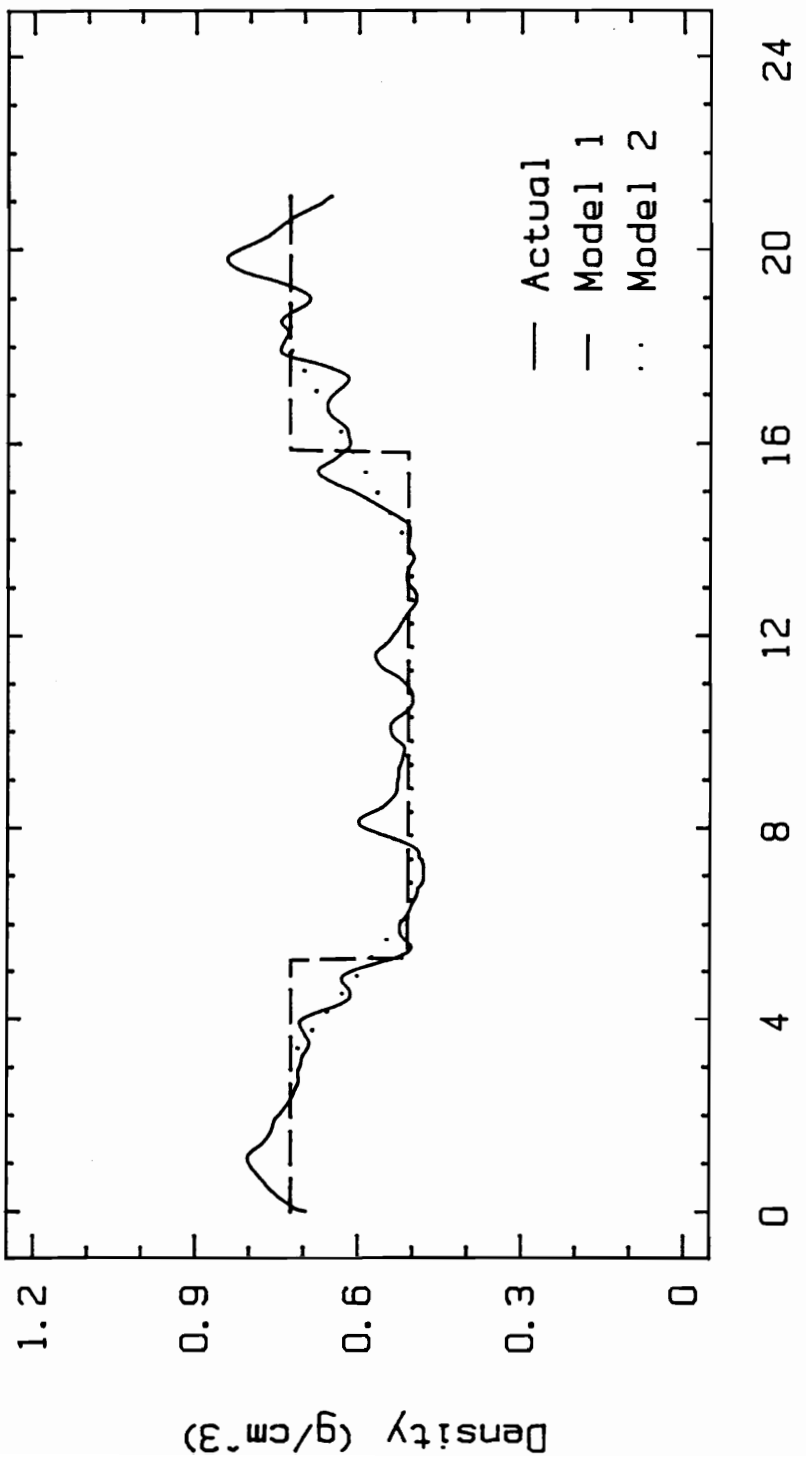

Figure 49. - Comparison of predicted and actual density profile (#34).

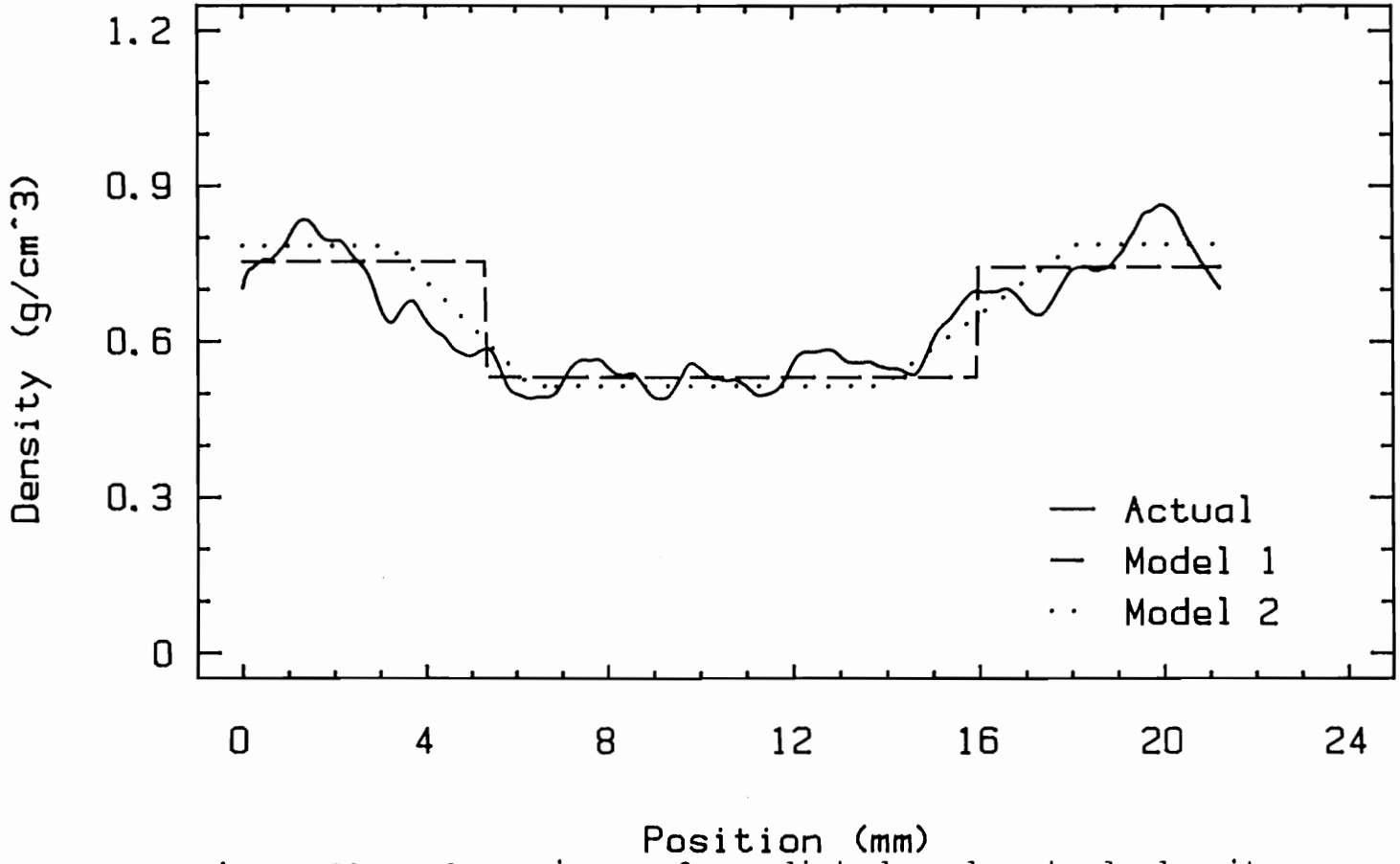

Figure 50. - Comparison of predicted and actual density profile (#35).

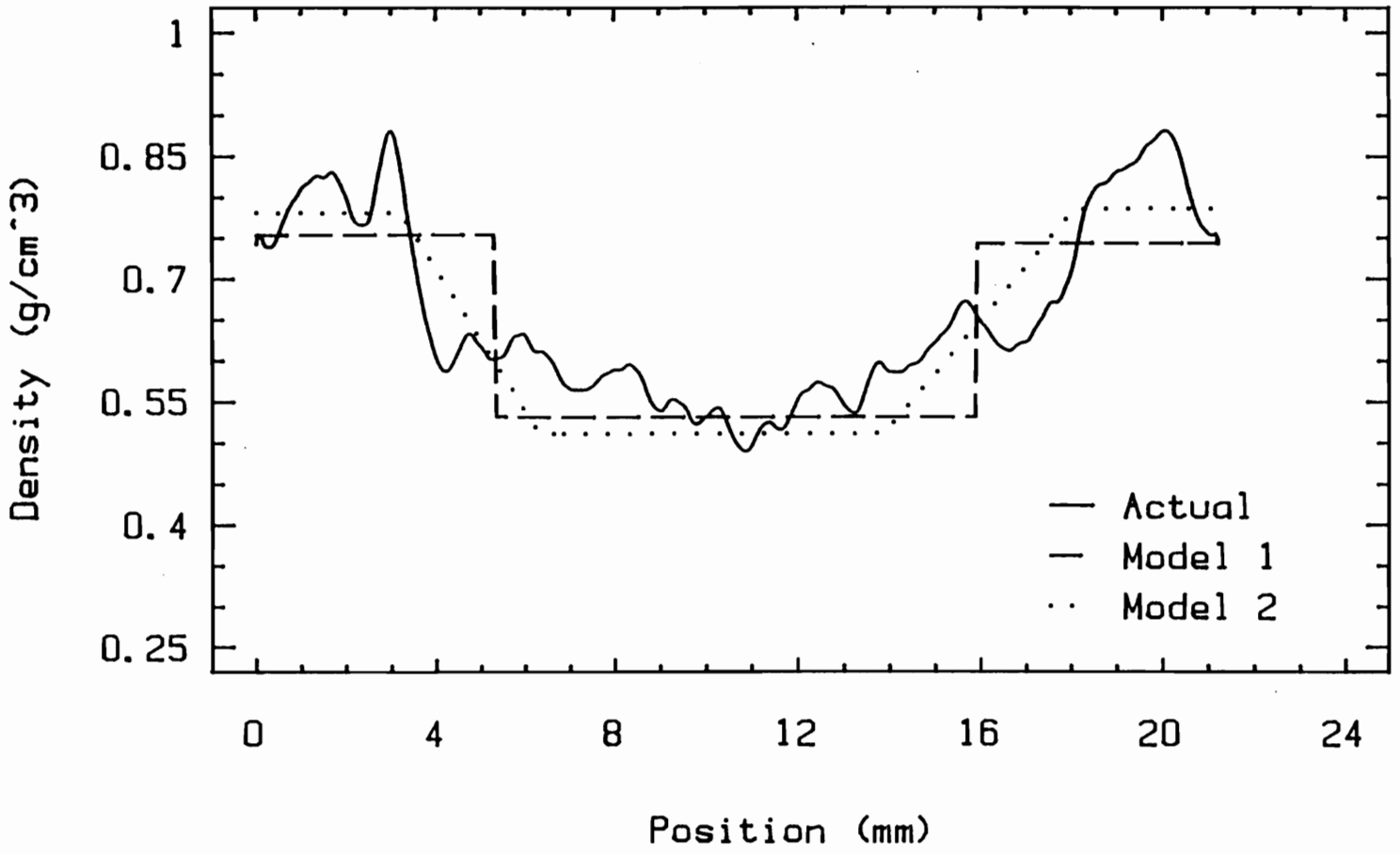

Figure 51. - Comparison of predicted and actual density profile (#36).